

**Preparation, Thermal stability and Photocatalytic Activity of Fluorinated
Organic/Silica/Anatase Titanium Oxide Nanocomposites**

Doctoral Course
Graduate School of Science and Technology
Hirosaki University

Doctor Thesis

September 2014

Sujuan Guo

Contents

General Introduction	1
1. Fluoroalkyl end-capped vinyltrimethoxysilane oligomer/anatase titanium oxidenanocomposites possessing photocatalytic activity even after calcination at 1000 °C	35
1.1. Introduction	36
1.2. Experimental	38
1.2.1. Measurements	38
1.2.2. Materials	38
1.2.3. Preparation of fluoroalkyl end-capped vinyltrimethoxysilane oligomer/anatase titanium oxide nanocomposites	39
1.3. Results and discussion	40

1.4.	Conclusions	47
2.	Preparation and photocatalytic activity of fluoroalkyl end-capped vinyltrimethoxysilane oligomer/anatase titanium oxide nanocomposites – encapsulated low molecular weight aromatic compounds	55
2.1.	Introduction	56
2.2.	Experimental	59
2.2.1.	Measurements	59
2.2.2.	Materials	59
2.2.3.	Preparation of fluoroalkyl end-capped vinyltrimethoxysilane oligomer/anatase titanium oxide nanocomposites – encapsulated BPA	60
2.2.4.	Decolorization of methyl blue under UV light irradiation in the presence of fluoroalkyl end-capped vinyltrimethoxysilane	

	oligomer/anatase titanium oxide nanocomposites – encapsulated BPA	61
2.3.	Results and discussion	61
2.4.	Conclusion	88
3.	Vinylidene fluoride - containing copolymers/anatase titanium oxide/silica nanocomposites exhibiting photocatalytic activity even after calcination at 1000 °C	95
3.1.	Introduction	96
3.2.	Experimental	99
3.2.1.	Measurements	99
3.2.2.	Materials	100
3.2.3.	Preparation of poly(VDF- <i>co</i> -M ₂) copolymer/silica/anatase titanium oxide nanocomposites	100

3.2.4.	Discoloration of methylene blue under UV light irradiation in the presence of fluorinated copolymers/silica/anatase titanium oxide nanocomposites	101
3.3.	Results and discussion	102
3.3.1	Preparation of poly(VDF- <i>co</i> -M) copolymer/ <i>an</i> -TiO ₂ nanocomposites and poly(VDF- <i>co</i> -M) copolymer/SiO ₂ / <i>an</i> -TiO ₂ nanocomposites	102
3.3.2	Photocatalytic activity of fluorinated copolymers/ <i>an</i> -TiO ₂ and fluorinated copolymers/SiO ₂ / <i>an</i> -TiO ₂ nanocomposites	112
3.4.	Conclusion	123
4.	Preparation and properties of fluorinated aliphatic alcohols/silica nanocomposites - Application to the encapsulation of anatase titanium oxide nanoparticles into these composite cores	134
4.1.	Introduction	135

4.2.	Experimental	138
4.2.1.	Measurements	138
4.2.2.	Materials	138
4.2.3.	Preparation of 1 <i>H</i> , 1 <i>H</i> , 2 <i>H</i> , 2 <i>H</i> -tridecafloro-1- <i>n</i> -octanol (FA6)/SiO ₂ nanocomposites	139
4.2.4.	Preparation of 1 <i>H</i> , 1 <i>H</i> , 2 <i>H</i> , 2 <i>H</i> -tridecafloro-1- <i>n</i> -octanol (FA6)/SiO ₂ /anataase TiO ₂ nanocomposites	140
4.2.5	Preparation of 1 <i>H</i> , 1 <i>H</i> , 2 <i>H</i> , 2 <i>H</i> -tridecafloro-1- <i>n</i> -octanol (FA6)/SiO ₂ /anataase TiO ₂ nanocomposites - encapsulated bisphenol A	141
4.2.6	Preparation of modified glass treated with fluorinated aliphatic alcohols/silica nanocomposites by dipping method	142
4.3.	Results and discussion	143

4.3.1	Preparation of a variety of fluorinated aliphatic alcohols/SiO ₂ nanocomposites and application to the surface modification of glass treated with these nanocomposites	143
4.3.2	Preparation and photocatalytic activity of 1 <i>H</i> , 1 <i>H</i> , 2 <i>H</i> , 2 <i>H</i> -tridecafloro-1- <i>n</i> -octanol (FA6)/SiO ₂ /anataase TiO ₂ nanocomposites and 1 <i>H</i> , 1 <i>H</i> , 2 <i>H</i> , 2 <i>H</i> -tridecafloro-1- <i>n</i> -octanol (FA6)/SiO ₂ /anataase TiO ₂ nanocomposites encapsulated <i>Ar</i> -H	154
4.4.	Conclusion	172
	Conclusions	180
	Publications	184
	Acknowledgements	186

General Introduction

1. Fluorinated polymers

In recent years, fluorinated polymers have been widely applied in the fields of surfactant, water and oil repellent agents, coating materials and so on.¹⁾ The properties of fluorinated polymers mainly depend on the fluorine atoms in the molecule. Table 1 compares the physical constants of hydrogen, fluorine, chlorine and bromine atoms. Fluorine atoms possess the highest electronegativity, strong electron affinity, low polarizability and refractive index. Therefore, fluorinated polymers can exhibit good electronic and optical properties. Their thermal stability, oxidative resistance, and resistance to chemical reagents are also very excellent due to the large bond energy of carbon-fluorine (441 kJ mol^{-1}) compared to those of the corresponding non-fluorinated ones.^{2, 3)} In addition, fluorinated polymers are endowed with high resistance to water, oil and stain by the low cohesion between fluorinated polymer molecules, poor intermolecular forces between the air and the fluoropolymer interface, and the small surface free energy.

Table 1 Physical properties of hydrogen, fluorine, chlorine and bromine.

	H	F	Cl	Br
Electronic structure	1S ¹	2S ² 2P ⁵	3S ² 3P ⁵	4S ² 4P ⁵
Electronegativity (Pauling)	2.1	4.0	3.0	2.8
Electron affinity (kJ mol ⁻¹)	75	350	365	343
C-X bond length (10 ⁻¹⁰ m)	1.100	1.271	1.767	1.937
C-X bond energy (kJ mol ⁻¹)	414	441	329	276
Polarizability (10 ⁻²⁴ cm ³)	0.66	0.68	2.58	6.94

The first fluoropolymer: poly(tetrafluoroethylene) [PTFE: $-(CF_2-CF_2)_n-$], was synthesized in 1938. Since then, much effort has been made on the synthesis and application of fluorinated polymers. ⁴⁾ Up to date, there have been many commercial products of fluoropolymers, such as poly(vinylidene fluoride) [PVDF], poly(ethylene-tetrafluoroethylene) [PETFE], and poly(chlorotrifluoroethylene) [PCTFE]. Although these fluoropolymers are well known to exhibit their extremely high chemical stability and thermal stability, their poor solubility in organic solvents limits their applications. From this point of view, it is of particular interest to develop novel fluorinated polymers possessing functional groups such as amide, carboxyl, hydroxyl, and so on.

Lagow et al. reported that fluorinating functionalized polymeric materials, which contain pendant ester, carboxylic acid, acid halide or acid anhydride groups, are useful as ion exchange membranes, solid electrolytes, and conductive films. ⁵⁾ In addition, various reactants

can be tacked onto such fluorinated polymers thereby making them useful in many other applications. For example, M. Yamabe et al. reported on the preparation of a variety of fluorinated copolymer using fluorinated ethylenically unsaturated monomers and functional monomers having carboxylic group (-COOH group).⁶⁾ These fluoropolymers can be dissolved in a variety of traditional organic solvents with a small amount of water.⁶⁾

Among numerous fluorinated polymers, fluoroalkyl end-capped oligomers are attractive materials because they can exhibit many unique properties such as high solubility, surface-active properties, biological activities, and nanometer size-controlled self-assembled molecular aggregates through the aggregations of end-capped fluoroalkyl groups, which cannot be achieved by the corresponding nonfluorinated and randomly fluoroalkylated ones.⁷⁾ As shown in Figure 1-[A], these fluorinated molecular aggregates can form the suitable host moieties to interact with a variety of guest molecules, although the corresponding non-fluorinated ones can not form such molecular aggregates (see Fig. 1-[B]).^{7-a)}

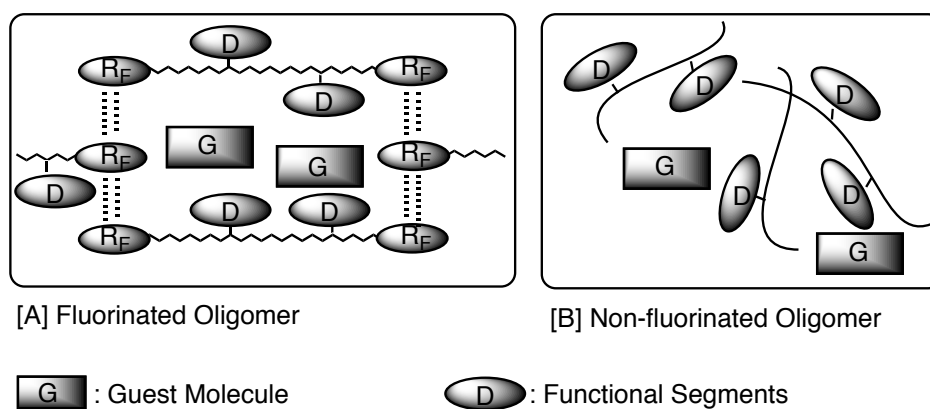
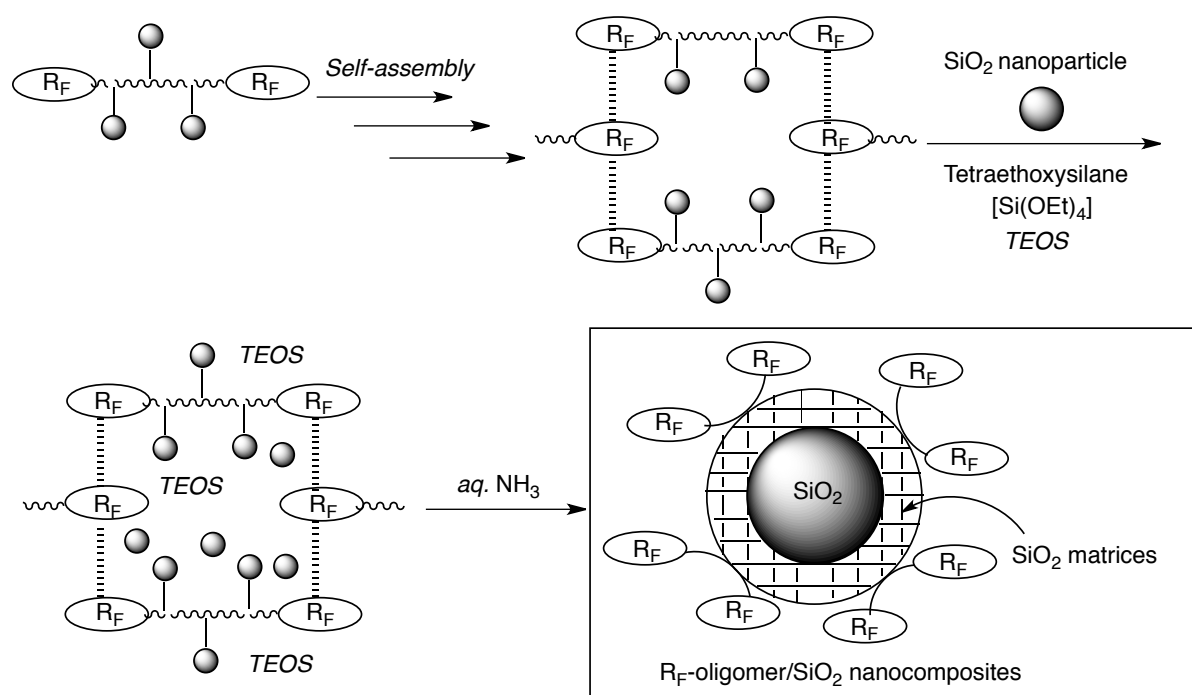


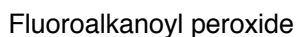
Fig. 1 Schematic illustration for the interaction of self-assembled fluoroalkyl end-capped oligomers with guest molecules.^{7a)}

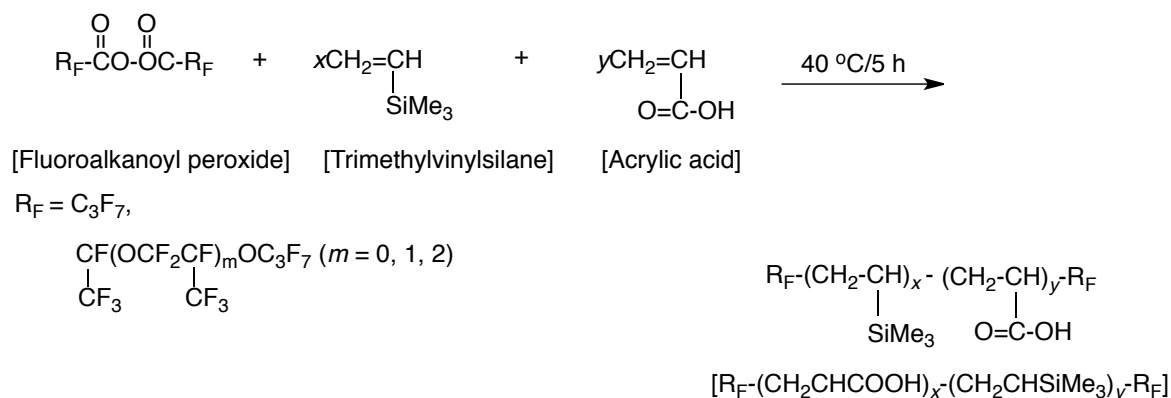
Taking silica nanoparticles as an example, fluoroalkyl end-capped oligomers can form the nanometer size-controlled selfassemblies and react with tetraethoxysilane (TEOS) as a cross-linker for guest silica nanoparticles under alkaline conditions to produce fluorinated oligomer/silica nanocomposites (see Scheme 1).⁸⁾



Scheme 1 Preparation of fluoroalkyl end-capped oligomer/ SiO_2 nanocomposites.⁸⁾

Fluoroalkyl end-capped oligomers can be easily prepared by using fluoroalkanoyl peroxide as a key intermediate. Scheme 2 shows the preparation of two fluoroalkyl end-capped acrylic acid oligomers, which can be easily synthesized by primary radical termination or radical chain transfer to the fluoroalkanoyl peroxide under the oligomeric

acid. ⁹⁾Scheme 2 Preparation of fluoroalkyl end-capped acrylic acid oligomers. ⁹⁾Scheme 3. ¹⁰⁾



Scheme 3 Preparation of $\text{R}_F\text{-(CH}_2\text{CHCOOH)}_x\text{-(CH}_2\text{CHSiMe}_3)_y\text{-R}_F$ cooligomers. ¹⁰⁾

These obtained cooligomers are readily soluble in not only water but also traditional organic solvents such as methanol, tetrahydrofuran, carbon tetrachloride, chloroform, *N*, *N*-dimethylformamide, dimethyl sulfoxide, benzene, toluene and xylene. Interestingly, the molecular aggregates formed through the aggregation of end-capped fluoroalkyl segments in these cooligomers can interact with positively charged HIV-1 as a guest molecule to exhibit a potent and selective anti-HIV-activity by the electrostatic interaction (see Figure 2). ¹⁰⁾

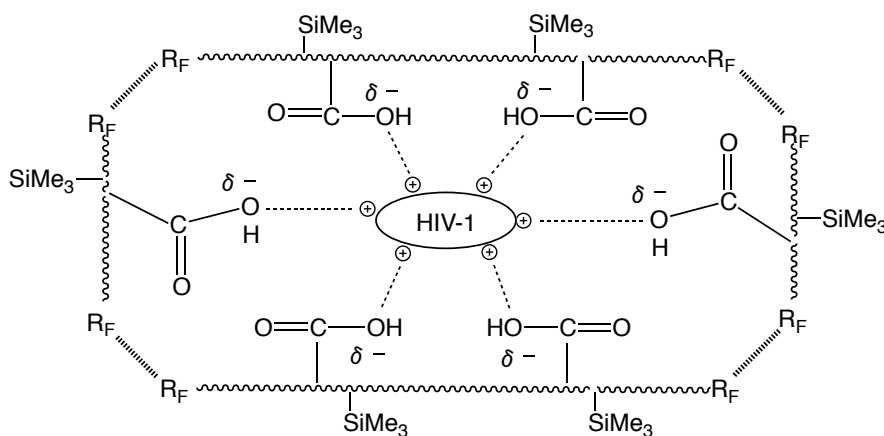


Fig. 2 Schematic illustration for the interaction of HIV-1 and the intermolecular aggregates of $\text{R}_F\text{-(CH}_2\text{CHCO}_2\text{H)}_x\text{-(CH}_2\text{CHSiMe}_3)_y\text{-R}_F$. ¹⁰⁾

2. Fluorinated polymers/inorganic hybrid materials

Organic–inorganic hybrid materials have received much attention as a new class of composite materials because of the novel properties arisen from the combination of organic and inorganic material, which can not be achieved by a single-phase material.¹¹⁾ Since fluorinated polymers possess outstanding properties, it is of particular interest to develop fluorinated polymers/inorganic hybrid materials.

Table 2 Examples of fluorinated polymers/inorganic hybrid materials.

Inorganic materials	Fluorinated polymers	Properties	Ref.
TiO ₂	poly (MAA-co-TFA)/PVDF ^{a)}	good photocatalytic activity	12
SiO ₂	PFMA ^{b)}	switchable superoleophilicity and high oleophobicity	13
ZnO	PTFE ^{c)}	superhydrophobicity	14
Katoite	R _F -(MES) _n -R _F ^{d)}	good antibacterial activity and oleophobicity	15
Hydroxyapatite	R _F -(VM) _n -R _F ^{e)}	good hydro- and oleophobicity	16
Au	R _F -(AMPS) _x -(Ad-HAc) _y -R _F ^{f)}	extremely red-shifted plasmon absorption behavior	17
Cu	R _F -(DMAA) _n -R _F ^{g)}	stable copper nanoparticles	18

a) poly (MAA-co-TFA)/PVDF: poly(methacrylic acid-co-trifluoroethyl acrylate)/poly(vinylidene difluoride)

b) PFMA: poly(fluoroalkyl ethyl methacrylates)

c) PTFE: poly(tetrafluoroethylene)

d) R_F-(MES)_n-R_F: fluoroalkyl end-capped 2-methacryloyloxyethanesulfonic acid oligomer

e) R_F-(VM)_n-R_F: fluoroalkyl end-capped vinyltrimethoxysilane oligomer

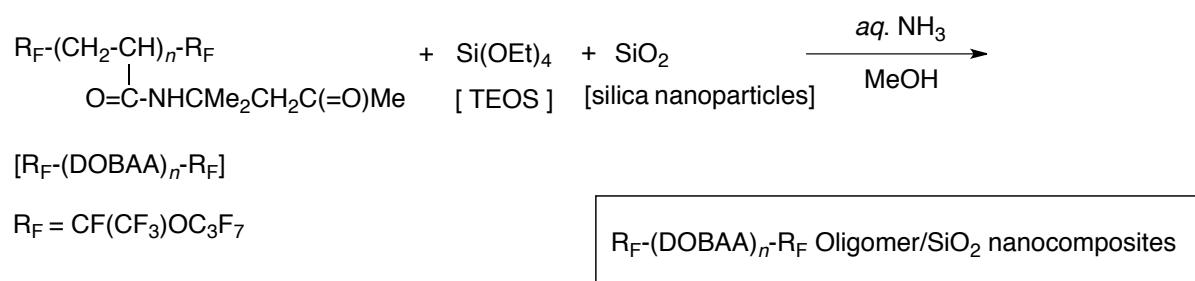
f) R_F-(AMPS)_x-(Ad-HAc)_y-R_F: fluoroalkyl end-capped (2-acrylamido-2-methylpropanesulfonic acid-co-1-hydroxy-5-adamantylacrylate) oligomer

g) R_F-(BTRI)_x-(DMAA)_y-R_F: fluoroalkyl end-capped *N,N*-dimethylacrylamide oligomer

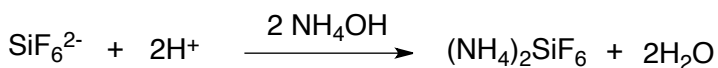
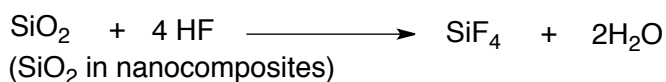
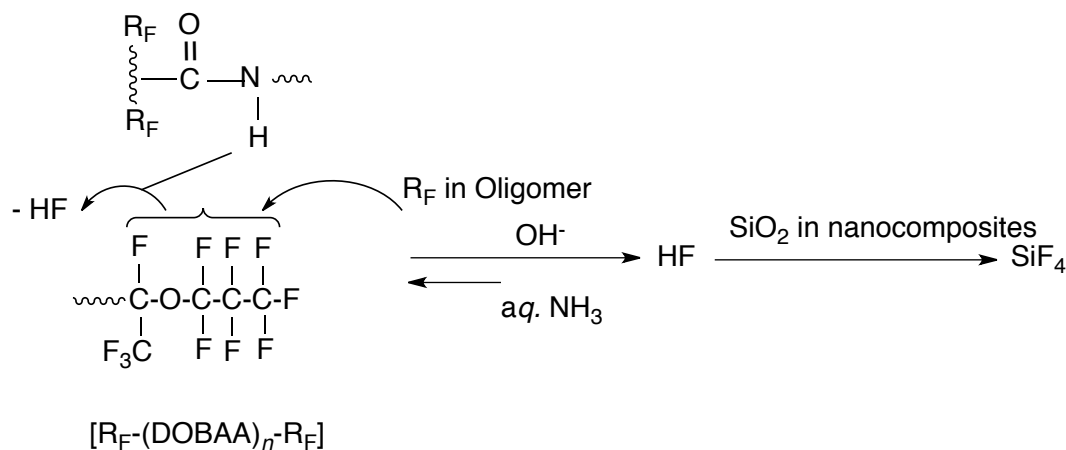
The commonly used inorganic materials are titanium oxide (TiO₂), silica (SiO₂), zinc oxide (ZnO), calcium carbonate (CaCO₃), magnetite (Fe₃O₄), gold (Au), silver (Ag), copper (Cu)

and so on. Table 2 shows some examples of the recently reported fluorinated polymers/inorganic hybrid materials, including their unique characteristics imparted by fluorinated polymers and inorganic materials.¹²⁻¹⁸⁾

As shown in Scheme 4, fluoroalkyl end-capped *N*-(1, 1-dimethyl-3-oxobutyl)acrylamide oligomer [R_F-(DOBAA)_{*n*}-R_F]/silica nanocomposites were prepared by reaction of the corresponding fluorinated oligomer with tetraethoxysilane and silica nanoparticles under alkaline conditions.¹⁹⁾ R_F-(DOBAA)_{*n*}-R_F oligomer in the nanocomposites can exhibit a nonflammable characteristic even after calcination at 800 °C through the formation of ammonium hexafluorosilicate during the sol-gel process (see Scheme 5).¹⁹⁾

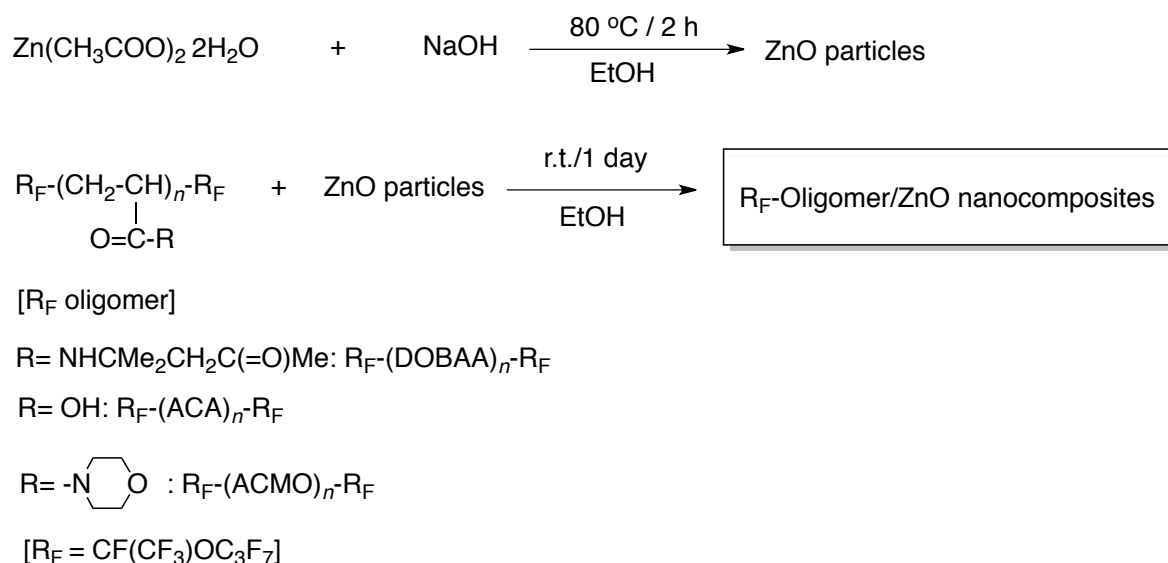


Scheme 4 Preparation of R_F-(DOBAA)_{*n*}-R_F Oligomer/SiO₂ nanocomposites.¹⁹⁾



Scheme 5 Plausible reaction mechanism for the formation of ammonium hexafluorosilicate. ¹⁹⁾

Fluoroalkyl end-capped oligomers/ZnO nanocomposites have been also prepared by the interaction of the corresponding oligomers with ZnO particles (see Scheme 6). ²⁰⁾ These nanocomposites can give unique characteristics such as nanometer size-controlled fine particles, good dispersibility and stability in water and traditional organic solvents. ²⁰⁾ These composites can also exhibit the surface electric conductivity of *ca* 10⁻¹¹ S cm⁻¹ at room temperature and yellow-green luminescence under UV irradiation. ²⁰⁾



Scheme 6 Preparation of fluoroalkyl end-capped oligomers/ZnO nanocomposites. ²⁰⁾

A variety of fluoroalkyl end-capped oligomers/silver nanocomposites have been prepared by the reactions of silver ions with poly (methylhydrosiloxane) in the presence of the corresponding oligomers in organic media. ²¹⁾ These fluorinated silver nanocomposites were found to exhibit not only a good oleophobicity imparted by fluorine but also high surface antibacterial activity related to the presence of silver nanoparticles on their surface. ²¹⁾ In this way, fluoroalkyl end-capped oligomer/silver nanocomposites have high potential for the application to the coating areas through their unique surface characteristics. ²¹⁾

Among these fluorinated polymers/inorganic hybrid materials, fluorinated polymers/titanium oxide nanocomposites have attracted much attention due to the high chemical stability, nontoxicity and excellent photocatalytic activity for the degradation of pollutants in natural environment.

3. Titanium oxide

TiO₂ belongs to the family of transition metal oxides. It has been widely used in pigment, porcelain glaze, cosmetics and additives from the early twentieth century because of its low cost, high chemical stability and nontoxicity. In 1972, Fujishima and Honda discovered the photocatalytic splitting of water on TiO₂ electrodes under ultraviolet light.²²⁾ Since then, notable progress has been made on investigating the photocatalytic activity of TiO₂.

There are three major stable polymorphs, named as anatase, rutile and brookite, with band gaps of 3.2 eV, 3.02 eV and 2.96 eV respectively, corresponding to a wavelength around 390 nm.²³⁾ Figure 3 shows the crystal structures of anatase and rutile phase of TiO₂.

Anatase has been already found to exhibit the higher photocatalytic activity²⁴⁾, while rutile is a catalytically inactive or much less active form of TiO₂.²⁵⁾ The reason for the different photocatalytic activities between anatase and rutile may be due to their crystal structures. As shown by the crystal structure of anatase in Figure 3, the position of oxygen ions on the exposed crystal surface shows a triangular arrangement, allowing effective absorption of organics. In addition, the position of titanium ions creates a favorable reaction condition with the absorbed organics. However, such favorable structure arrangement is not available for the rutile structure.²⁶⁾

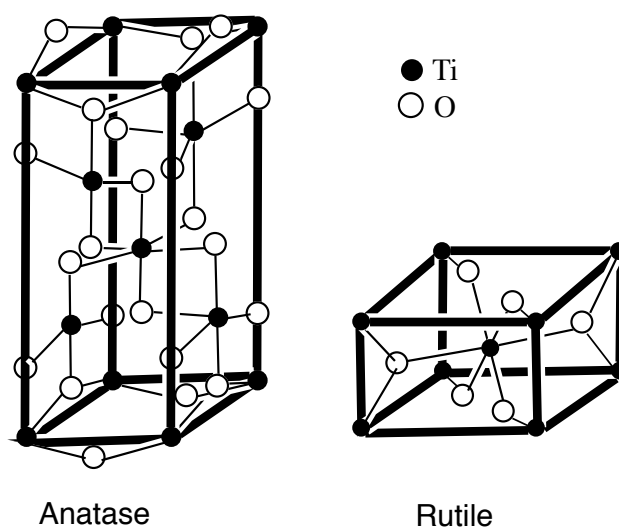


Fig. 3 Crystal structures of the anatase and rutile phases of TiO₂.²⁶⁾

The particle size also has an effect on the photocatalytic activity. Investigations have showed that the photocatalytic activity is much higher in the form of nanoparticles compared with the micrometric powders.²⁷⁾ Generally, we can obtain the higher photocatalytic activity related to the TiO₂ particles with smaller particle size and larger surface area. This should be due to the increase of active sites per square meter, as well as greater adsorbability of the pollutants on the catalyst surface.

The photodegradation process usually can be simply characterized by Figure 4. Electron-hole pairs (e^-h^+) are generated when the semiconductor photocatalyst is irradiated by light whose energy is equal or higher than the band-gap energy of the semiconductor. The oxygen adsorbed on the surface of the semiconductor trapped the electron to produce superoxide, while the hydroxyl radicals are formed via the oxidation of hydroxyl groups by

holes.²⁸⁾ These superoxides and hydroxyl radicals possess strong oxidation ability to degrade the pollutants.

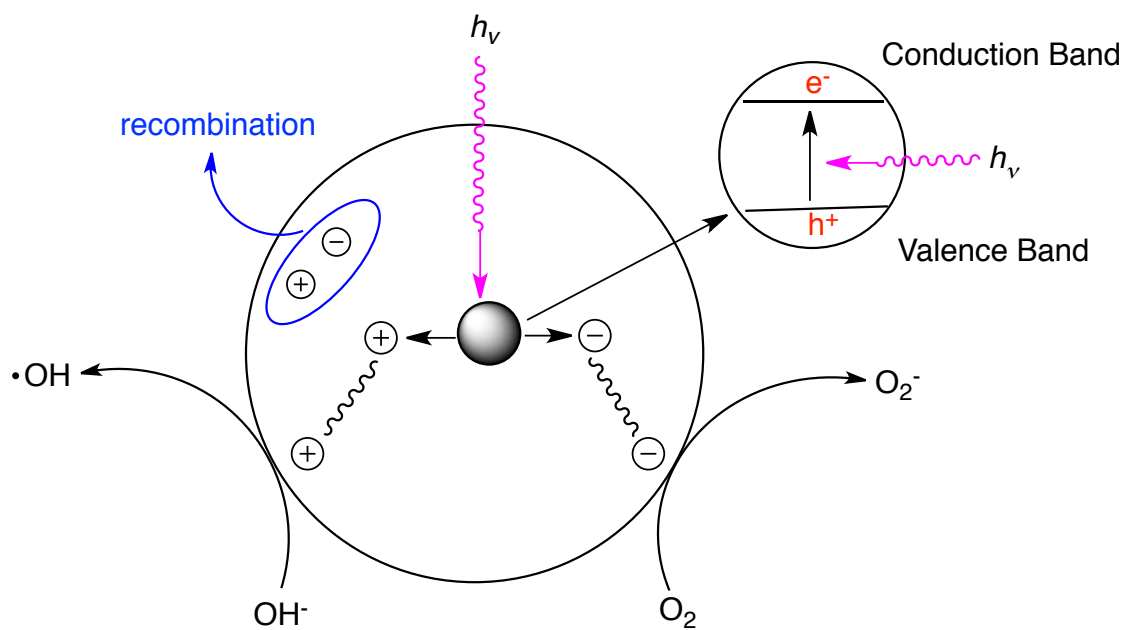


Fig. 4 Photocatalytic process over TiO_2 .²⁸⁾

A lot of research works have been performed to enhance the photocatalytic activity of titanium oxide,²⁹⁾ and it has been recently found that fluorine doping is a very effective way to enhance the photocatalytic activity of titanium oxide, due to the inhibition of the electron-hole recombination, high percentage of (001) facets, enhanced generation of free hydroxyl radicals, oxygen vacancies, the large surface area, and so on.³⁰⁾ One of the proposed explanations is shown in Fig. 5.³¹⁾ The $\equiv\text{Ti}-\text{F}$ group on the surface can trap the photogenerated electrons due to the strong electronegativity of the fluorine and then

transferring them to O_2 adsorbed on the surface of titanium oxide, inhibiting the recombination rate of electron and hole.

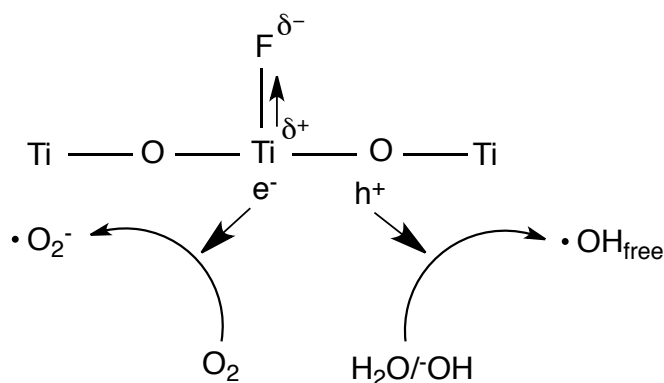


Fig. 5 Proposed mechanism for generation and transfer of charge carriers in F-TiO₂.³¹⁾

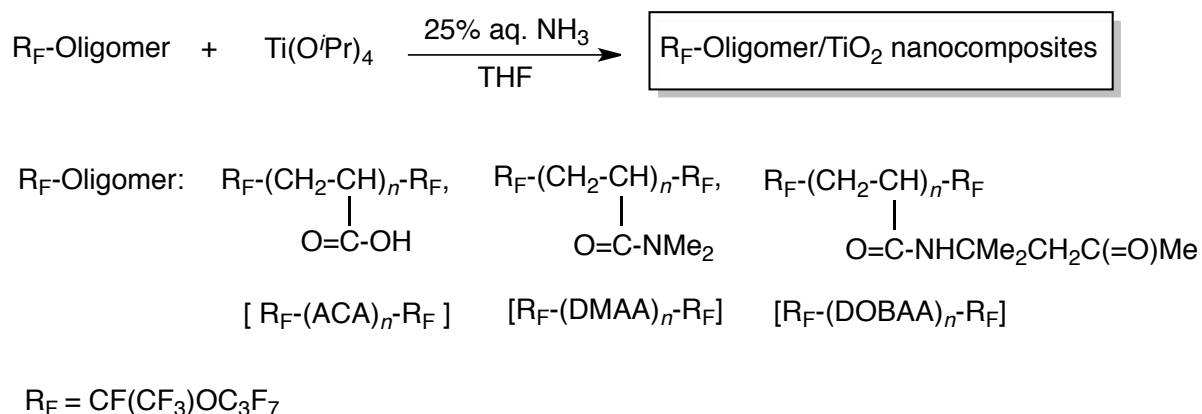
Generally, fluorine doped TiO₂ (F-TiO₂) is prepared by treating titanium plates with HF solution, and HF acts as the fluorine source for F-TiO₂.³²⁾ However, it has been reported that fluorine can easily transfer from poly(tetrafluoroethylene) [PTFE] to TiO₂ by comilling and annealing of a TiO₂-PTFE mixture.³³⁾

The sol-gel reactions of fluorinated polymers and silica should generate HF molecules as mentioned above (see Scheme 5). Therefore, fluorinated polymers are expected to be useful as one kind of fluorine source to offer fluorine doped TiO₂ with enhanced photocatalytic activity.

4. Fluorinated polymers/TiO₂ nanocomposites

Since fluorine doped TiO₂ possesses enhanced photocatalytic activity, and fluorides cannot be oxidized by the oxygen vacancies formed on the surface of TiO₂,³¹⁾ fluorinated polymers should be applied to prepare titanium oxide nanocomposites possessing unique characteristics imparted by both fluorine and titanium oxide.

Some of fluorinated polymers nanocomposites have been already prepared. For example, three kinds of fluoroalkyl end-capped oligomers/titanium oxide nanocomposites have been prepared by the hydrolysis of titanium isopropoxide [Ti(OⁱPr)₄] in the presence of the corresponding oligomers under mild conditions (see Scheme 7).³⁴⁾ R_F-(ACA)_n-R_F oligomer is the most effective one among these oligomers for the preparation of the corresponding oligomers/titanium oxide nanocomposites through the formation of the C(=O)O-Ti bonds by the interaction of carboxyl groups in R_F-(ACA)_n-R_F oligomer with Ti(OⁱPr)₄.³⁴⁾



Scheme 7 Preparation of fluoroalkyl end-capped oligomers/titanium oxide nanocomposites.³⁴⁾

The modified film treated with these nanocomposites can exhibit a good oleophobic characteristic imparted by fluoroalkyl segments, and a hydrophilic characteristic, which is due to the replacement from the hydrophobic fluoroalkyl segments to the hydrophilic segments in oligomers such as carboxyl groups at the water interface when the environment is changed from air to water (see Figure 6).³⁴⁾

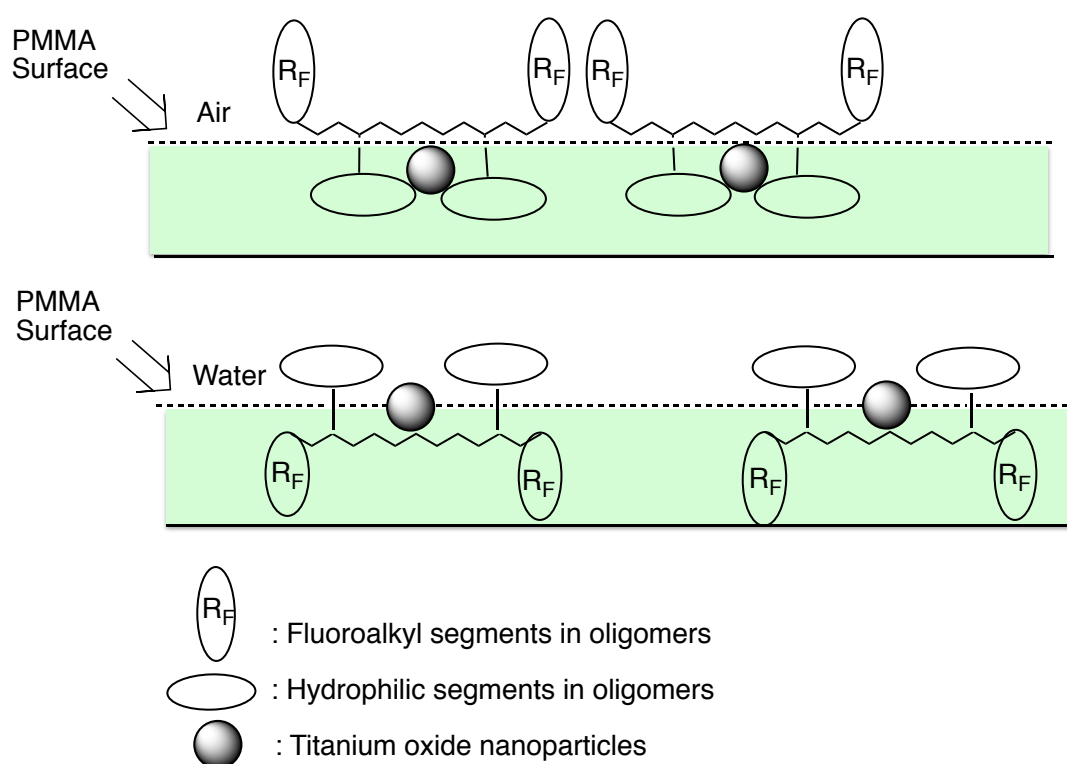
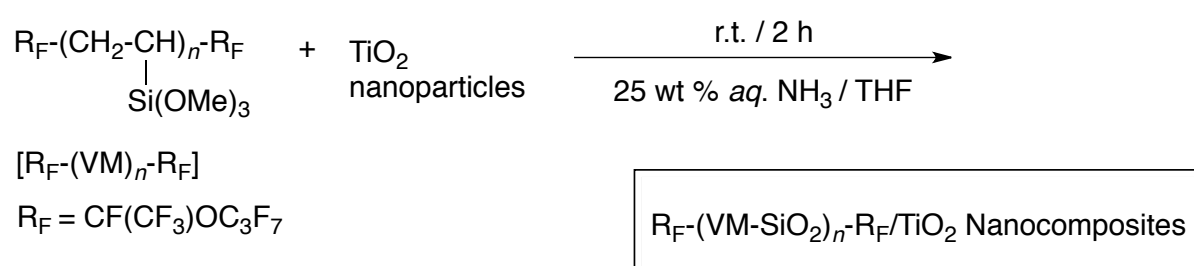


Fig. 6 Schematic illustration for the arrangement of fluoroalkyl end-capped oligomers/TiO₂ on the PMMA film surface.³⁴⁾

Fluoroalkyl end-capped vinyltrimethoxysilane oligomer is also applied to the preparation of fluorinated titanium oxide nanocomposites through the sol-gel reaction of the

corresponding oligomer in the presence of TiO₂ nanoparticles under alkaline conditions (see Scheme 8).³⁵⁾ These fluorinated composites thus obtained were nanometre size-controlled fine particles, and exhibited good dispersibility and stability in traditional organic solvents except for water.³⁵⁾



Scheme 8 Preparation of R_F-(VM-SiO₂)_n-R_F/TiO₂ Nanocomposites.³⁵⁾

The modified glass surface treated with R_F-(VM-SiO₂)_n-R_F/anatase TiO₂ nanocomposites can exhibit not only a superhydrophobic characteristic but also a good oleophobicity imparted by fluoroalkyl segments in the composites.³⁵⁾ Very interestingly, it has been reported that the wettability for water can be switched between superhydrophobicity and superhydrophilicity by alternation of ultraviolet (UV) irradiation and dark storage while keeping a good oleophobicity on the modified surface treated with these nanocomposites.³⁵⁾

It is well known that transition metal oxides exhibit photoinduced hydrophilicity and UV-driven reversible switching behaviors between superhydrophobicity and

superhydrophilicity.³⁶⁾ However, there are no reports related to such switching behaviour with a good oleophobic characteristic so far. From this point of view, $R_F-(VM-SiO_2)_n-R_F$ /anatase TiO_2 nanocomposites are interesting functional materials, which can exhibit the photoinduced hydrophilicity while keeping a good oleophobicity imparted by fluorine.^{8, 35)}

Poly(vinylidene fluoride)/poly(methyl methacrylate) grafted TiO_2 composite nanofibrous membrane as polymer electrolyte for lithium-ion batteries has been recently fabricated by electrospinning method.³⁷⁾ This composite nanofibrous membrane was proven to be a good absorbent for the liquid electrolyte, and it exhibits a high electrolyte uptake and a high electrolyte retention ratio.

Although fluorinated polymers possess so many excellent properties, the low thermal stability of anatase titanium oxide limits the application of these nanocomposites. Usually, anatase titanium oxide transforms into rutile phase when the temperature is above 600 °C, which may result in the decrease of photocatalytic ability of titanium oxide.³⁸⁾ In order to take good advantages of anatase titanium dioxide for its application in various environments, a great effort should be made to improve the thermal stability of anatase titanium oxide at such higher temperatures.

In fact, many research works have been performed to overcome the phase transformation from anatase to rutile at higher temperatures. For example, Lv et al. synthesized $TiOF_2$ by a

simple microwave-assisted hydrothermal route using tetrabutyl titanate and hydrofluoric acid as raw materials.³⁹⁾ The prepared anatase TiO_2 from TiOF_2 shows very high thermal stability and the phase transformation temperature from anatase to rutile is up to 1000 °C. The high thermal stability and the photocatalytic enhancement of catalysts were attributed to the adsorbed fluoride ion on the surface of anatase after calcination.³⁹⁾

5. Silica/titanium oxide nanocomposites

Not only fluorinated titanium oxide composites, but also silica nanoparticles have been applied to the preparation of titanium oxide nanocomposites, exhibiting higher photocatalytic activity and thermal stability compared with that of the parent TiO_2 nanoparticles.⁴⁰⁾

The higher thermal stability of silica/titanium oxide composites is due to the surrounding silica phase through the Ti-O-Si bonds.⁴¹⁾ The silica lattice locks the Ti-O species at the interface of the TiO_2 domains, preventing the nucleation that is necessary for the phase transformation to rutile.⁴¹⁾

The Ti-O-Si bonds strongly modify the electronic structure of the Ti atoms in silica/titanium oxide composites.⁴²⁾ The effective positive charge on the Ti atoms increased due to the surrounding Si (IV) with a higher electronegativity.⁴²⁾ Thus, the electron-accepting ability of Ti (IV) in Ti-O-Si bonds is higher than in Ti-O-Ti bonds, which is effective for the

electron-hole separation, as shown in Fig. 7.⁴²⁾ Compared with the photocatalytic process over pure titanium oxide (see Fig. 4), the silica/titanium oxide composites can inhibit the recombination of photogenerated electrons and holes, resulting in higher photocatalytic activity.⁴²⁾

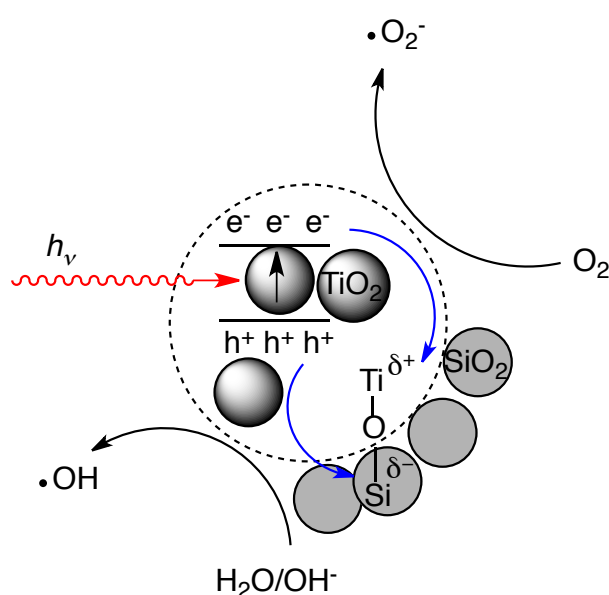
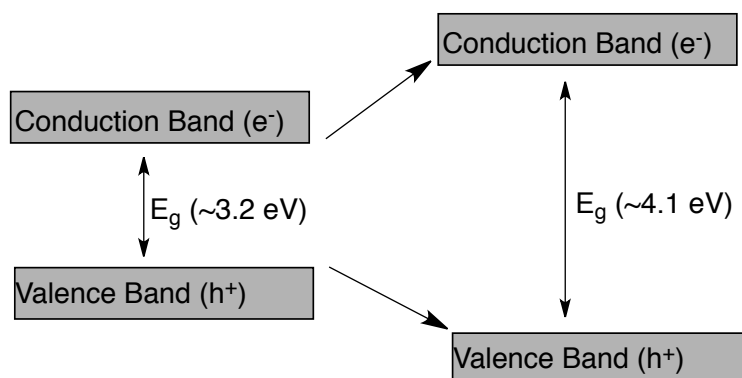


Fig. 7 Proposed mechanism for the efficient electron-hole separation on the silica/titanium oxide nanocomposites.⁴²⁾

In addition, the band gap enlarged through lowering the valence band edge and elevating the conduction band edge (see Scheme 9).⁴²⁾ The oxidizing potential of the photogenerated holes and the reducing potential of the photogenerated electrons will increase with increasing band gap.⁴²⁾ Therefore, the silica/titanium oxide composites possess high photooxidation and photoreduction abilities.⁴²⁾



Scheme 9 Enlarged band gap (~ 4.1 eV) of silica/titanium oxide nanocomposites compared with that of anatase TiO_2 nanoparticles (~ 3.2 eV).⁴²⁾

Such silica-coated TiO_2 nanocomposites can be prepared by a simple catalytic hydrolysis method.⁴³⁾ The enhanced photocatalytic behavior of these nanocomposites should be observed.⁴³⁾ Not only the lower recombination rate of photogenerated electrons and holes resulted from the interaction between silica and titanium oxide, but also the increased adsorption of organic materials by silica are contributed to the higher photocatalytic ability of silica/titanium oxide nanocomposites.⁴³⁾

Besides the enhanced photocatalytic activity of silica/titanium oxide nanocomposites, silica also endows titanium oxide with molecular selective photocatalysis by incorporation of TiO_2 nanoparticles into mesoporous silica (see Figure 8).⁴⁴⁾ The molecular selectivity of

mesoporous silica/titanium oxide nanocomposites can be tuned by controlling the pore diameter of mesoporous silica.⁴⁴⁾

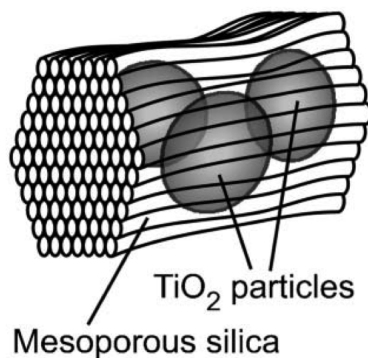


Fig. 8 Schematic illustration of the mesoporous silica/titanium oxide nanocomposites.⁴⁴⁾

Silica/titanium oxide composites also have great potential in commercial applications for self-cleaning coatings.⁴⁵⁾ These nanocomposites are able to adhere firmly on the surface of stone or cotton textile, improving the mechanical resistance of the coatings and giving hydrophobic properties to the coatings.⁴⁵⁾

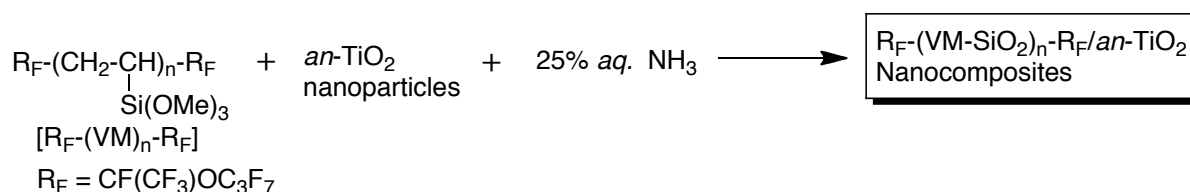
6. Thesis outline

Fluorinated polymers, especially fluoroalkyl end-capped oligomers are very convenient and effective tool for the preparation of titanium oxide based nanocomposites due to their unique properties such as good solubility in water and organic solvents, high surface modification ability, and the ability to form nanometer size controlled molecular aggregates, which can not be achieved by the corresponding non-fluorinated ones. The sol-gel reactions of

fluorinated polymers in the presence of alkyl silanes and silica nanoparticles under alkaline conditions would generate HF molecules, offering fluorine source for F-TiO₂ with enhanced photocatalytic activity and thermal stability. In addition, silica doped titanium oxide also should possess an enhanced photocatalytic activity and thermal stability without phase transformation from anatase to rutile at higher temperatures, due to the formation of Ti-O-Si bond. From this point of view, it is of great interest to explore novel fluorinated polymers/silica/titanium oxide nanocomposites.

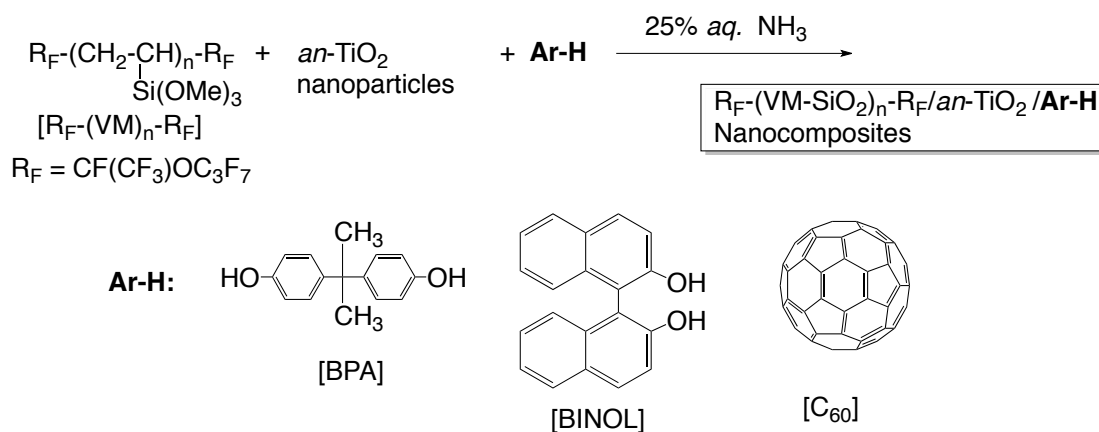
In this study, a variety of fluorinated polymers including low molecular weight fluorinated compounds/silica/titanium oxide nanocomposites are prepared, and their not only photocatalytic activity but also thermal stability are investigated.

In chapter 1, fluoroalkyl end-capped vinyltrimethoxysilane oligomer/anatase titanium oxide nanocomposites keeping anatase structure and possessing a higher photocatalytic activity even after calcination at 1000 ° are described (see Scheme 10).



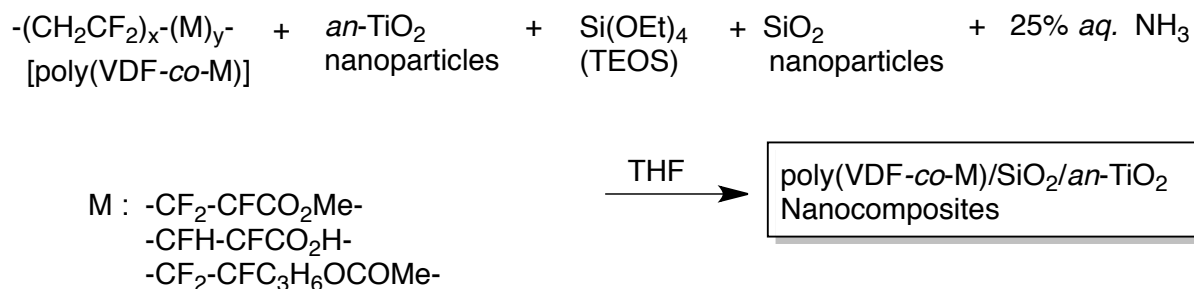
Scheme 10 Preparation of R_F-(VM-SiO₂)_n-R_F/an-TiO₂ Nanocomposites

In chapter 2, fluoroalkyl end-capped vinyltrimethoxysilane oligomer/anatase titanium oxide nanocomposites - encapsulated low molecular weight aromatic compounds such as bisphenol A [BPA], 1,1'-bi(2-naphthol) [BINOL], and fullerene are described (see Scheme 11), including their higher photocatalytic activity and nonflammable characteristics related to the encapsulated BPA, BINOL and fullerene in the nanocomposite cores.



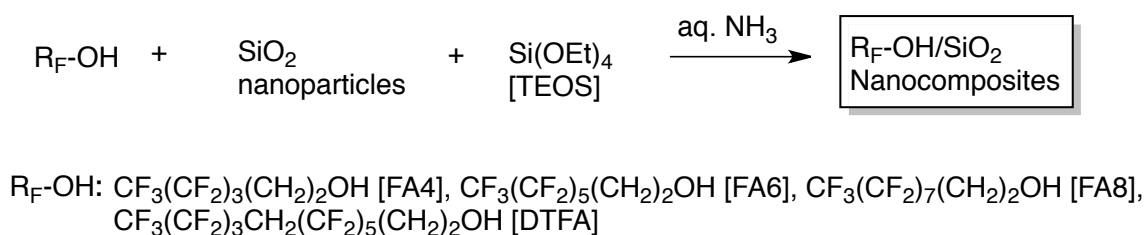
Scheme 11 Preparation of $\text{R}_F\text{-(VM-SiO}_2\text{)}_n\text{-R}_F/\text{an-TiO}_2/\text{Ar-H}$ nanocomposites

In chapter 3, preparation and photocatalytic activity of poly(vinylidene fluoride copolymers)/silica/anatase titanium oxide nanocomposites (see Scheme 12) are described.

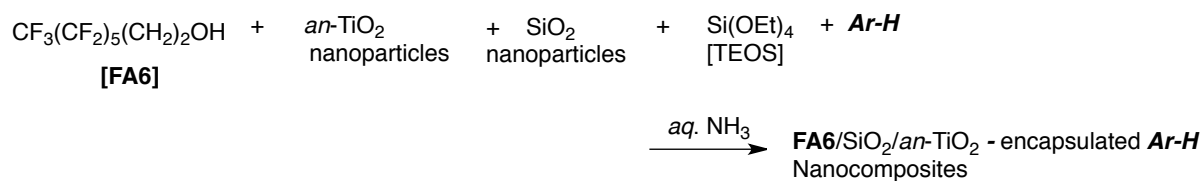
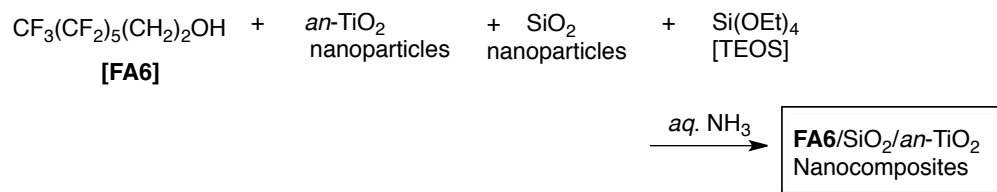


Scheme 12 Preparation of poly(VDF-co-M)/SiO₂/an-TiO₂ nanocomposites.

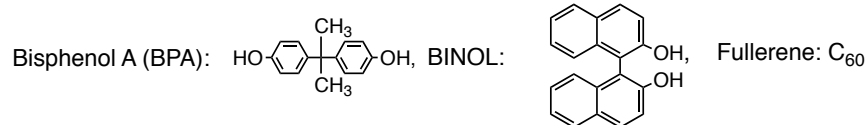
In chapter 4, a variety of fluorinated aliphatic alcohols/silica nanocomposites (see scheme 13), fluorinated aliphatic alcohol (FA6)/silica/anatase titanium oxide nanocomposites, and the encapsulation of low molecular weight aromatic compounds such as BPA, BINOL, and fullerene into these fluorinated silica/anatase titanium oxide nanocomposite cores (see Scheme 14) are described.



Scheme 13 Preparation of R_F-OH/SiO₂ nanocomposites



Ar-H: bisphenol A; BINOL, Fullerene



Scheme 14 Preparation of FA6/SiO₂/an-TiO₂ nanocomposites and FA6/SiO₂/an-TiO₂ - encapsulated Ar-H nanocomposites.

Reference

- 1) a) S. C. Sharma, H. Kunieda, J. Esquena, C. R. Abreu, *J. Colloid Interface Sci.*, **299**, 297 (2006);
b) X. Yu, A. Roy, S. Dunn, A. S. Badami, J. Yang, A. S. Good, and J. E. McGrath, *J. Polym. Sci. Part A: Polym. Chem.*, **47**, 1038 (2009);
c) K. Tanaka, M. Kogoma, and Y. Ogawa, *Thin Solid Films*, **506-507**, 159 (2006).
- 2) L. Pauling, “*The Nature of the Chemical Bond and the Structure of Molecules and Crystals: An Introduction to Modern Structural Chemistry*”, Cornell University Press, New York (1960).
- 3) W. R. Dolbier Jr., *J. Fluorine Chem.*, **126**, 157 (2005).
- 4) a) J. J. Reisinger and M. A. Hillmyer, *Prog. Polym. Sci.*, **27**, 971 (2002);
b) T. Imae, *Curr. Opin. Colloid Interface Sci.*, **8**, 307 (2003);
c) B. Stadlober, M. Zirkel, M. Beutl, and G. Leising, *Appl. Phys. Lett.*, **86**, 242902 (2005);
d) K. Tanaka, T. Inomata, and M. Kogoma, *Thin Solid Films*, **386**, 217 (2001);
e) L. Andruzzi, A. Hexemer, X. Li, C. K. Ober, E. J. Kramer, G. Galli, E. Chiellini, and D. A. Fischer, *Langmuir*, **20**, 10498 (2004).

- 5) D. F. Persico and R. J. Lagow, *J. Polym. Sci. Part A: Polym. Chem.*, **29**, 233 (1991).
- 6) H. Miyake, Y. Sugaya, and M. Yamabe, *J. Fluorine Chem.*, **92**, 137 (1998).
- 7) a) H. Sawada, K. Ikeno, and T. Kawase, *Macromolecules*, **35**, 4306 (2002);
- b) M. O. Hunt, Jr., A. M. Belu, R. W. Linton, and J. M. Desimone, *Macromolecules*, **26**, 4854 (1993);
- c) J. Wang, G. Mao, C. K. Ober, and E. Kramer, *J. Polym. Prepr. (Am. Chem. Soc., Div. Polym. Chem.)*, **38**, 953 (1997);
- d) J. F. Elman, B. D. Johs, T. E. Long, and J. T. Koberstein, *Macromolecules*, **27**, 5341 (1994);
- e) M. A. Hillmyer and T. P. Lodge, *J. Polym. Sci. Part A: Polym. Chem.*, **40**, 1 (2002);
- f) S. Affrossman, P. Bertrand, M. Hartshorne, T. Kiff, D. Leonard, R. A. Pethrick, and R. W. Richards, *Macromolecules*, **29**, 5432 (1996).
- 8) a) H. Sawada, T. Narumi, A. Kajiwara, K. Ueno, and K. Hamazaki, *Colloid Polym. Sci.*, **284**, 551(2006);
- b) H. Sawasa, *Polym. Chem.*, **3**, 46 (2012).
- 9) H. Sawada, Y. Minoshima, and H. Nakajima, *J. Fluorine Chem.*, **65**, 169 (1993).
- 10) a) H. Sawada, K. Tanba, N. Itoh, C. Hosoi, M. Oue, M. Baba, T. Kawase, M. Mitani, and H. Nakajima, *J. Fluorine Chem.*, **77**, 51 (1996);

- b) H. Sawada, *Prog. Polym. Sci.*, **32**, 509 (2007).
- 11) a) P. Gomez-Romero, *Adv. Mater.*, **13**, 163 (2001);
- b) A. P. Wight and M. E. Davis, *Chem. Rev.*, **102**, 3589 (2002);
- c) Y. H. Han, A. Taylor, M. D. Mantle, and K. M. Knowles, *J. Non-Cryst. Solids*, **353**, 313 (2007);
- d) A. Maurya and P. Chauhan, *Polym. Bull.*, **68**, 961 (2012).
- 12) T. He, Z. Zhou, W. Xu, F. Ren, H. Ma, and J. Wang, *Polymer*, **50**, 3031 (2009).
- 13) H. Yang, X. Hu, R. Chen, S. Liu, P. Pi, and Z. Yang, *Appl. Surf. Sci.*, **280**, 113 (2013).
- 14) M. Srivastava, B. B. J. Basu, and K. S. Rajam, *J. Nanotechnol.*, 1 (2011).
- 15) H. Sawada, S. Sekiguchi, H. Kakehi, T. Mori, M. Miura, and N. Isu, *J. Compos. Mater.*, **43**, 3291 (2009).
- 16) H. Takashima, K. Iwaki, K. Takishita, and H. Sawada, *Polym. Adv. Technol.*, **20**, 887 (2009).
- 17) M. Mugisawa and H. Sawada, *Langmuir*, **24**, 9215 (2008).
- 18) a) H. Sawada, R. Furukuwa, K. Sasazawa, K. Toriba, K. Ueno, and K. Hamazaki, *J. Appl. Polym. Sci.*, **100**, 1328 (2006);
- b) H. Sawada, R. Furukuwa, K. Sasazawa, M. Mugisawa, and K. Ohnishi, *Eur. Polym. J.*, **43**, 3258 (2007).

- 19) a) H. Sawada, T. Narumi, S. Kodama, M. Kamijo, R. Ebara, M. Sugiya, and Y. Iwasaki, *Colloid Polym. Sci.*, **285**, 977 (2007);
- b) H. Sawada, T. Tashima, H. Kakehi, Y. Nishiyama, M. Kikuchi, M. Miura, Y. Sato, and N. Isu, *Polym. J.*, **42**, 167 (2010);
- c) H. Sawada, H. Kakehi, T. Tashima, Y. Nishiyama, M. Miura, and N. Isu, *J. Appl. Polym. Sci.*, **112**, 3482 (2009).
- 20) K. Sasazawa, Y. Hirayama and H. Sawada, *Polym. Int.*, **58**, 177(2009).
- 21) H. Sawada, A. Sasaki, K. Sasazawa, K. Toriba, H. Kakehi, M. Miura, and N. Isu, *Polym. Adv. Technol.*, **19**, 419 (2008).
- 22) A. Fujishima and K. Honda. *Nature*, **238**, 37 (1972).
- 23) G. S. Mitall and T. Manoj, *Chinese Sci. Bulletin*, **56**, 1639 (2011).
- 24) J. Augustynski, *J. Electrochim. Acta.*, **38**, 43 (1993).
- 25) S. T. Martin, C. L Morrison, and M. R. Hoffmann, *J. Phys. Chem.*, **98**, 13695 (1994).
- 26) R. Thiruvengkatachari, S. Vigneswaran, and II S. Moon. *Korean J. Chem. Eng.*, **25**, 64 (2008).
- 27) N. Xu, Z. Shi, Y. Fan, J. Dong, J. Shi, and M. Z. C. Hu, *Ind. Eng. Chem. Res.*, **38**, 373 (1999).
- 28) a) A. L. Linsebigler, G. Lu, and J. T. Y. Jr., *Chem. Rev.*, **95**, 735 (1995);

- b) J. M. Herrmann, *Catal. Today*, **53**, 115 (1999);
- c) W. Wang, J. Zhang, F. Chen, D. He, and M. Anpo, *J. Colloid Interface Sci.*, **323**, 182 (2008).
- 29) a) G. Liu, H. G. Yang, X. Wang, L. Cheng, J. Pan, G. Q. (Max) Lu, and H. M. Cheng, *J. Am. Chem. Soc.*, **131**, 12868 (2009);
- b) R. Asahi, T. Morikawa, T. Ohwaki, K. Aoki, and Y. Taga, *Science*, **293**, 269 (2001);
- c) T. Ihara, M. Miyoshi, Y. Triyama, O. Marumato, and S. Sugihara, *Appl. Catal. B*, **42**, 403 (2003);
- d) Y. Xu, K. Lv, Z. Xiong, W. Leng, W. Du, D. Liu, and X. Xue, *J. Phys. Chem. C*, **111**, 19024 (2007);
- e) J. Pan, G. Liu, G. Q. (Max) Lu, and H. M. Cheng, *Angew. Chem. Int. Ed.*, **50**, 2133 (2011).
- 30) a) W. Ho, J. C. Yu, and S. Lee. *Chem. Commun.*, 1115 (2006);
- b) J. K. Zhou, L. Lv, J. Yu, H. L. Li, P. Z. Guo, H. Sun, and X. S. Zhao, *J. Phys. Chem. C*, **112**, 5316 (2008);
- c) D. Zhang, G. Li, X. Yang, and J. C. Yu, *Chem. Commun.*, 4381 (2009);
- d) D. Huang, S. Liao, S. Quan, L. Liu, Z. He, J. Wan, and W. Zhou, *J. Mater. Sci.*, **42**, 8193 (2007).

- 31) J. Yu, W. Wang, B. Cheng, and B. L. Su, *J. Phys. Chem. C*, **113**, 6743 (2009).
- 32) G. Wu, J. Wang, D. F. Thomas, and A. Chen, *Langmuir*, **24**, 3503 (2008).
- 33) M. Senna, A. Duvel, V. Sepelak, J. Shi, K. L. D. Silva, V. Laporte, S. Lebedkin, C. Kubel, D. Wang, D. Schunemann, K. D. Becker, and P. Heitjans, *J. Phys. Chem. C*, **117**, 15272 (2013).
- 34) H. Sawada, E. Sawada, H. Kakehi, T. Kariya, M. Mugisawa, Y. Chounan, M. Miura, and N. Isu, *Polym. Compos.*, **30**, 1848 (2009).
- 35) E. Sawada, H. Kakehi, Y. Chounan, M. Miura, Y. Sato, N. Isu, and H. Sawada, *Composites Part B*, **41**, 498 (2010).
- 36) a) R. Wang, K. Hashimoto, A. Fujishima, M. Chikuni, E. Kojima, A. Kitamura, M. Shimohigoshi, and T. Watanabe, *Adv. Mater.*, **10**, 135 (1998);
- b) X. Feng, L. Feng, M. Jin, J. Zhai, L. Jiang, and D. Zhu, *J. Am. Chem. Soc.*, **126**, 62 (2004);
- c) H. S. Lim, D. Kwak, D. Y. Lee, S. G. Lee, and K. Cho, *J. Am. Chem. Soc.*, **129**, 4128 (2007);
- d) B. Yan, J. Tao, C. Pamg, Z. Zheng, Z. Shen, C. H. A. Huan, and T. Yu, *Langmuir*, **24**, 10569 (2008);
- e) S. Wang, X. Feng, J. Yao, and L. Jiang, *Angew. Chem., Int. Ed.*, **45**, 1264 (2006).

- 37) W. Cui, D. Tang, and Z. Gong, *J. Power Sources*, **223**, 206 (2013).
- 38) a) X. Peng and A. Chen, *Adv. Funct. Mater.*, **16**, 1355 (2006);
- b) N. Wetchakun, B. Incessungvorn, K. Wetchakun, and S. Phanichphant, *Mater. Lett.*, **82**, 195 (2012);
- c) Q. Gao, X. Wu, and Y. Fan, *Dyes Pigments*, **95**, 96 (2012);
- d) K. Elghniji, J. Soro, S. Rossignol, and M. Ksibi, *J. Taiwan Inst. Chem. E.*, **43**, 132 (2012).
- 39) K. Lv, J. Yu, L. Cui, S. Chen, and M. Li, *J. Alloys Compd.*, **509**, 4557 (2011).
- 40) a) C. Anderson and A. J. Bard, *J. Phys. Chem. C*, **99**, 9882 (1995);
- b) X. Fu, L. A. Clark, Q. Yang, and M. A. Anderson, *Environ. Sci. Technol.*, **30**, 647 (1996);
- c) K. Okada, N. Yamamoto, Y. Kameshima, A. Yasumori, and K. J. D. MacKenzie, *J. Am. Ceram. Soc.*, **84**, 1591 (2001);
- d) L. Sikong and P. Masom, *Adv. Mater. Res.*, **602-604**, 139 (2013).
- 41) a) A. Hilonga, J. K. Kim, P. B. Sarawade, and H. T. Kim, *J. Mater. Sci.*, **45**, 1255 (2010);
- b) A. Hilonga, J. K. Kim, P. B. Sarawade, and H. T. Kim, *J. Mater. Sci.*, **45**, 1264 (2010).
- 42) a) X. Gao and I. E. Wachs, *Catalysis Today*, **51**, 233 (1999);
- b) N. Seriani, C. Pinilla, S. Cereda, A. D. Vita, and S. Scandolo, *J. Phys. Chem. C*, **116**,

11062 (2012).

43) S. Hu, F. Li, and Z. Fan, *Bull. Korean Chem. Soc.*, **33**, 1895 (2012).

44) K. Inumaru, T. Kasahara, M. Yasui, and S. Yamanaka, *Chem. Commun.*, 2131 (2005).

45) a) L. Pinho and J. Mosquera, *J. Phys. Chem. C*, **115**, 22851 (2011);

b) K. Qi, X. Chen, Y. Liu, J. H. Xin, C. L. Mark, and W. A. Daoud, *J. Mater. Chem.*, **17**, 3504 (2007).

CHAPTER 1

Fluoroalkyl End-capped Vinyltrimethoxysilane Oligomer/Anatase Titanium Oxide Nanocomposites Possessing Photocatalytic Activity even after Calcination at 1000 °C

1.1. Introduction

There has been great interest in titanium oxide (TiO_2) due to its attraction for not only the most important white pigment in the plastic industry and cosmetic materials, but also the extensive applications in a wide variety of fields such as photocatalyst, chemical sensor and energy conversions.¹⁾ Titanium oxide occurs as two important polymorphs, the stable rutile and metastable anatase.²⁾ Titanium oxide having the anatase structure is one of the most important semiconductors, playing a central role in many applications such as photovoltaic cells, photo/electrochromics, photocatalysis, and smart surface coatings.³⁾ It is well-known that anatase transforms irreversibly to rutile at elevated temperatures.⁴⁾ Normally, the phase transformation temperature in air from anatase to rutile titanium oxide is between 600 and 750 °C.⁵⁾ From an applicable viewpoint of anatase titanium oxide into a variety of fields, it is deeply desirable to develop thermally stable anatase titanium oxide composites without the phase transformation to rutile under such higher temperature conditions. In fact, titania-silica composites have been prepared by the sol-gel reaction of titanium oxychloride and sodium silicate in the presence of surfactants such as cetyltrimethylammonium bromide.⁶⁾ This titanium-silica composite shows that the rutile phase appears at a calcination temperature of 1000 °C; however, this composite can keep anatase structure around 600 ~ 900 °C. ⁶⁾ On the

other hand, during the comprehensive studies on the fluoroalkyl end-capped oligomeric nanocomposites⁷⁾, fluoroalkyl end-capped vinyltrimethoxysilane oligomer has been recently reported to be a convenient tool for the preparation of the expected fluorinated oligomer/titanium oxide nanocomposites.⁸⁾ In addition, these nanocomposites were applied to the surface modification of glass to exhibit not only a completely superhydrophobic characteristic with a non-wetting property against water droplets but also a good oleophobicity on their surface.⁸⁾ Especially, the wettability for water can be switched between superhydrophobicity and superhydrophilicity by alternation of ultraviolet (UV) irradiation and dark storage with keeping a good oleophobicity on the modified surface treated with these anatase titanium oxide nanocomposite.⁸⁾ This chapter shows that fluoroalkyl end-capped vinyltrimethoxysilane oligomer/anatase titanium oxide nanocomposites $[R_F-(VM-SiO_2)_n-R_F/an-TiO_2]$ can keep completely its structure without phase transformation to rutile even after calcination at 1000 °C, and $R_F-(VM-SiO_2)_n-R_F/an-TiO_2$ nanocomposite after calcination can exhibit the same photocatalytic activity as that before calcination.

1.2. Experimental

1.2.1 Measurements

Molecular weight was measured using a Shodex DS-4 (pump, Tokyo, Japan) and Shodex RI-71 (detector) gel permeation chromatography (GPC) calibrated with polystyrene standard using tetrahydrofuran (THF) as the eluent. Dynamic light-scattering (DLS) measurements were measured using Otsuka Electronics DLS-7000 HL (Tokyo, Japan). Ultraviolet-visible (UV-vis) spectra were measured using Shimadzu UV-1600 UV-vis spectrophotometer (Kyoto, Japan). Field emission scanning electron micrographs (FE-SEM) and energy dispersive X-ray (EDX) spectra were obtained using JEOL JSM-7000F (Tokyo, Japan). X-ray diffraction (XRD) measurements were performed by the use of Mac Science M18XHF-SRA (Tokyo, Japan).

1.2.2. Materials

Titanium oxide nanoparticles (average particle size: 20 nm) were received from Ishihara Sangyo Kaisha Ltd. (Osaka, Japan). Fluoroalkyl end-capped vinyltrimethoxysilane oligomer

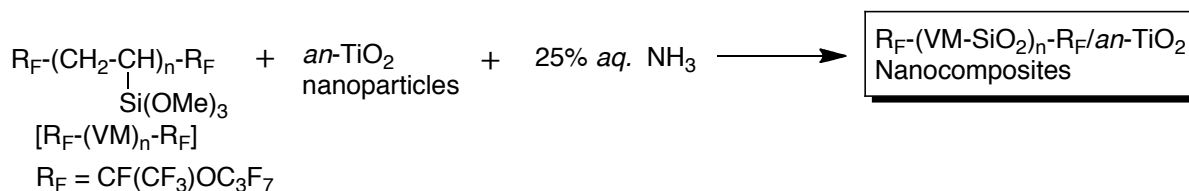
was prepared by reaction of fluoroalkanoyl peroxide with the corresponding monomer according to the previously reported method.⁹⁾

1.2.3. Preparation of fluoroalkyl end-capped vinyltrimethoxysilane oligomer/anatase titanium oxide nanocomposites

A typical procedure for the preparation of fluorinated oligomer/anatase titanium oxide nanocomposites is as follows: to a tetrahydrofuran (THF) solution (20 ml) of fluoroalkyl end-capped vinyltrimethoxysilane oligomer: $R_F-[CH_2CHSi(OMe)_3]_n-R_F$ [$R_F-(VM)_n-R_F$]; $R_F = CF(CF_3)OC_3F_7$; $M_n = 1030, 400$ mg] were added anatase TiO_2 nanoparticles [*an*- TiO_2 : 500 mg) and 25 % aqueous ammonia solution (0.25 ml). The mixture was stirred with a magnetic stirring bar at room temperature for 2 hr, and then was centrifuged for 30 min. The expected fluorinated TiO_2 nanocomposites were easily separated from the THF solution. THF (20 ml) was added to the obtained crude product. The THF solution was stirred with magnetic stirring bar at room temperature for 1 day. After centrifugal separation of this solution, the obtained product was dried in vacuum at 50 °C for 2 days to produce purified fluorinated composite white colored powders (549 mg).

1.3. Results and discussion

Fluoroalkyl end-capped vinyltrimethoxysilane oligomer/*an*-TiO₂ nanocomposites were prepared by the sol-gel reactions of the corresponding oligomer [R_F-(VM)_n-R_F] in the presence of anatase titanium oxide nanoparticles in tetrahydrofuran (THF) under alkaline conditions according to the previously reported method (see Scheme 2-1 and Table 2-1).^{8-b)}



Scheme 1-1 Preparation of R_F-(VM-SiO₂)_n-R_F/*an*-TiO₂ Nanocomposites.

Table 1-1 Preparation of R_F-(VM-SiO₂)_n-R_F/*an*-TiO₂ nanocomposites.

Run	R _F -(VM) _n -R _F (mg)	<i>an</i> -TiO ₂ ^{b)} (mg)	aq. NH ₃ (ml)	Product yield ^{a)} (%)	Size of composites ^{b)} (after calcination) (nm) ± STD
1	400	100	0.25	67	48.5 ± 8.7 (11.5 ± 0.7)
2	400	250	0.25	71	30.6 ± 5.4 (33.1 ± 7.4)
3	400	400	0.25	76	71.0 ± 19.5 (27.2 ± 8.6)
4	400	500	0.25	61	10.8 ± 1.7 (68.3 ± 31.3)
5	400	600	0.25	77	30.0 ± 5.2 (28.1 ± 4.9)
6	400	800	0.25	76	85.4 ± 30.1 (11.2 ± 1.6)
7	400	900	0.25	79	20.9 ± 5.0 (29.3 ± 3.9)
8	400	1000	0.25	71	20.3 ± 4.9 (11.7 ± 1.1)

a) Yield based on R_F-(VM)_n-R_F and TiO₂

b) Determined by DLS (dynamic light scattering) measurements in methanol solutions.

$R_F-(VM-SiO_2)_n-R_F/an-TiO_2$ nanocomposites thus obtained can exhibit not only good dispersibility and stability in traditional organic solvents such as 1,2-dichloroethane, chloroform, THF, methanol, ethanol, and 2-propanol, ethyl acetate, acetone, dimethyl sulfoxide, and *N,N*-dimethylformamide but also a relatively good dispersibility in water. Thus, we have measured the size of $R_F-(VM-SiO_2)_n-R_F/an-TiO_2$ composites before and after calcination at 1000 °C in methanol by dynamic light-scattering (DLS) measurements at 25 °C. Each size of these obtained fluorinated TiO_2 composites before and after calcination is nanometer size-controlled fine particles: 11 ~ 85 nm and 11 ~ 68 nm (number-average diameter), respectively.

The field-emission scanning electron micrograph (FE-SEM) of well-dispersed methanol solutions of nanocomposites (Run 4 in Table 1-1) has been measured before and after calcination at 1000 °C, and the results were shown in Fig. 1-1.

Electron micrographs of the nanocomposites before and after calcination at 1000 °C showed the formation of composite fine particles with a mean diameter of 77 nm and 75 nm, respectively, and it was demonstrated that the appearance of white colored nanocomposite powders did not change at all before and after calcination at 1000 °C. The difference in the average sizes determined by DLS (Run 4 before calcination in Table 1-1) and FE-SEM would be due to the coagulation or agglomeration of the nanocomposites particles during sample

preparation for FE-SEM measurements.

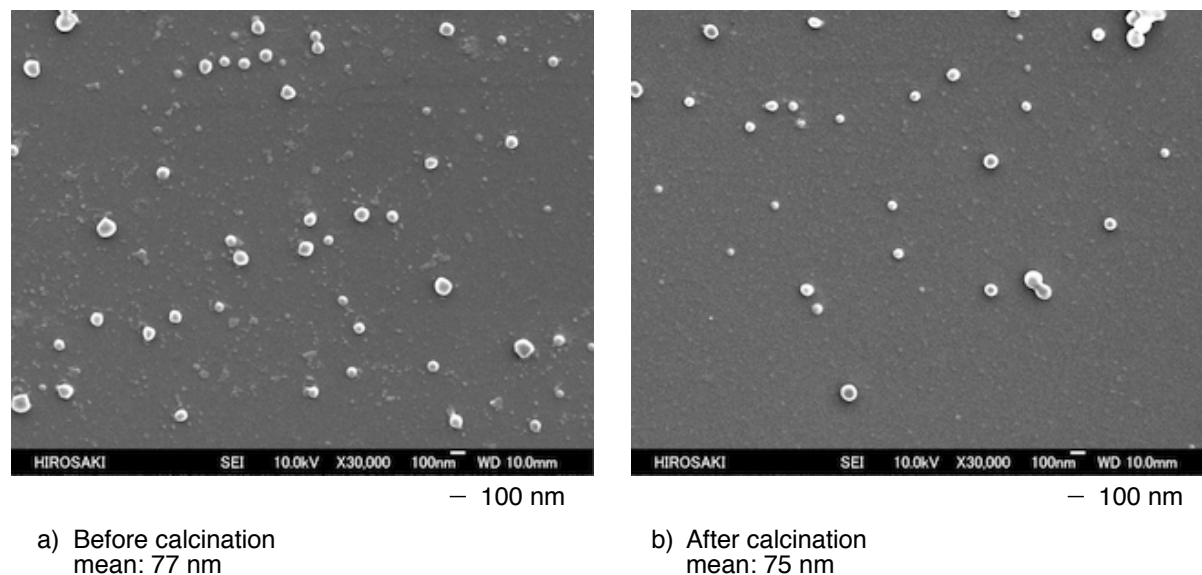


Fig. 1-1 FE-SEM (Feild Emission-Scanning Electron Microscopy) images of methanol solutions of $R_F-(VM-SiO_2)_n-R_F/an-TiO_2$ nanocomposites (Run 4 in Table 1) before and after calcination at 1000 °C.

Fig. 1-2 shows separately the XRD spectra of $R_F-(VM-SiO_2)_n-R_F/an-TiO_2$ nanocomposites (Run 4 in Table 1-1) before and after calcination at 1000 °C. The XRD spectra of parent *an*-TiO₂ nanoparticles were also demonstrated in Fig. 1-2, for comparison. The characteristic peaks of the nanocomposites before and after calcination were completely agreement with those of the parent *an*-TiO₂ particles.

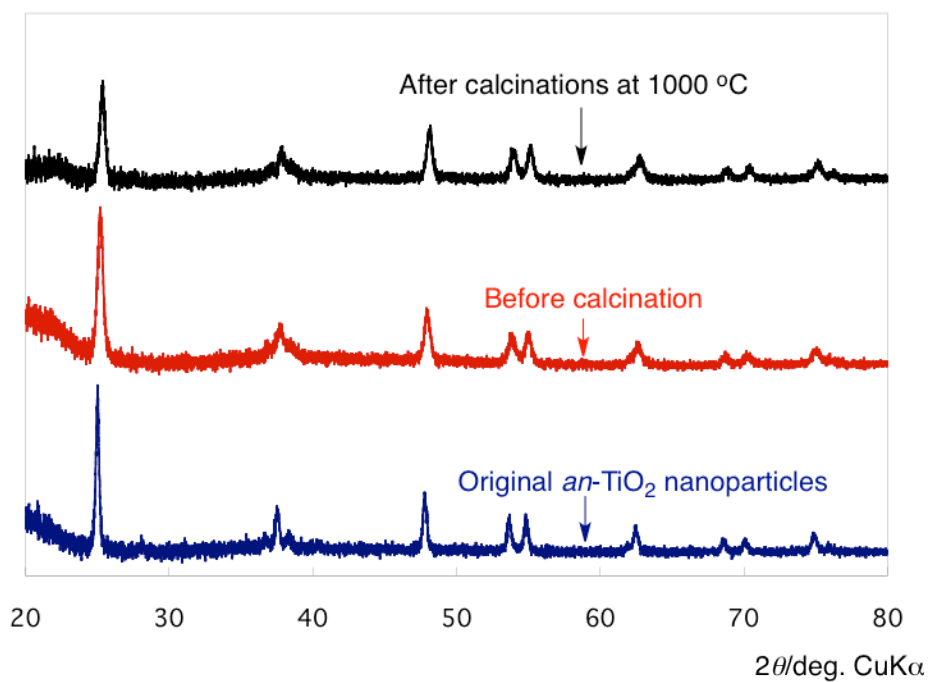


Fig. 1-2 X-ray diffraction patterns of original an-TiO_2 nanoparticles and $\text{R}_\text{F}-(\text{VM-SiO}_2)_n-\text{R}_\text{F}/\text{an-TiO}_2$ nanocomposites before and after calcinations at 1000 °C.

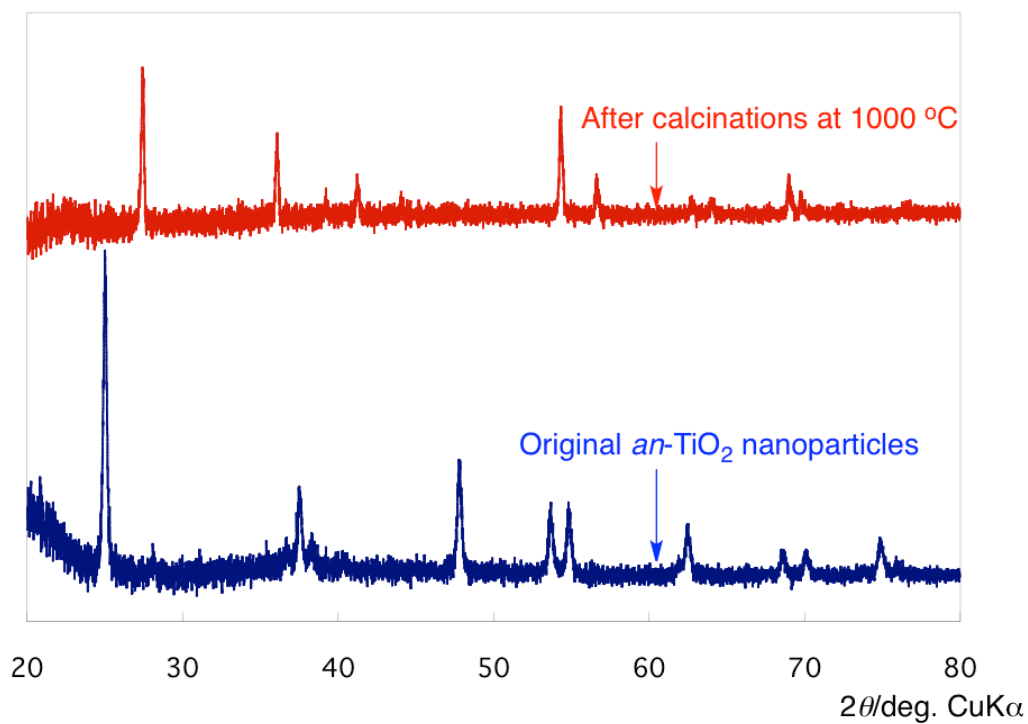


Fig. 1-3 X-ray diffraction patterns of original an-TiO_2 nanoparticles before and after calcinations at 1000 °C.

Other nanocomposites before and after calcination at 1000 °C shown in Table 1-1 were found to exhibit the same XRD characteristic peaks as that of anatase structure. In contrast, parent *an*-TiO₂ nanoparticles suffered a complete phase transformation to rutile under similar calcination conditions (see Fig. 1-3). These findings suggest that R_F-(VM-SiO₂)_n-R_F oligomeric nanocomposite lattice locks the Ti-O species at the interface of the TiO₂ domains, preventing the nucleation that is necessary for the phase transformation to rutile at 1000 °C.

In order to clarify the presence of *an*-TiO₂ in the present R_F-(VM-SiO₂)_n-R_F/*an*-TiO₂ nanocomposites after calcination at 1000 °C, the photocatalytic activity of R_F-(VM-SiO₂)_n-R_F/*an*-TiO₂ nanocomposites before and after calcination at 1000 °C was evaluated in terms of the decolorization of methylene blue dye (MB) under UV light irradiation. The residual amounts of MB were estimated by the decrease of the absorbance at λ_{max} : 652 nm related to MB by UV light irradiation, and the results were shown in Fig. 1-4.

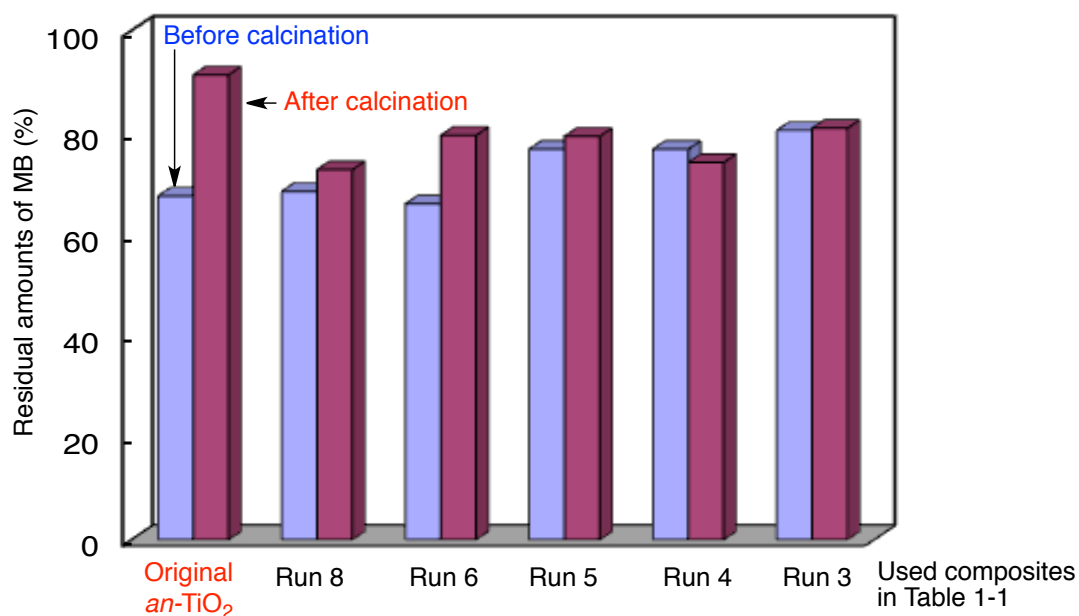


Fig. 1-4 Photo-decolorization of MB in aqueous solutions of $R_F-(VM-SiO_2)_n-R_F/an-TiO_2$ nanocomposites before and after calcination at 1000 °C shown in Table 1-1.

Concentration of $R_F-(VM-SiO_2)_n-R_F/an-TiO_2$ composites (or parent *an*-TiO₂ nanoparticles): 25 mg/dm³

Concentration of MB : 2.5 mg/dm³

UV irradiation (λ_{max} : 365 nm) time: 1 min

As shown in Fig. 1-4, original *an*-TiO₂ nanoparticles exhibit a photocatalytic activity toward MB, although the corresponding original TiO₂ nanoparticles with complete phase transformation to rutile after calcination at 1000 °C (see Fig. 1-3) exhibit no photocatalytic activity under similar conditions. However, interestingly, the $R_F-(VM-SiO_2)_n-R_F/an-TiO_2$ nanocomposites, which were prepared under a variety of feed ratios as shown in Table 1-1, were found to exhibit a good photocatalytic activity for the decolorization of MB before and after calcination at 1000 °C, as well as those of original *an*-TiO₂ nanoparticles. The contents of Ti, O, Si, C, and F in the $R_F-(VM-SiO_2)_n-R_F/an-TiO_2$ nanocomposite (Run 4 in Table 1-1) before calcination were estimated to be 19.0, 62.2, 1.3, 15.1, and 2.4 %, respectively, by the

use of EDX (Energy Dispersive X-ray) spectra measurements. Thus, this nanocomposite could possess a higher photocatalytic activity than that of original TiO_2 nanoparticles. In addition, the relationship between the contents of the residual amounts of MB and UV light irradiation time has been studied, and the results were shown in Fig. 1-5.

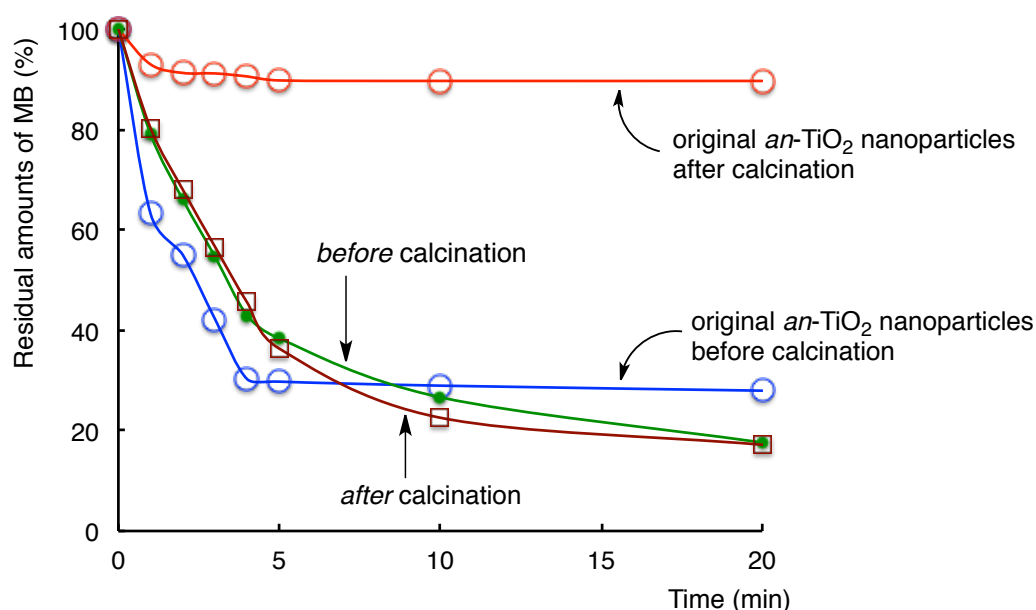


Fig. 1-5 Relationship between the residual amounts of MB and photoirradiation (λ_{max} : 365 nm) time in the presence of original an-TiO_2 nanoparticles and $\text{R}_F\text{-(VM-SiO}_2)_n\text{-R}_F/\text{an-TiO}_2$ nanocomposites before and after calcination at 1000 °C.
(used sample: Run 3 in Table 1-1)
Concentration of MB: 2.5 mg/dm³;
Concentration of nanocomposites: 25 mg/dm³

Fig. 1-5 shows that $\text{R}_F\text{-(VM-SiO}_2)_n\text{-R}_F/\text{an-TiO}_2$ nanocomposite after calcination at 1000 °C can give an effect decoloring ability of MB with the increase of the UV light irradiation time as well as that before calcination. Fig. 1-6 also shows the UV light irradiation time (λ_{max} : 365 nm) dependence for UV-vis spectra of aqueous solutions containing MB and

$R_F-(VM-SiO_2)_n-R_F/an-TiO_2$ nanocomposites after calcination at 1000 °C.

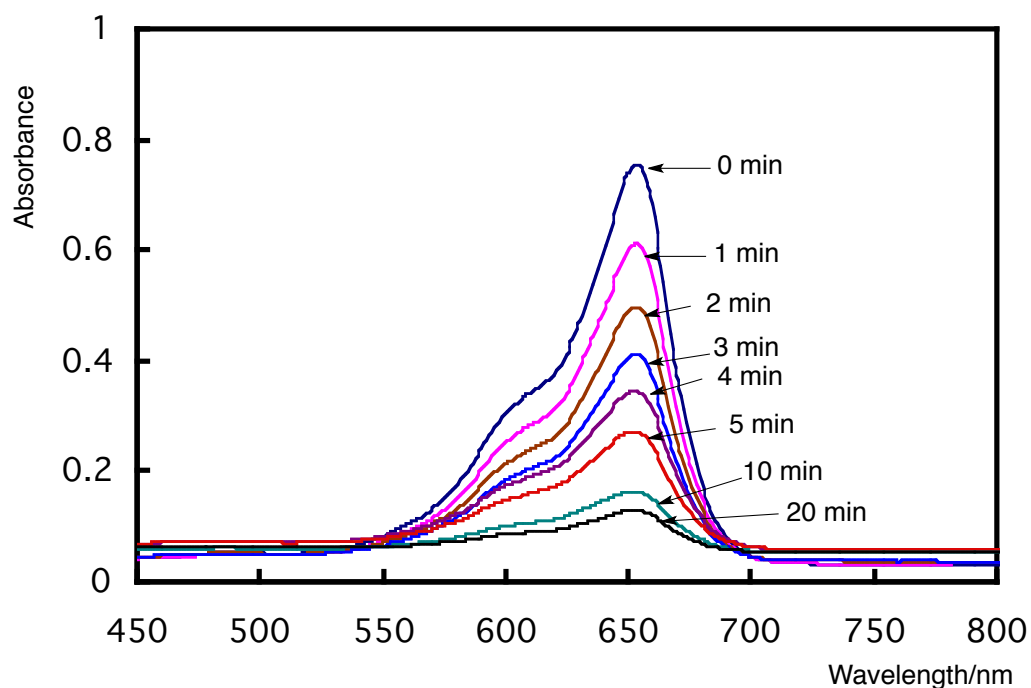


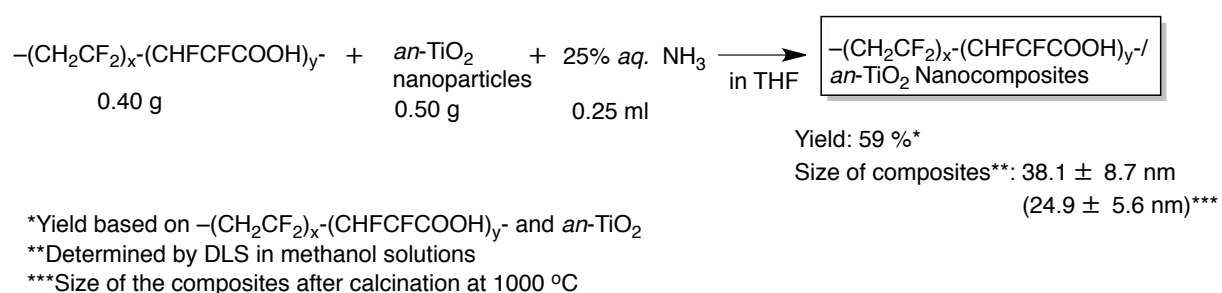
Fig. 1-6 UV light irradiation (λ_{max} : 365 nm) time dependence for UV-vis spectra of aqueous solutions containing 2.5 mg/dm³ methylene blue and 25 mg/dm³ $R_F-(VM-SiO_2)_n-R_F/TiO_2$ nanocomposites after calcination at 1000 °C.
(used sample: Run 3 in Table 1-1)

1.4. Conclusions

It was verified that the crystalline structure of *an*-TiO₂ in the present $R_F-(VM-SiO_2)_n-R_F/an-TiO_2$ nanocomposites can keep completely its structure without phase transformation to rutile even after calcination at 1000 °C. In general, the phase transformation of titanium oxide from anatase to rutile can be observed during calcination process from 600

to 750 °C.^{2, 5)} However, titania-silica composite, which was prepared from sodium silicate and titanium oxychloride, can keep the anatase structure around 900 °C, although the rutile phase in this composite appears at a calcination temperature of 1000 °C.⁶⁾ This stabilization of anatase TiO₂ is due to the formation of Ti-O-Si interface to prevent the phase transformation to rutile.¹⁰⁾

Vinylidene fluoride copolymer/*an*-TiO₂ nanocomposites [–(CH₂CF₂)_x–(CHFCFCOOH)_y–/*an*-TiO₂] possessing no silica source has been prepared according to the preparative method shown in Scheme 1-1 (See Scheme 1-2).



Scheme 1-2 Preparation of –(CH₂CF₂)_x–(CHFCFCOOH)_y–/*an*-TiO₂ nanocomposites.

The parent fluorinated copolymer has been prepared based on the previously reported method.¹¹⁾ *An*-TiO₂ in the nanocomposites was found to exhibit a complete phase transformation to rutile after calcination at 1000 °C (See Fig. 1-7).

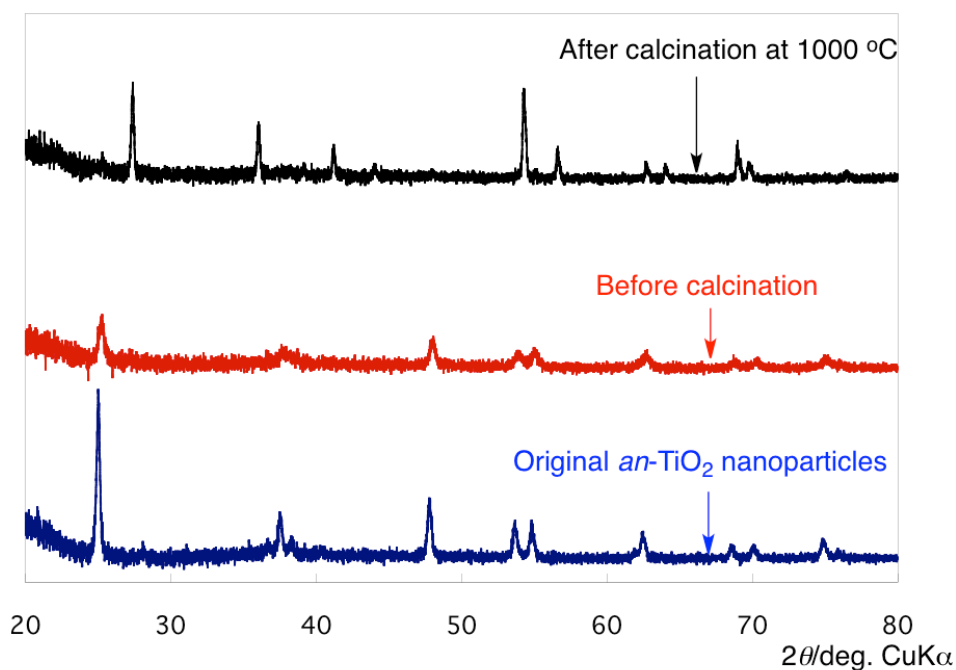


Fig. 1-7 X-ray diffraction patterns of original *an*-TiO₂ nanoparticles and $-(\text{CH}_2\text{CF}_2)_x-(\text{CHFCFCOOH})_y-/an\text{-TiO}_2$ nanocomposites before and after calcination at 1000 °C.

However, interestingly, the introduction of silica gel into $[-(\text{CH}_2\text{CF}_2)_x-(\text{CHFCFCOOH})_y-/an\text{-TiO}_2$ nanocomposites through the composite reaction with silica nanoparticles (average particle size: 10 nm) enabled the crystalline structure of *an*-TiO₂ to keep its structure without phase transformation to rutile even after calcination at 1000 °C (see Scheme 1-3 and Fig. 1-8).



Scheme 1-3 Preparation of $\text{-(CH}_2\text{CF}_2\text{)}_x\text{-(CHFClFCOOH)}_y\text{-an-TiO}_2\text{/SiO}_2$ nanocomposites.

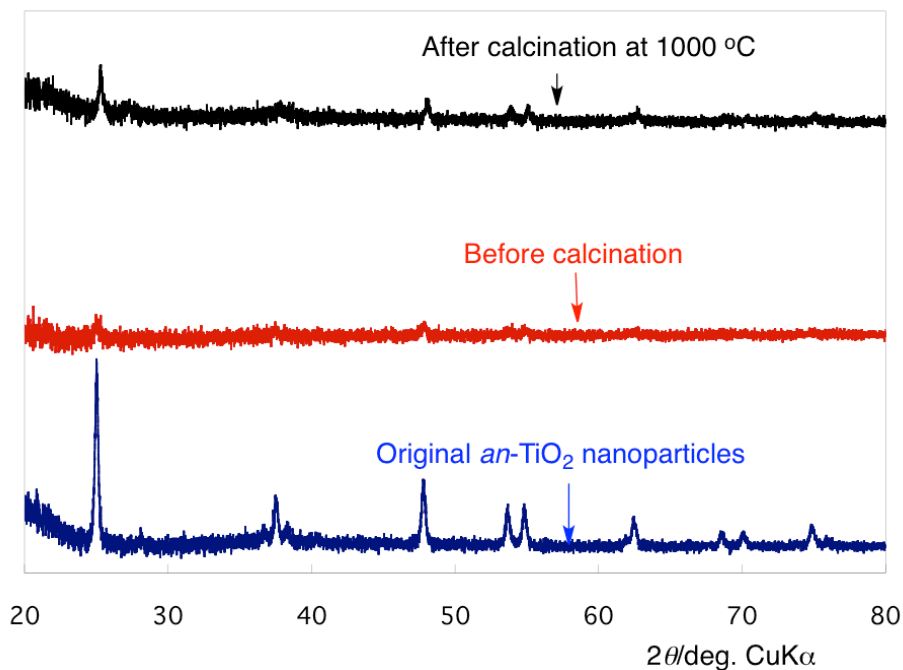


Fig. 1-8 X-ray diffraction patterns of original an-TiO_2 nanoparticles and $\text{-(CH}_2\text{CF}_2\text{)}_x\text{-(CHFClFCOOH)}_y\text{-SiO}_2\text{/an-TiO}_2$ nanocomposites before and after calcination at 1000°C .

These findings suggest that the SiO_2 lattice in the nanocomposites can lock the Ti-O species through the formation of Ti-O-Si species to prevent the phase transformation to rutile during the calcination process. Fluorine-doped nanosized anatase TiO_2 particles can be in

general prepared by using hydrofluoric acid as a source of fluorine, and these fluorine-doped TiO₂ nanoparticles can enhance the photocatalytic activity, compared to that of original one.¹²⁾ This finding is due to the formation of Ti-F species on the facets, especially surface terminating Ti-F bonds in the surface Ti-O-Ti networks.¹²⁾ Hydrogen fluoride can be easily formed in R_F-(VM-SiO₂)_n-R_F nanocomposite matrices to give a nonflammable characteristic for the encapsulated low molecular weight aromatic compounds into their composite matrices.¹³⁾ Thus, higher photocatalytic activity and extremely thermostable anatase titanium oxide in the R_F-(VM-SiO₂)_n-R_F/*an*-TiO₂ nanocomposites even after calcination at 1000 °C would be due to the formation of Ti-F and Ti-O-Si species. It is suggested that such extremely thermostable characteristic and higher photocatalytic activity of anatase titanium oxide in the composites after calcination at 1000 °C is the first example. Especially, the thermally stable R_F-(VM-SiO₂)_n-R_F/*an*-TiO₂ nanocomposites will have high potential for the applications to a variety of fields such as dye sensitized solar cell, because these nanocomposites can exhibit good photocatalytic activity relative to anatase titanium oxide even after calcination at 1000 °C.

References

- 1) a) M. R. Hoffmann, S. T. Martin, W. Choi, and D. W. Bahnemann, *Chem. Rev.*, **95**, 69 (1995);
b) M. Gratzel, *Nature*, **414**, 338 (2001);
c) B. O'Regan and M. Gratzel, *Nature*, **353**, 737 (1991);
d) A. L. Linsebigler, G. Q. Lu, and J. T. Yates, *Chem. Rev.*, **95**, 735 (1995);
e) S. Liu and A. Chen, *Langmuir*, **21**, 8409 (2005).
- 2) G. Madras, B. J. McCoy, and A. Navrotsky, *J. Am. Ceram. Soc.*, **90**, 250 (2007).
- 3) a) X. Chen and S. Mao, *Chem. Rev.*, **107**, 2891 (2007);
b) H. J. Snaith and L. Schmidt-Mende, *Adv. Mater.*, **19**, 3187 (2007).
- 4) D. A. H. Hanaor and C. C. Sorrell, *J. Mater. Sci.*, **46**, 855 (2011).
- 5) X. Peng and A. Chen, *Adv. Funct. Mater.*, **16**, 1355 (2006).
- 6) a) A. Hilonga, J.-K. Kim, P. B. Sarawade, and H. T. Kim, *J. Mater. Sci.*, **45**, 1255 (2010);
b) A. Hilonga, J.-K. Kim, P. B. Sarawade, and H. T. Kim, *J. Mater. Sci.*, **45**, 1264 (2010).
- 7) a) H. Sawada, *Polym. Chem.*, **3**, 46 (2012);
b) H. Sawada, *Prog. Polym. Sci.*, **32**, 509 (2007);
c) H. Sawada, *Polym. J.*, **39**, 637 (2007).

- 8) a) H. Sawada, E. Sawada, H. Kakehi, T. Kariya, M. Mugisawa, Y. Chounan, M. Miura, and N. Isu, *Polym. Composites*, **30**, 1848 (2009);
- b) E. Sawada, H. Kakehi, Y. Chounan, M. Miura, Y. Sato, N. Isu, and H. Sawada, *Composites Part B*, **41**, 498 (2010).
- 9) H. Sawada and M. Nakayama, *J. Chem. Soc., Chem. Commun.*, 677 (1991).
- 10) a) X. Gao and I. E. Wachs, *Catalysis Today*, **51**, 233 (1999);
- b) L. Sikong, J. Damchan, K. Kooptarnond, and S. Niyomwas, *Songklanakarin J. Sci. Technol.*, **30**, 385 (2008).
- 11) H. Sawada, T. Tashima, Y. Nishiyama, M. kikuchi, Y. Goto, G. Kostov, and B. Ameduri, *Macromolecules*, **44**, 1114 (2011).
- 12) a) G. Liu, C. Sun, H. G. Yang, S. C. Smith, L. Wang, G. Q. Lu, and H.-M. Cheng, *Chem. Commun.*, **46**, 755 (2010);
- b) W. Ho, J. C. Yu, and S. Lee, *Chem. Commun.*, 1115 (2006);
- c) H. Zhang, P. Liu, P. F. Li, H. Liu, Y. Qang, S. Zhang, M. Guo, H. Cheng, and H. Zhao, *Chem. Eur. J.*, **17**, 5949 (2011);
- d) D. Zhang, G. Li, X. Yang, and J. C. Yu, *Chem. Commun.*, 4381 (2009);
- e) G. Wu, J. Wang, D. F. Thomas, and A. Chen, *Langmuir*, **24**, 3503 (2008);
- f) M. Liu, L. Zhao, S. Ju, Z. Yan, T. He, C. Zhou, and W. Wang, *Chem. Commun.*, **46**,

1664 (2010);

g) X. Han, Q. Kuang, M. Jin, Z. Xie, and L. Zheng, *J. Am. Chem. Soc.*, **131**, 3152 (2009);

h) G. H. Yang, G. Liu, S. Z. Qiao, C. H. Sun, Y. G. Jin. S. C. Smith, J. Zou,

H. M. Cheng, and G. Q. Lu, *J. Am. Chem. Soc.*, **131**, 4078 (2009);

i) D. Li, H. Haneda, N. K. Labhsetwar, S. Hishita, and N. Ohashi, *Chem. Phys. Lett.*, **401**,

579 (2005);

j) J. C. Yu, J. Yu, W. Ho, Z. Jiang, and L. Zhang, *Chem. Mater.*, **14**, 3808 (2002).

13) H. Sawada, Y. Matsuki, Y. Goto, S. Kodama, M. Sugiya, and Y. Nishiyama, *Bull. Chem. Soc. Jpn.*, **83**, 75 (2010).

CHAPTER 2

Preparation and Photocatalytic Activity of Fluoroalkyl End-capped Vinyltrimethoxysilane Oligomer/Anatase Titanium Oxide Nanocomposites – Encapsulated Low Molecular Weight Aromatic Compounds

2.1. Introduction

Polymer nanocomposites, which consist of a polymer matrix filled with nanoscale particles, have emerged as a new class of high performance materials. In these nanoscale particles, especially, titanium oxide has been widely used as a white pigment in the plastic industry mainly because of the high refractive index of titanium oxide nanoparticles (~ 2.6), which enables it to produce high gloss composites.^{1, 2)} Titanium oxide is also the most commonly used semiconducting photocatalyst, because it is highly photoactive, photostable, biologically and chemically inert, and nontoxic.^{3, 4)} However, in general, nanoparticles can agglomerate or coalesce very easily forming larger particles, thus making them difficult to disperse uniformly through the polymer matrix, which results in an adverse effect on the catalyst efficiency.^{5 ~ 7)} Therefore, from the developmental viewpoint of organic polymer/titanium oxide nanocomposites having a good dispersibility and stability in a variety of solvents, it is of particular interest to use fluorinated polymers possessing a high surface active characteristic for the preparation of these titanium oxide nanocomposites.⁸⁾ In fact, fluoroalkyl end-capped vinyltrimethoxysilane oligomer/anatase titanium oxide nanocomposites $[R_F-(VM-SiO_2)_n-R_F/an-TiO_2]$ have been prepared by the sol-gel reaction of the corresponding oligomer $[R_F-(VM)_n-R_F]$ in the presence of anatase titanium oxide

nanoparticles (*an*-TiO₂) under alkaline conditions.⁹⁾

It is widely accepted that the anatase titanium oxide is a more efficient photocatalyst than the rutile titanium oxide due to the relatively high adsorptive affinity for organics and superior hole-trapping ability of the anatase titanium oxide.^{10 ~ 17)} However, the anatase titanium oxide transforms irreversibly to rutile at elevated temperatures around 600 and 750 °C.^{18 ~ 21)} From an applicable viewpoint of anatase titanium oxide into a variety of fields, it is deeply desirable to develop thermally stable anatase titanium oxide nanocomposites without the phase transformation into rutile under such higher temperature conditions. It has been very recently reported that fluoroalkyl end-capped vinyltrimethoxysilane oligomer/anatase titanium oxide nanocomposites [$R_F-(VM-SiO_2)_n-R_F/an-TiO_2$] can keep completely its structure without phase transformation into rutile even after calcination at 1000 °C, and $R_F-(VM-SiO_2)_n-R_F/an-TiO_2$ nanocomposite before and after calcination at 1000 °C exhibited the similar photocatalytic activity for the decolorization of methylene blue under UV light irradiation.²²⁾ This chapter shows that $R_F-(VM-SiO_2)_n-R_F/an-TiO_2$ nanocomposites are applicable to the encapsulation of low molecular weight aromatic compounds such as bisphenol A [BPA], 1,1'-bi(2-naphthol) [BINOL] and fullerene, and encapsulated aromatic compounds such as BPA and BINOL into these nanocomposite cores can exhibit no weight loss corresponding to the contents of the aromatic compounds even after calcination at 800 °C.

Especially, it has been found that the fluorinated titanium oxide nanocomposites - encapsulated these aromatic compounds before and after calcination at 1000 °C can exhibit a higher photocatalytic activity for the decolorization of methylene blue under UV light irradiation than that of the corresponding $R_F-(VM-SiO_2)_n-R_F/an-TiO_2$ nanocomposites or the original *an*-TiO₂ nanoparticles. These results will be described herein.

2.2. Experimental

2.2.1 Measurements

Molecular weight was measured using a Shodex DS-4 (pump, Tokyo, Japan) and Shodex RI-71 (detector) gel permeation chromatography (GPC) calibrated with polystyrene standard using tetrahydrofuran (THF) as the eluent. Dynamic light-scattering (DLS) measurements were recorded using Otsuka Electronics DLS-7000 HL (Tokyo, Japan). Ultraviolet-visible (UV-vis) spectra were carried out using Shimadzu UV-1600 UV-vis spectrophotometer (Kyoto, Japan). Field emission scanning electron micrographs (FE-SEM) and energy dispersive X-ray (EDX) spectra were recorded by means of JEOL JSM-7000F (Tokyo, Japan). X-ray diffraction (XRD) measurements were performed by the use of Mac Science M18XHF-SRA (Tokyo, Japan).

2.2.2. Materials

Titanium oxide nanoparticles (average particle size: 20 nm) were received from Ishihara Sangyo Kaisha Ltd. (Osaka, Japan). Bisphenol A (BPA), 1,1'-bi(2-naphthol) [BINOL] and

fullerene were purchased from Tokyo Chemical Industry Co., Ltd. (Tokyo, Japan).

Fluoroalkyl end-capped vinyltrimethoxysilane oligomer was prepared by reaction of fluoroalkanoyl peroxide with the corresponding monomer according to the previously reported method.²³⁾

2.2.3. Preparation of fluoroalkyl end-capped vinyltrimethoxysilane oligomer/anatase titanium oxide nanocomposites - encapsulated BPA

To a tetrahydrofuran (THF) solution (20 ml) containing fluoroalkyl end-capped vinyltrimethoxysilane oligomer: $R_F-[CH_2CHSi(OMe)_3]_n-R_F$ [$R_F-(VM)_n-R_F$]; $R_F = CF(CF_3)OC_3F_7$; $M_n = 1030$ (400 mg)] and BPA (250 mg) were added anatase TiO_2 nanoparticles [*an*- TiO_2 (500 mg)] and 25 % aqueous ammonia solution (0.25 ml). The mixtures were stirred with a magnetic stirring bar at room temperature for 2 hrs, and then were centrifuged for 30 min. The expected fluorinated TiO_2 nanocomposites were easily separated from the THF solution. THF (20 ml) was added to the obtained crude product. The THF solution was stirred with magnetic stirring bar at room temperature for 1 day. After centrifugal separation of this solution, the obtained product was dried in vacuum at 50 °C for 2 days to produce purified fluorinated composite white colored powders in 51 % (590

mg) isolated yield based on the used $R_F-(VM)_n-R_F$ oligomer, *an*-TiO₂ and BPA.

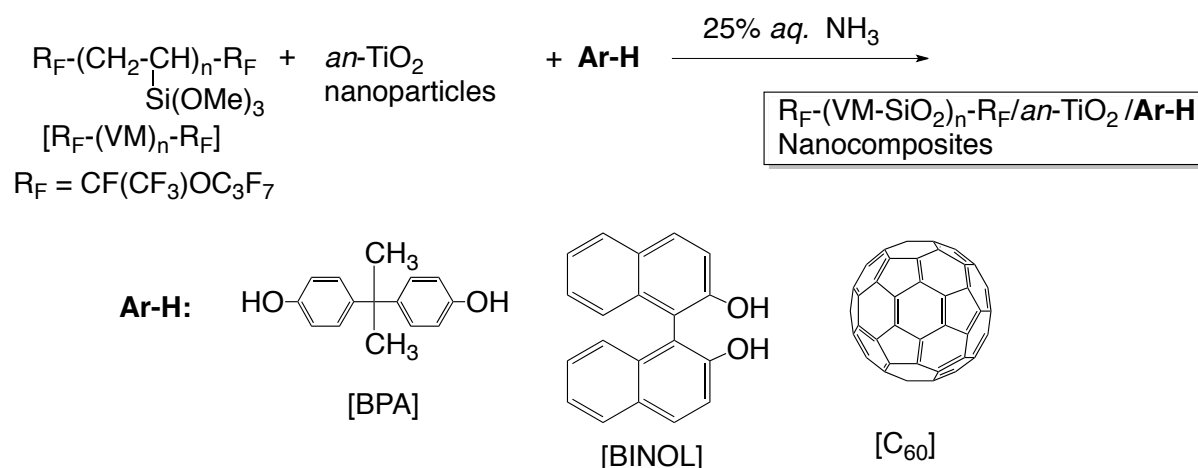
2.2.4. Decolorization of methyl blue under UV light irradiation in the presence of fluoroalkyl end-capped vinyltrimethoxysilane oligomer/anatase titanium oxide nanocomposites - encapsulated BPA

Methanol solution (0.8 ml) of methylene blue (10 mg/dm³) and well-dispersed $R_F-(VM-SiO_2)_n-R_F/an-TiO_2$ – encapsulated BPA nanocomposites (200 mg/dm³) methanol solution (0.4 ml) were added in 2 ml methanol solution. UV-vis spectra of the suspension methanol solution thus obtained exhibited an absorption band around 652 nm related to methylene blue dye. The decolorization of methylene blue dye was examined by irradiating this suspension solution with the UV lamp (λ_{max} : 365 nm) for 20 min at room temperature.

2.3. Results and discussion

2.3.1. Preparation of fluoroalkyl end-capped vinyltrimethoxysilane oligomer/anatase titanium oxide nanocomposites - encapsulated Ar-H

The sol-gel reactions of fluoroalkyl end-capped vinyltrimethoxysilane oligomer $[R_F-(VM)_n-R_F]$ under alkaline conditions were found to proceed smoothly in the presence of *an*-TiO₂ nanoparticles and bisphenol A (BPA) to give the corresponding fluorinated oligomer/*an*-TiO₂ nanocomposites - encapsulated BPA $[R_F-(VM-SiO_2)_n-R_F/an-TiO_2/BPA]$ in 34 ~ 51 % isolated yields. Similarly, $R_F-(VM-SiO_2)_n-R_F/an-TiO_2/BINOL$ and $/C_{60}$ nanocomposites were prepared in 37 ~ 49 % and 76 ~ 81 % isolated yields, respectively. These results were shown in Scheme 2-1 and Table 2-1.



Scheme 2-1 Preparation of $R_F-(VM-SiO_2)_n-R_F/an-TiO_2/Ar-H$ nanocomposites.

Table 2-1 Preparation of $R_F-(VM-SiO_2)_n-R_F/an-TiO_2/Ar-H$ nanocomposites.

Run	R _F -(VM) _n -R _F (mg)	an-TiO ₂ (mg)	Ar-H (mg)	25 % aq. NH ₃ (ml)	Product yield* (%)	Size of the composites** (after calcination) (nm) ± STD		
BPA								
1	400	500	250	0.25	51	17.8 ± 4.0	(11.5 ± 2.8)	
2	400	500	350	0.25	45	20.8 ± 5.2	(11.8 ± 4.9)	
3	400	500	850	0.25	34	74.9 ± 19.0	(44.1 ± 8.7)	
BINOL								
4	400	500	250	0.25	49	69.2 ± 16.1	(42.7 ± 9.8)	
5	400	500	350	0.25	46	47.2 ± 9.7	(72.2 ± 14.6)	
6	400	500	850	0.25	37	75.8 ± 15.0	(36.1 ± 9.0)	
C ₆₀								
7	400	500	5	0.25	76	27.2 ± 6.0	(20.3 ± 5.1)	
8	400	500	25	0.25	81	19.8 ± 5.0	(18.3 ± 4.4)	
9	400	500	50	0.25	79	21.6 ± 5.1	(21.1 ± 5.4)	

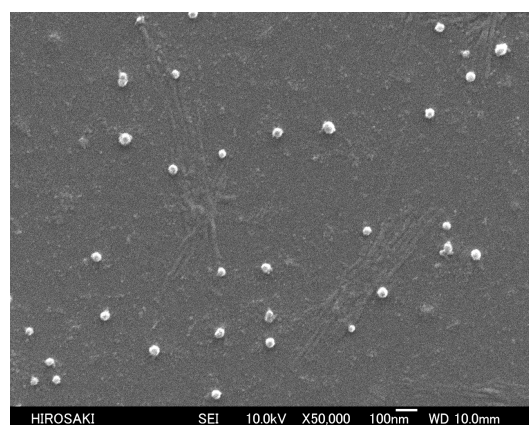
*Yield based on $R_F-(VM)_n-R_F$, $an-TiO_2$ and Ar-H

** Determined by DLS (dynamic light scattering) measurements in methanol solutions

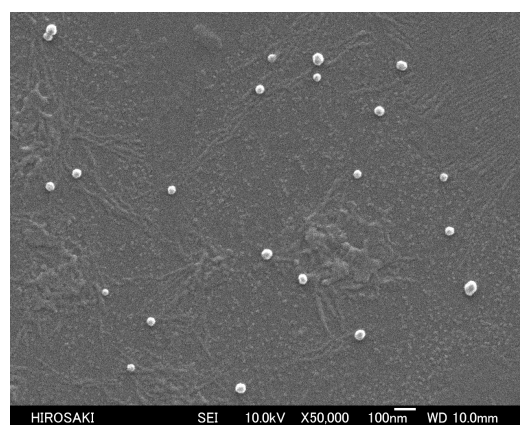
These obtained nanocomposites were found to exhibit a good dispersibility and stability for the traditional organic solvents such as methanol, ethanol, 2-propanol, tetrahydrofuran, chloroform, 1,2-dichloroethane, ethyl acetate, *N,N*-dimethylformamide and dimethyl sulfoxide. Thus, we have measured the size of $R_F-(VM-SiO_2)_n-R_F/an-TiO_2$ nanocomposites - encapsulated aromatic compounds before and after calcination at 1000 °C in methanol by dynamic light-scattering (DLS) measurements at 25 °C. Each size of these obtained fluorinated TiO_2 composites before and after calcination at 1000 °C is nanometer size-controlled fine particles: 18 ~ 76 nm and 12 ~ 72 nm (number-average diameter), respectively (see Table 2-1).

The field-emission scanning electron micrograph (FE-SEM) of well-dispersed methanol

solutions of nanocomposites has been measured before and after calcination at 1000 °C, and the results were shown in Fig. 2-1 (Run 1 in Table 2-1) and Figs. 2-2 ~ 2-3 (Runs 4 and 8 in Table 2-1).

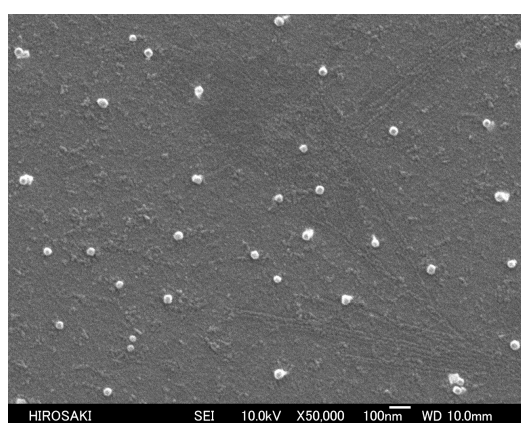


a) before calcination
mean: 52 nm

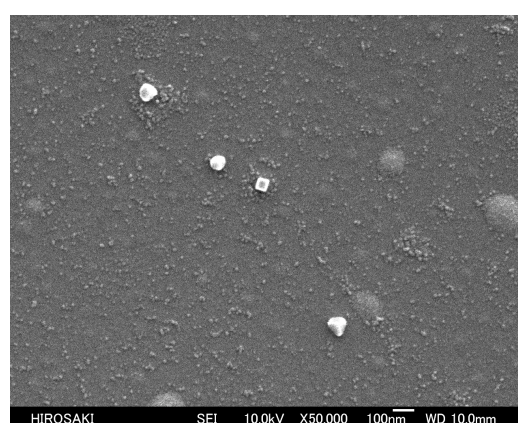


b) after calcination
mean: 43 nm

Fig. 2-1 FE-SEM (Field Emission-Scanning Electron Microscopy) images of $R_F-(VM-SiO_2)_n-R_F/TiO_2/BPA$ nanocomposites (Run 1 in Table 2-1) before and after calcination at 1000 °C.



a) before calcination
mean: 47 nm



b) after calcination
mean: 71 nm

Fig. 2-2 FE-SEM (Field Emission-Scanning Electron Microscopy) images of $R_F-(VM-SiO_2)_n-R_F/TiO_2/BINOL$ nanocomposites (Run 4 in Table 2-1) before and after calcination at 1000 °C.

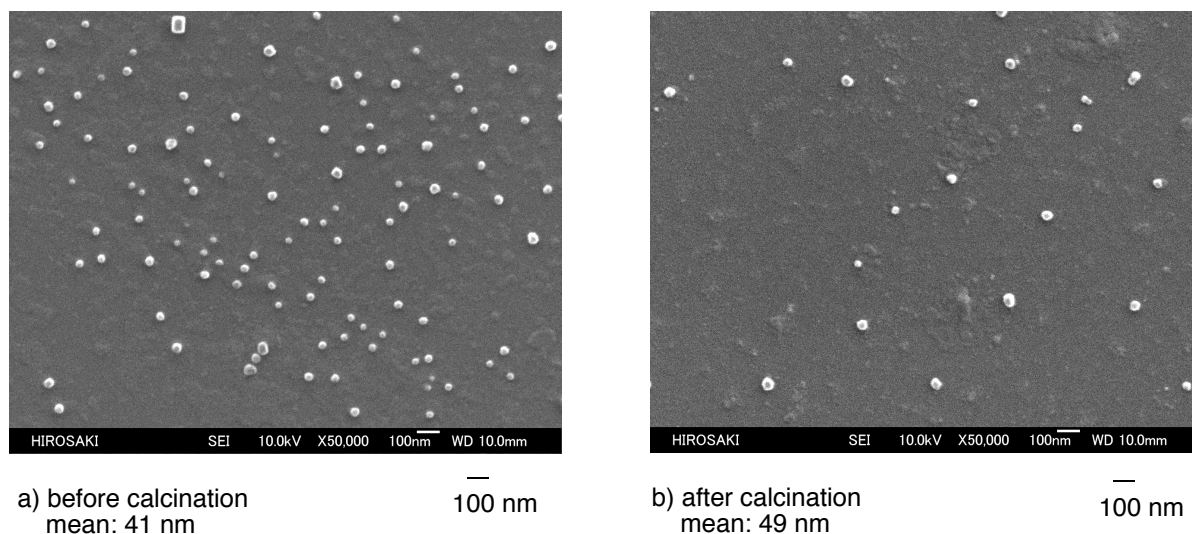


Fig. 2-3 FE-SEM (Field Emission-Scanning Electron Microscopy) images of $R_F-(VM-SiO_2)_n-R_F/TiO_2/C_{60}$ nanocomposites (Run 8 in Table 2-1) before and after calcination at 1000 °C.

FE-SEM pictures of nanocomposites before and after calcination at 1000 °C in Fig. 2-1 also showed the formation of composite fine particles with an average diameter of 52 nm and 43 nm, respectively, and the composite particles of the almost same size were obtained before and after calcination.

The thermal stability of $R_F-(VM-SiO_2)_n-R_F/an-TiO_2$ nanocomposites - encapsulated BPA by the use of thermogravimetric analyses (TGA), in which the weight loss of the nanocomposites was measured by raising the temperature around 800 °C at 10 °C/min heating ratio under air atmospheric conditions have been studied, and the results were shown in Fig. 2-4. $R_F-(VM-SiO_2)_n-R_F$ nanoparticles, which were prepared by the sol-gel reaction of $R_F-(VM)_n-R_F$ oligomer under alkaline conditions, markedly dropped around 420 °C and

decomposed gradually, reaching 63 % around 800 °C, of whose weight loss corresponds to the flammable organic moieties in $R_F-(VM-SiO_2)_n-R_F$ nanoparticles (see Fig. 2-4).²⁴⁾ $R_F-(VM-SiO_2)_n-R_F/an-TiO_2$ nanocomposites, which were prepared according to Scheme 2-1, afforded a clear weight loss (18 %) at 800 °C, indicating that the contents of titanium oxide nanoparticles in the composites is estimated to be 45 %.

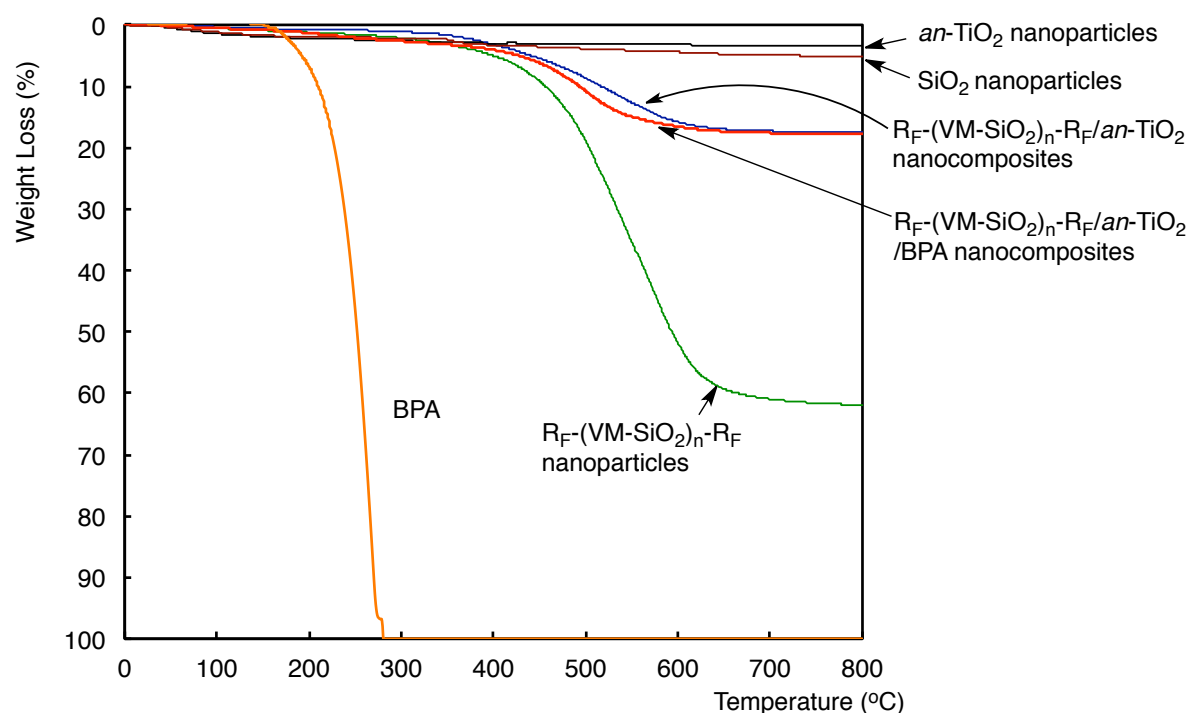


Fig. 2-4 Thermogravimetric analyses of BPA, *an*-TiO₂ nanoparticles, SiO₂ nanoparticles, $R_F-(VM-SiO_2)_n-R_F$ nanoparticles, $R_F-(VM-SiO_2)_n-R_F/an-TiO_2$ nanocomposites and $R_F-(VM-SiO_2)_n-R_F/an-TiO_2$ nanocomposites - encapsulated BPA (Run 2 in Table 2-1).

Unexpectedly, $R_F-(VM-SiO_2)_n-R_F/an-TiO_2$ - encapsulated BPA (Run 2 in Table 2-1), in which the theoretical content of BPA in the composites is 32 %, were found to exhibit no weight loss corresponding to the contents of encapsulated BPA in the composites even after

calcination at 800 °C, although the original BPA decomposed completely around 280 °C (see Fig. 2-4). A similar result was obtained in $R_F\text{-(VM-SiO}_2)_n\text{-}R_F/an\text{-TiO}_2$ nanocomposites - encapsulated BPA [theoretical content of BPA in the composites: 25 % (Run 1 in Table 2-1)], of whose feed amount of BPA is 250 mg (see Fig. 2-5). However, in the case of the nanocomposites (theoretical content of BPA: 53 %) of Run 3 in Table 2-1, a clear weight loss corresponding to the content of BPA was observed at 800 °C (see Fig. 2-6). Especially, this nanocomposite gave a clear weight loss around 380 °C corresponding to the original BPA, indicating that BPA in the composites should exhibit a flammable characteristic during the calcination process. These findings suggest that $R_F\text{-(VM-SiO}_2)_n\text{-}R_F/an\text{-TiO}_2$ nanocomposites can encapsulate BPA as a guest molecule into fluorinated composite matrices to afford nonflammable characteristic toward BPA; in contrast, encapsulated BPA should give a flammable characteristic in the composite matrices above the theoretical encapsulation ratio: 32 %.

Thermal stability of $R_F\text{-(VM-SiO}_2)_n\text{-}R_F/an\text{-TiO}_2$ nanocomposites - encapsulated BINOL was also studied under similar conditions, and the results were shown in Fig. 2-7.

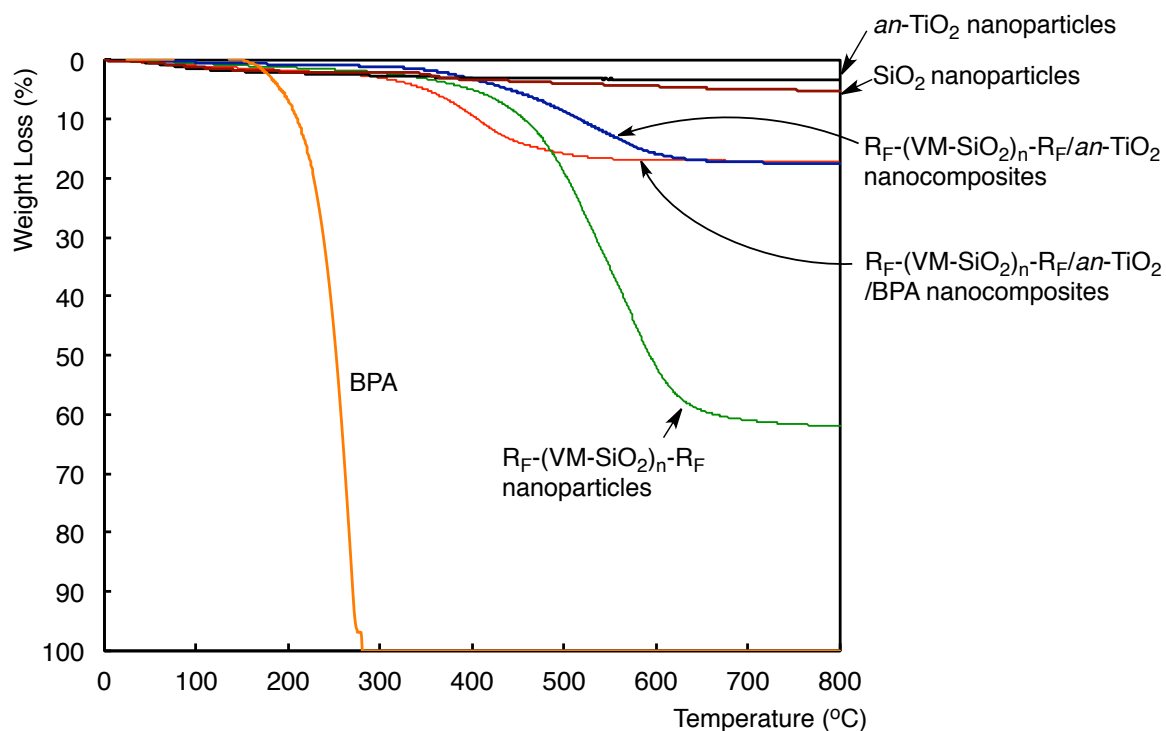


Fig. 2-5 Thermogravimetric analyses of BPA, $an\text{-TiO}_2$ nanoparticles, SiO_2 nanoparticles, $R_F\text{-(VM-SiO}_2)_n\text{-}R_F$ nanoparticles, $R_F\text{-(VM-SiO}_2)_n\text{-}R_F/an\text{-TiO}_2$ nanocomposites and $R_F\text{-(VM-SiO}_2)_n\text{-}R_F/an\text{-TiO}_2$ nanocomposites - encapsulated BPA (Run 1 in Table 2-1).

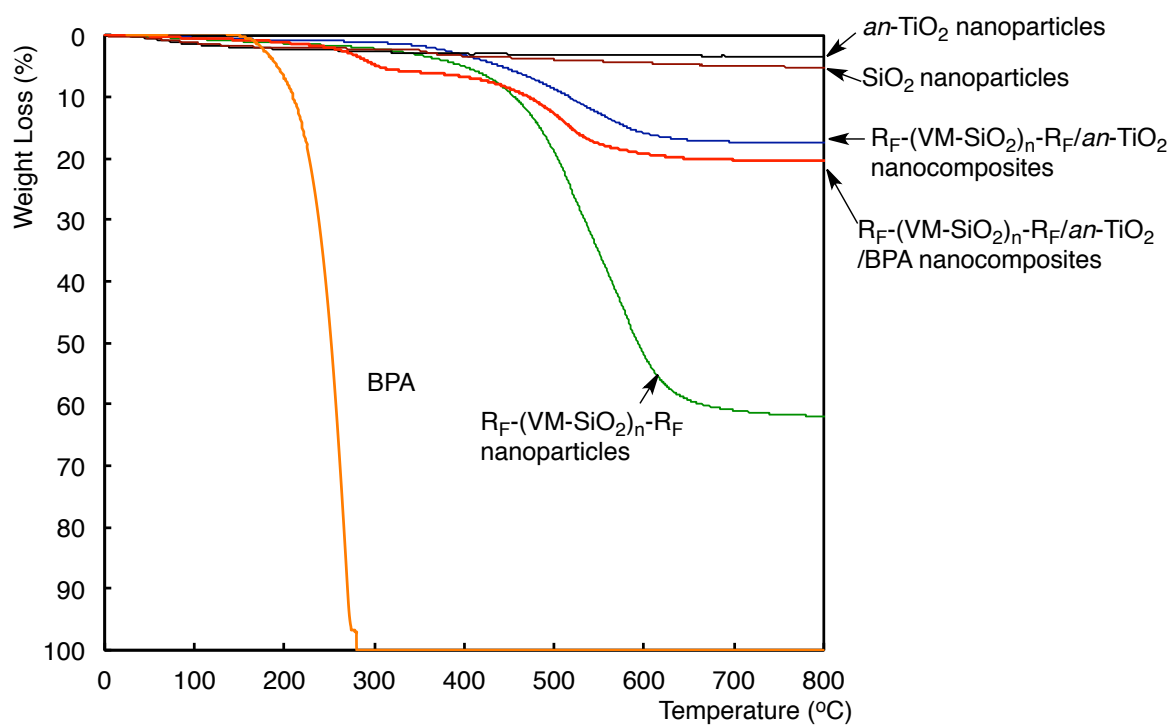


Fig. 2-6 Thermogravimetric analyses of BPA, $an\text{-TiO}_2$ nanoparticles, SiO_2 nanoparticles, $R_F\text{-(VM-SiO}_2)_n\text{-}R_F$ nanoparticles, $R_F\text{-(VM-SiO}_2)_n\text{-}R_F/an\text{-TiO}_2$ nanocomposites and $R_F\text{-(VM-SiO}_2)_n\text{-}R_F/an\text{-TiO}_2$ nanocomposites - encapsulated BPA (Run 3 in Table 2-1).

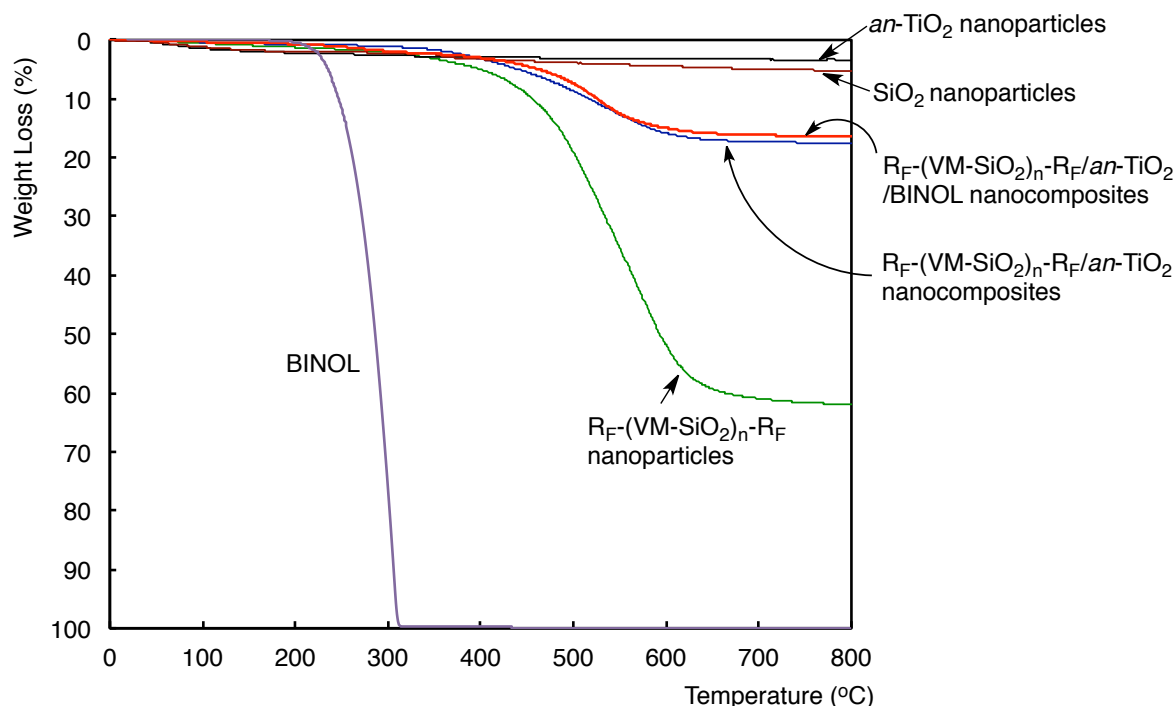


Fig. 2-7 Thermogravimetric analyses of BINOL, $an\text{-TiO}_2$ nanoparticles, SiO_2 nanoparticles, $R_F\text{-(VM-SiO}_2)_n\text{-R}_F$ nanoparticles, $R_F\text{-(VM-SiO}_2)_n\text{-R}_F/an\text{-TiO}_2$ nanocomposites and $R_F\text{-(VM-SiO}_2)_n\text{-R}_F/an\text{-TiO}_2$ nanocomposites - encapsulated BINOL (Run 4 in Table 2-1).

As shown in Fig. 2-7, fluorinated nanocomposites - encapsulated BINOL were found to exhibit a similar thermal stability to that of $R_F\text{-(VM-SiO}_2)_n\text{-R}_F/an\text{-TiO}_2$ nanocomposites - encapsulated BPA, and encapsulated BINOL, in which the theoretical contents of BINOL are 25 % (see Fig. 2-7: Run 4 in Table 2-1) and 32 % [see Fig. 2-8 (Run 5 in Table 2-1)], respectively, gave no weight loss behavior even after calcination at 800 °C. In contrast, a clear weight loss behavior was observed in $R_F\text{-(VM-SiO}_2)_n\text{-R}_F/an\text{-TiO}_2$ nanocomposites - encapsulated BINOL (see Fig. 2-9), in which the theoretical content of BINOL in the composites is 53 %, as well as that of the corresponding nanocomposites – encapsulated BPA in Fig. 2-6.

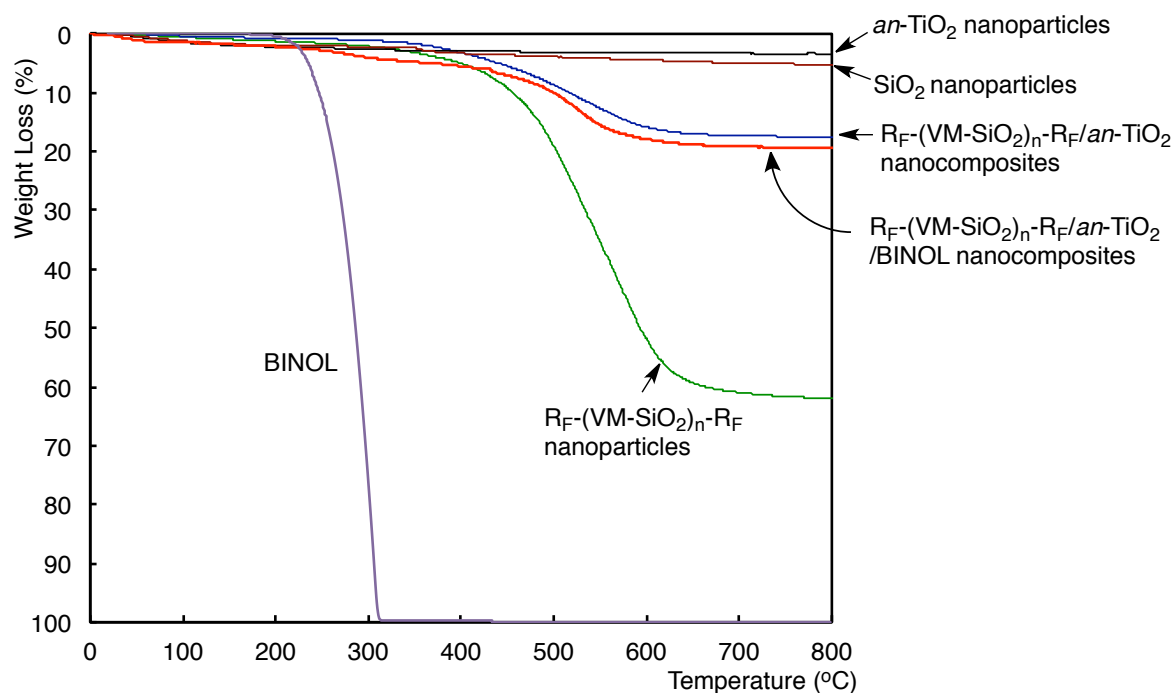


Fig. 2-8 Thermogravimetric analyses of BINOL, $an\text{-TiO}_2$ nanoparticles, SiO_2 nanoparticles, $R_F\text{-(VM-SiO}_2)_n\text{-}R_F$ nanoparticles, $R_F\text{-(VM-SiO}_2)_n\text{-}R_F/an\text{-TiO}_2$ nanocomposites and $R_F\text{-(VM-SiO}_2)_n\text{-}R_F/an\text{-TiO}_2$ nanocomposites - encapsulated BINOL (Run 5 in Table 2-1).

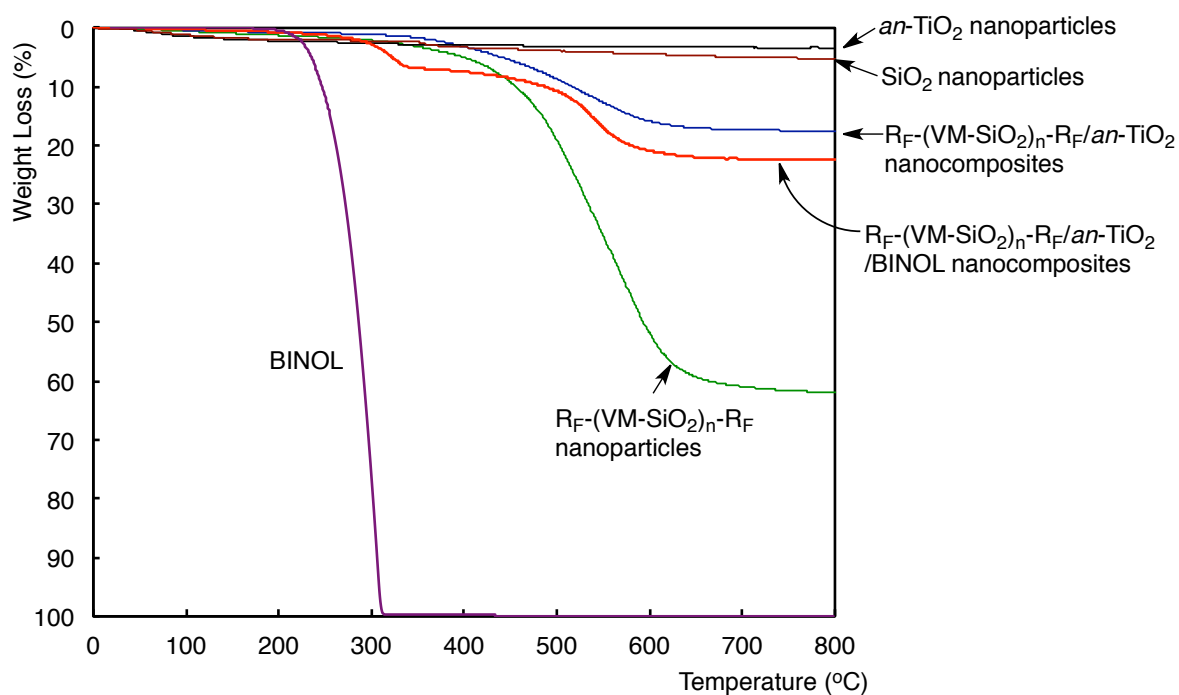


Fig. 2-9 Thermogravimetric analyses of BINOL, $an\text{-TiO}_2$ nanoparticles, SiO_2 nanoparticles, $R_F\text{-(VM-SiO}_2)_n\text{-}R_F$ nanoparticles, $R_F\text{-(VM-SiO}_2)_n\text{-}R_F/an\text{-TiO}_2$ nanocomposites and $R_F\text{-(VM-SiO}_2)_n\text{-}R_F/an\text{-TiO}_2$ nanocomposites - encapsulated BINOL (Run 6 in Table 2-1).

$R_F-(VM-SiO_2)_n-R_F/an-TiO_2$ nanocomposites - encapsulated fullerene exhibited clear weight loss at 800 °C in each nanocomposite (see Fig. 2-10 and Figs. 2-11, 2-12). It was previously reported that encapsulated aromatic compounds possessing acidic hydroxyl groups such as BPA in fluoroalkyl end-capped acrylic acid oligomer [$R_F-(CH_2CHCOOH)_n-R_F$; $R_F = CF(CF_3)OC_3F_7$]/silica nanocomposite matrices can exhibit a non-flammable characteristic due to the formation of hexafluorosilicate anions in the composite matrices through the dehydrofluorination of phenol-type acidic protons and fluorines in the composites catalyzed by both ammonia and silica nanoparticles.^{25 ~ 30)} Therefore, encapsulated fullerene into fluorinated nanocomposite matrices should exhibit a clear weight loss after calcination at 800 °C.

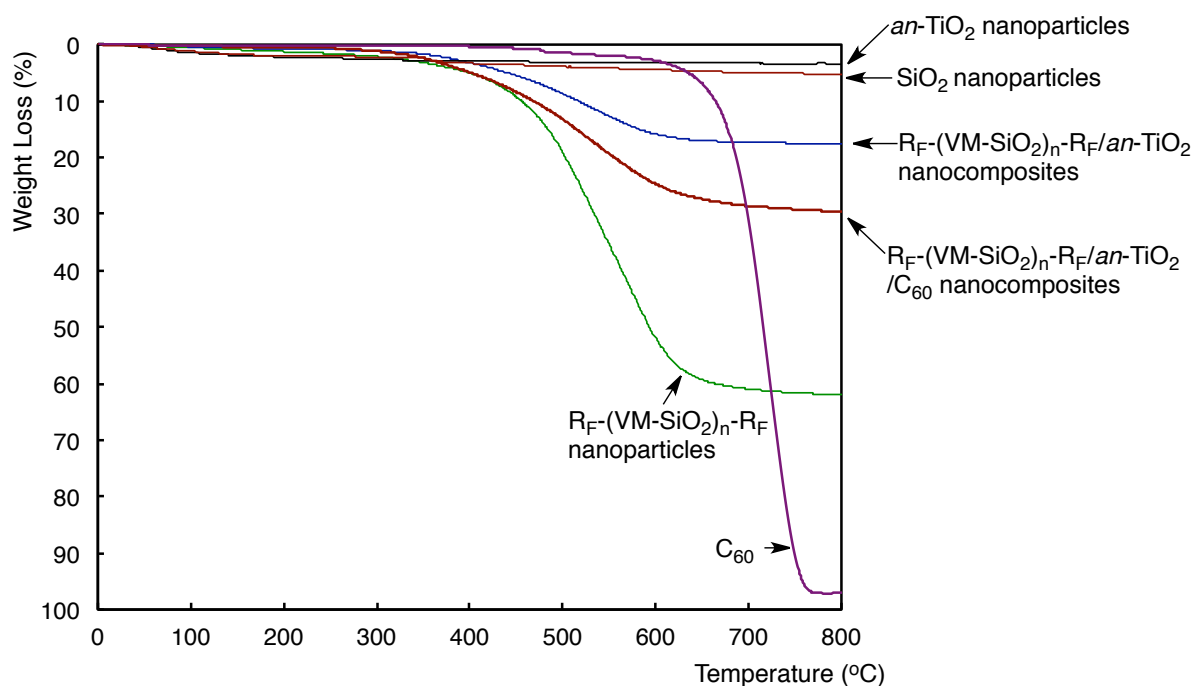


Fig. 2-10 Thermogravimetric analyses of C_{60} , $an-TiO_2$ nanoparticles, SiO_2 nanoparticles, $R_F-(VM-SiO_2)_n-R_F$ nanoparticles, $R_F-(VM-SiO_2)_n-R_F/an-TiO_2$ nanocomposites and $R_F-(VM-SiO_2)_n-R_F/an-TiO_2$ nanocomposites - encapsulated C_{60} (Run 7 in Table 2-1).

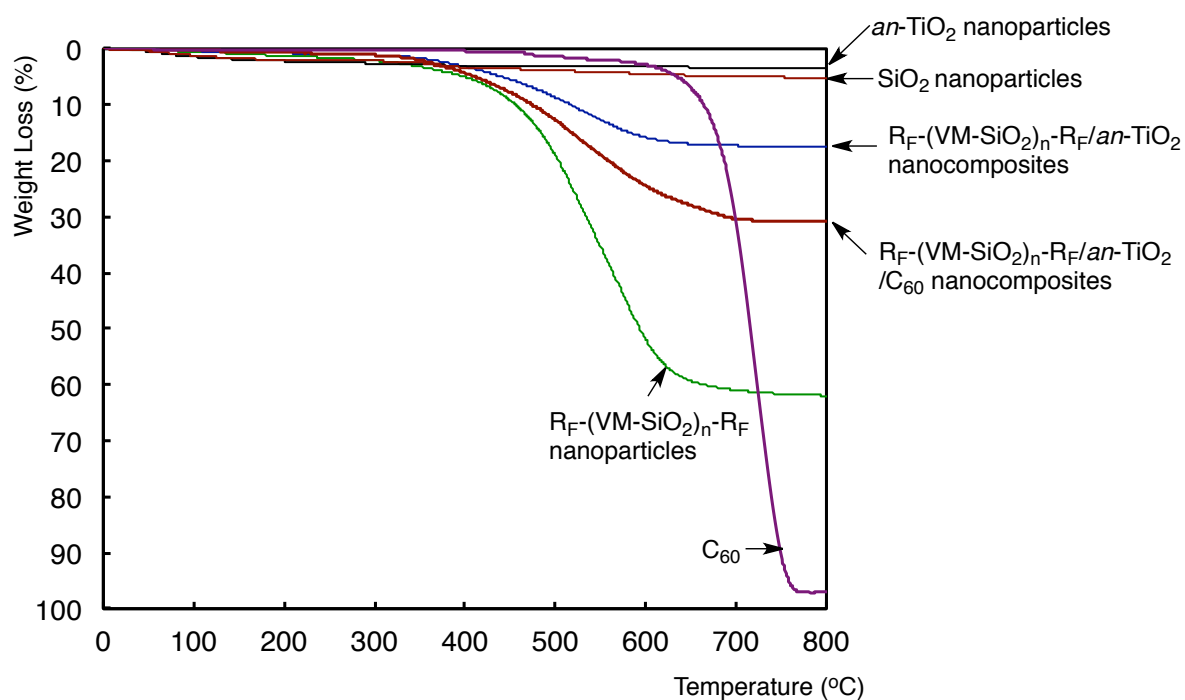


Fig. 2-11 Thermogravimetric analyses of C_{60} , $an\text{-TiO}_2$ nanoparticles, SiO_2 nanoparticles, $\text{R}_F\text{-(VM-SiO}_2)_n\text{-R}_F$ nanoparticles, $\text{R}_F\text{-(VM-SiO}_2)_n\text{-R}_F/an\text{-TiO}_2$ nanocomposites and $\text{R}_F\text{-(VM-SiO}_2)_n\text{-R}_F/an\text{-TiO}_2$ nanocomposites - encapsulated C_{60} (Run 8 in Table 2-1).

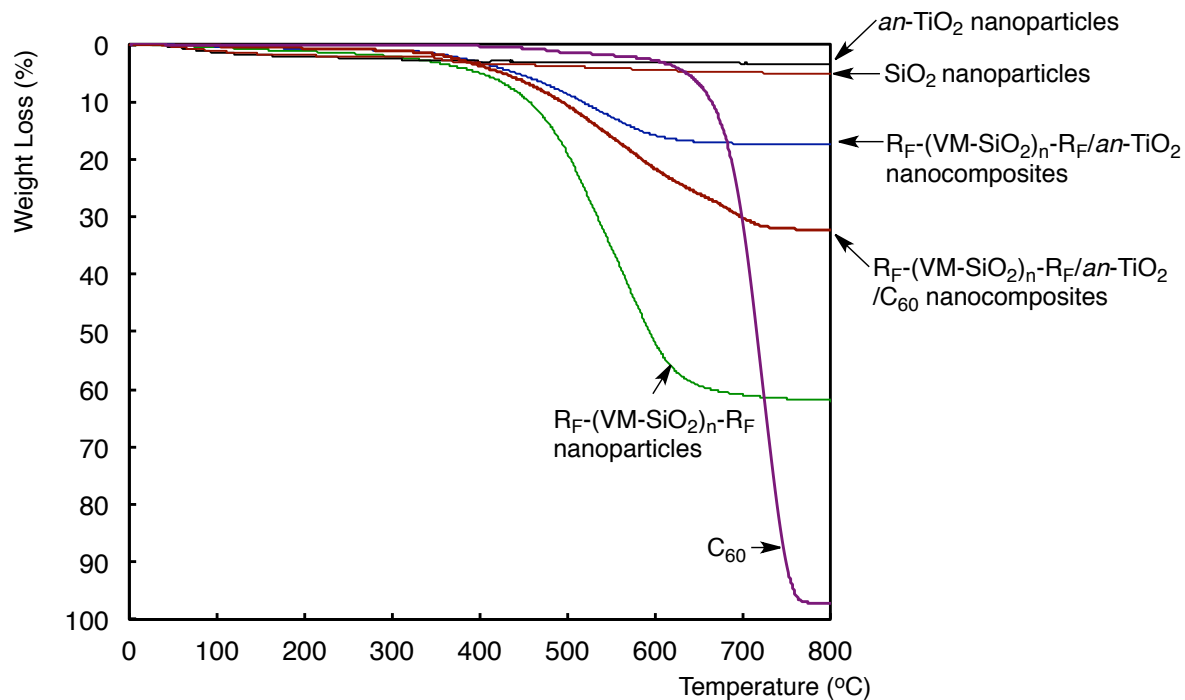


Fig. 2-12 Thermogravimetric analyses of C_{60} , $an\text{-TiO}_2$ nanoparticles, SiO_2 nanoparticles, $\text{R}_F\text{-(VM-SiO}_2)_n\text{-R}_F$ nanoparticles, $\text{R}_F\text{-(VM-SiO}_2)_n\text{-R}_F/an\text{-TiO}_2$ nanocomposites and $\text{R}_F\text{-(VM-SiO}_2)_n\text{-R}_F/an\text{-TiO}_2$ nanocomposites - encapsulated C_{60} (Run 9 in Table 2-1).

In order to clarify the presence of low molecular weight aromatic compounds in $R_F-(VM-SiO_2)_n-R_F/an-TiO_2$ nanocomposite matrices before and after calcination, the UV-vis spectra of well-dispersed methanol solutions of $R_F-(VMSiO_2)_n-R_F/an-TiO_2/BPA$ and /BINOL nanocomposites have been measured before and after calcination, and the results are shown in Figs. 2-13 and 2-14.

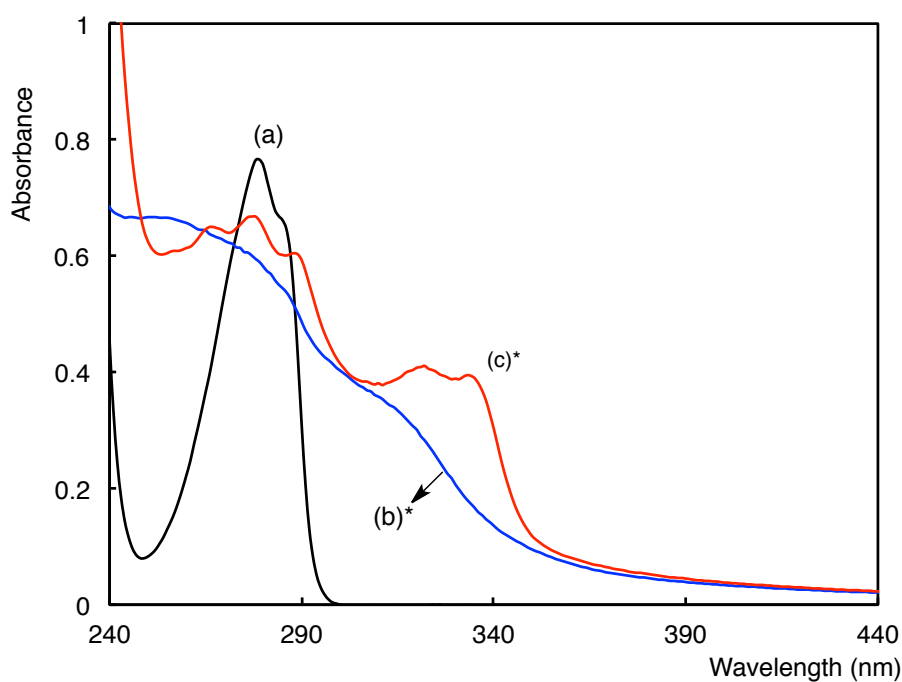


Fig. 2-13 UV-vis spectra of methanol solutions of original BPA (3 mg/dm^3) (a), $R_F-(VM-SiO_2)_n/an-TiO_2$ nanocomposites - encapsulated BPA before calcination (1.5 g/dm^3) (b)*, and $R_F-(VM-SiO_2)_n/an-TiO_2$ nanocomposites - encapsulated BPA after calcination at 1000°C (1.5 g/dm^3) (Run 2 in Table 2-1) (c)*. *The supernatant solutions, which were obtained from the centrifugal separation of the corresponding well-dispersed methanol solutions.

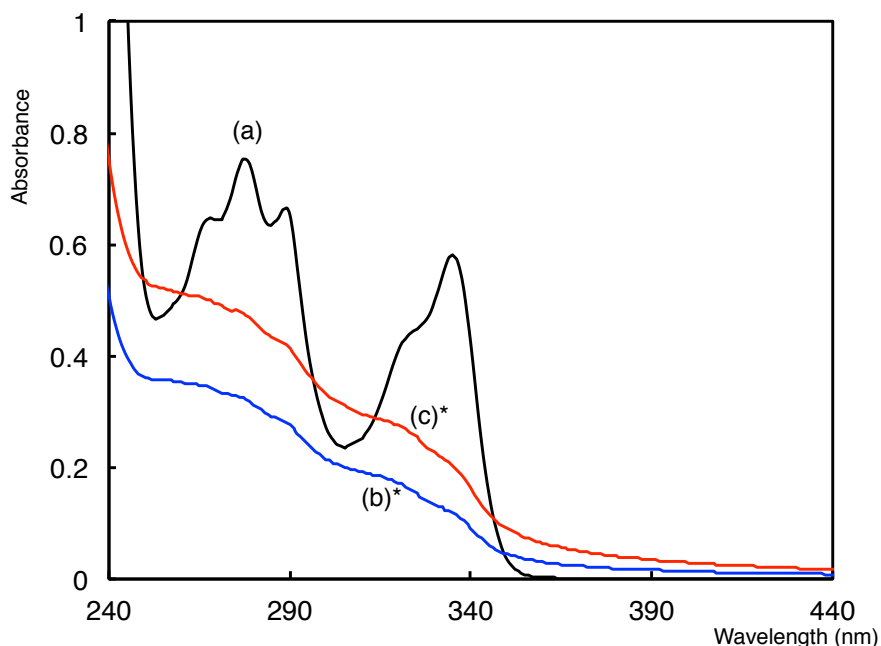


Fig. 2-14 UV-vis spectra of methanol solutions of original BINOL (3 mg/dm³) (a), R_F-(VM-SiO₂)_n/*an*-TiO₂ nanocomposites - encapsulated BINOL before calcination (1.5 g/dm³) (b)*, and R_F-(VM-SiO₂)_n/*an*-TiO₂ nanocomposites - encapsulated BINOL after calcination at 1000 °C (1.5 g/dm³) (Run 5 in Table 2-1) (c)*. *The supernatant solutions, which were obtained from the centrifugal separation of the corresponding well-dispersed methanol solutions.

R_F-(VM-SiO₂)_n-R_F/*an*-TiO₂/BPA and /BINOL nanocomposites before calcination were able to exhibit each clear absorption band related to BPA and BINOL around 280 nm, respectively (see Figs. 2-13 and 2-14). In particular interest, UV-vis spectra related to the released BPA and BINOL were observed around 280 nm from the well-dispersed methanol solutions of the composites even after calcination at 1000 °C. UV-vis absorption peaks related to the released BPA from the nanocomposites before and after calcination are different from that of parent BPA. This would be due to the presence of *an*-TiO₂ nanoparticles (λ_{max} : around 340 nm) in the composites. These findings suggest that encapsulated BPA and BINOL can exhibit a nonflammable characteristic in the fluorinated nanocomposite matrices even after

calcination at 800 °C.

UV-vis spectra of well-dispersed $R_F-(VM-SiO_2)_n-R_F/an-TiO_2/C_{60}$ nanocomposites (Run 7 in Table 2-1) aqueous methanol solutions were measured, and the results are displayed in Fig. 2-15. UV-vis spectra of the other composites (Runs 8 and 9 in Table 2-1) are shown in Figs. 2-16 and 2-17. The UV-vis spectra of the supernatant solution, which was obtained from the centrifugal separation of well-dispersed methanol solution of $R_F-(VM-SiO_2)_n-R_F/C_{60}$ nanocomposites (the preparative method of this nanocomposite: see Scheme 2-2) have been also measured, for comparison.

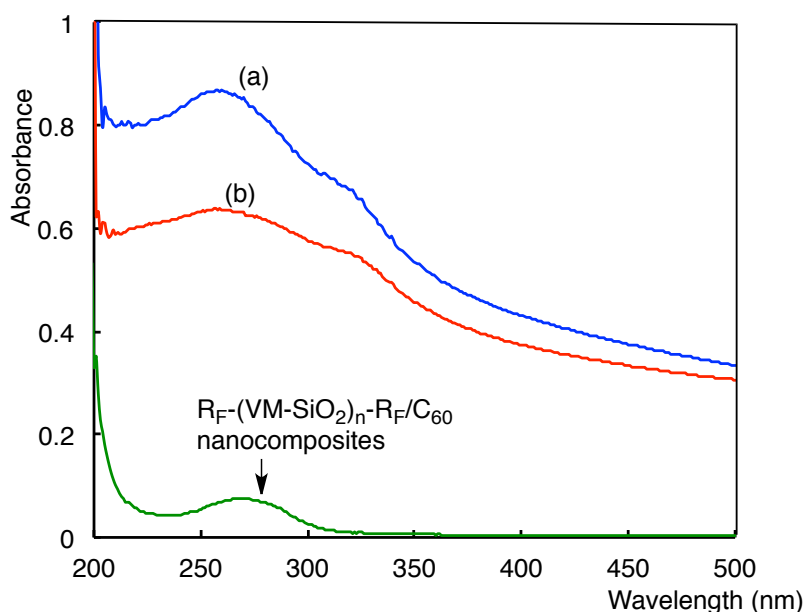


Fig. 2-15 UV-vis spectra of well-dispersed methanol/water (9/1: vol/vol) solutions of $R_F-(VM-SiO_2)_n-R_F/C_{60}$ nanocomposites (1.0 g/dm^3)*, $R_F-(VM-SiO_2)_n-R_F/an-TiO_2/C_{60}$ nanocomposites (25 mg/dm^3) before calcination (a) and $R_F-(VM-SiO_2)_n-R_F/an-TiO_2/C_{60}$ nanocomposites after calcination (b) at 1000 °C (25 mg/dm^3) (Run 7 in Table 2-1).
*the supernatant methanol solution.

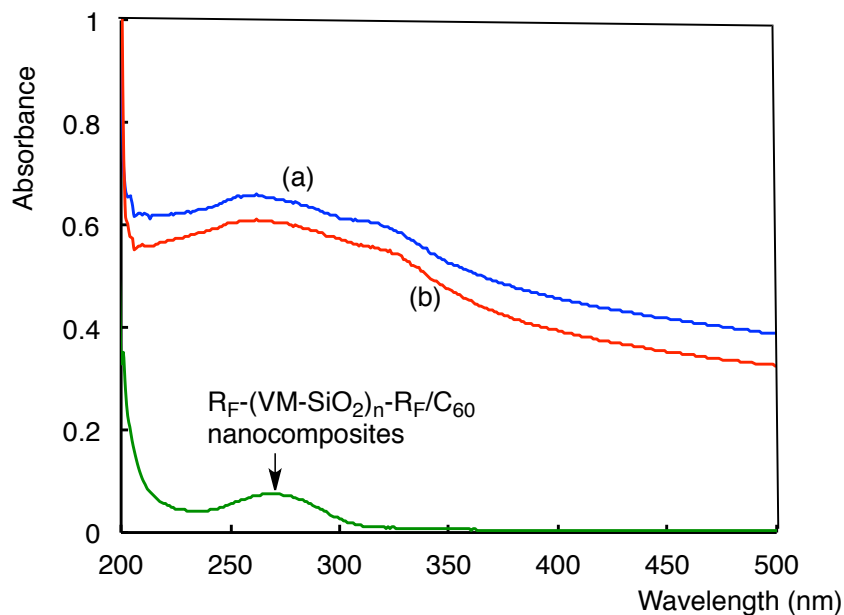


Fig. 2-16 UV-vis spectra of well-dispersed methanol/water (9/1: vol/vol) solutions of $R_F-(VM-SiO_2)_n-R_F/C_{60}$ nanocomposites (1.0 g/dm^3)*, $R_F-(VM-SiO_2)_n-R_F/an-TiO_2/C_{60}$ nanocomposites (25 mg/dm^3) before calcination (a) and $R_F-(VM-SiO_2)_n-R_F/an-TiO_2/C_{60}$ nanocomposites after calcination (b) at 1000°C (25 mg/dm^3) (Run 8 in Table 2-1).
*the supernatant methanol solution.

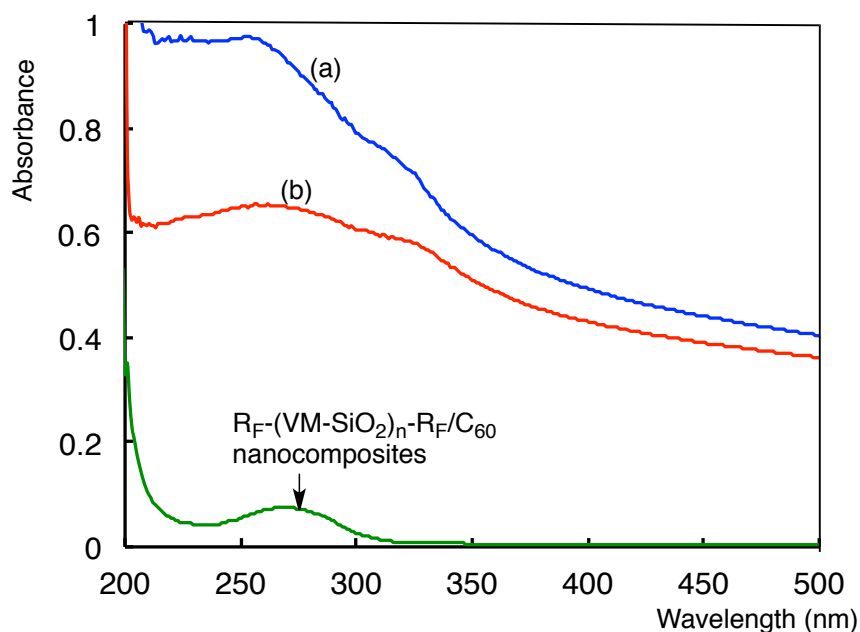
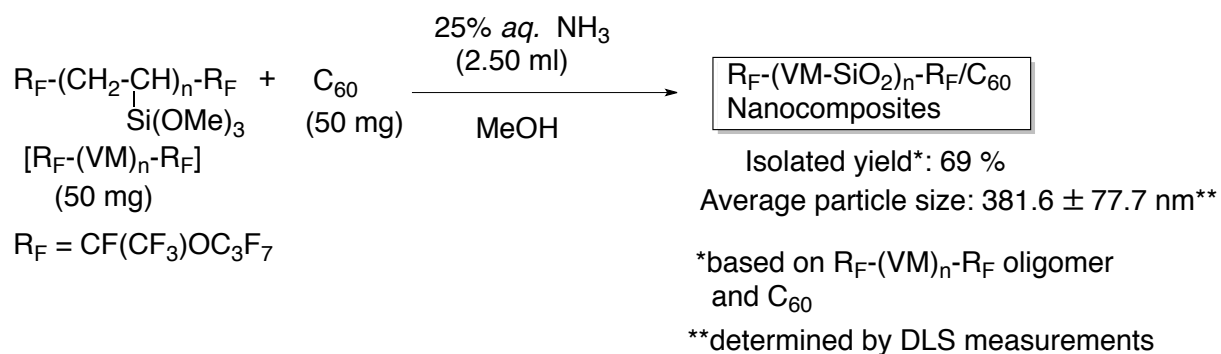


Fig. 2-17 UV-vis spectra of well-dispersed methanol/water (9/1: vol/vol) solutions of $R_F-(VM-SiO_2)_n-R_F/C_{60}$ nanocomposites (1.0 g/dm^3)*, $R_F-(VM-SiO_2)_n-R_F/an-TiO_2/C_{60}$ nanocomposites (25 mg/dm^3) before calcination (a) and $R_F-(VM-SiO_2)_n-R_F/an-TiO_2/C_{60}$ nanocomposites after calcination (b) at 1000°C (25 mg/dm^3) (Run 9 in Table 2-1).
*the supernatant methanol solution.



Scheme 2-2 Preparation of $\text{R}_F\text{-(VM-SiO}_2\text{)}_n\text{-R}_F/\text{C}_{60}$ nanocomposites.

$\text{R}_F\text{-(VM-SiO}_2\text{)}_n\text{-R}_F/\text{C}_{60}$ nanocomposites were obtained in 69 % isolated yield. The obtained composite afforded a good dispersibility in traditional organic solvents such as methanol, although the parent fullerene cannot give a dispersibility or solubility in methanol at all under similar conditions. DLS measurements show that the size of the composite is sub-micrometer size-controlled ($381.6 \pm 77.7 \text{ nm}$). This composite can exhibit a clear absorption peak around 270 nm related to the presence of fullerene (see Fig. 2-15 and Figs. 2-16, 2-17), and the content of fullerene in the composite was estimated to be 28 % by using TGA measurements (see Fig. 2-18).

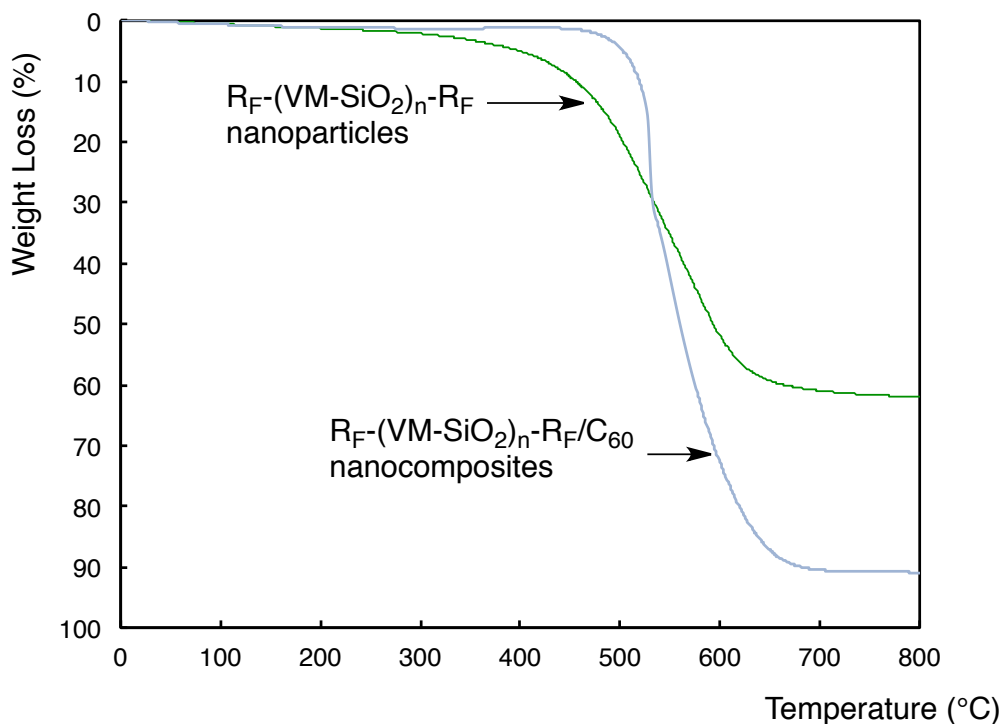


Fig. 2-18 Thermogravimetric analysis of $R_F-(VM-SiO_2)_n-R_F$ nanoparticles and $R_F-(VM-SiO_2)_n-R_F/C_{60}$ nanocomposites.

$R_F-(VM-SiO_2)_n-R_F/an-TiO_2/C_{60}$ nanocomposites (Runs 7 ~ 9 in Table 2-1) before calcination afforded not only the broad peak around 340 nm related to the presence of *an*- TiO_2 nanoparticles but also the similar absorption peak around 270 nm to that of $R_F-(VM-SiO_2)_n-R_F/C_{60}$ nanocomposites, indicating that fullerene should be encapsulated into $R_F-(VM-SiO_2)_n-R_F/an-TiO_2$ nanocomposite cores. However, an effective decrease of the absorption peaks related to the encapsulated fullerene has been observed after the calcination [see Figs. 2-15-(b) and Figs. 2-16-(b) ~ 2-17-(b)]. This finding suggests that fullerene could exhibit partially a flammable characteristic in the composite matrices during the calcination process.

It has been recently reported that $R_F-(VM-SiO_2)_n-R_F/an-TiO_2$ nanocomposites can keep the anatase TiO_2 structure even after calcination at 1000 °C, although the parent *an*- TiO_2 nanoparticles give a perfect phase transformation into rutile under similar conditions (see Fig. 2-19).²²⁾

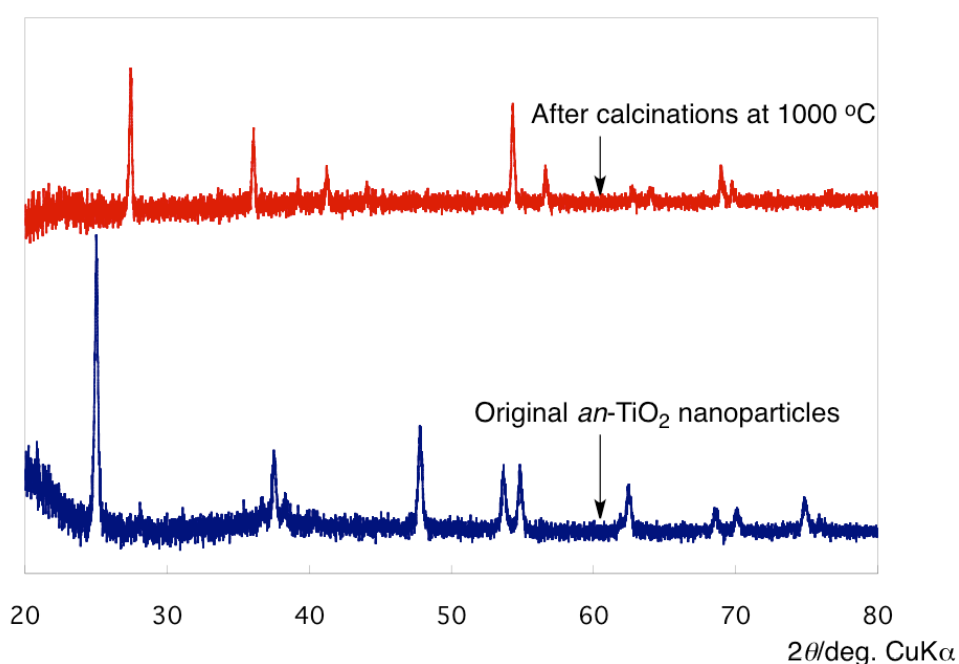


Fig. 2-19 X-ray diffraction patterns of original *an*- TiO_2 nanoparticles before and after calcinations at 1000 °C.

Thus, the XRD spectra of $R_F-(VM-SiO_2)_n-R_F/an-TiO_2/Ar-H$ nanocomposite in Table 2-1 have been studied, and the results were shown in Figs. 2-20 ~ 22.

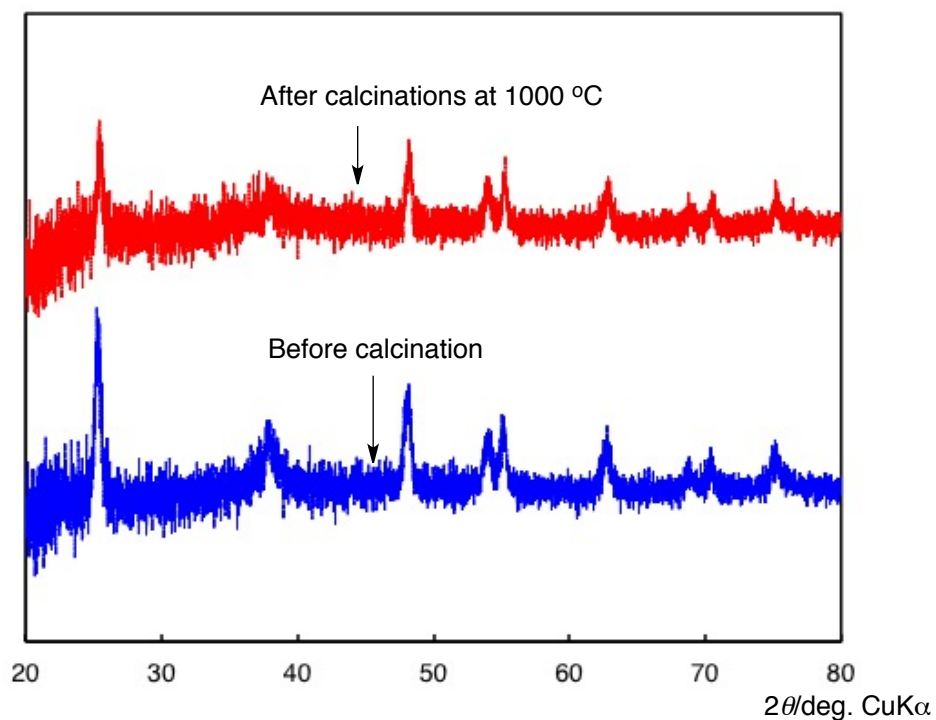


Fig. 2-20 X-ray diffraction patterns of $R_F-(VM-SiO_2)_n-R_F/an-TiO_2/BPA$ nanocomposites (Run1 in Table 2-1) before and after calcinations at 1000 °C.

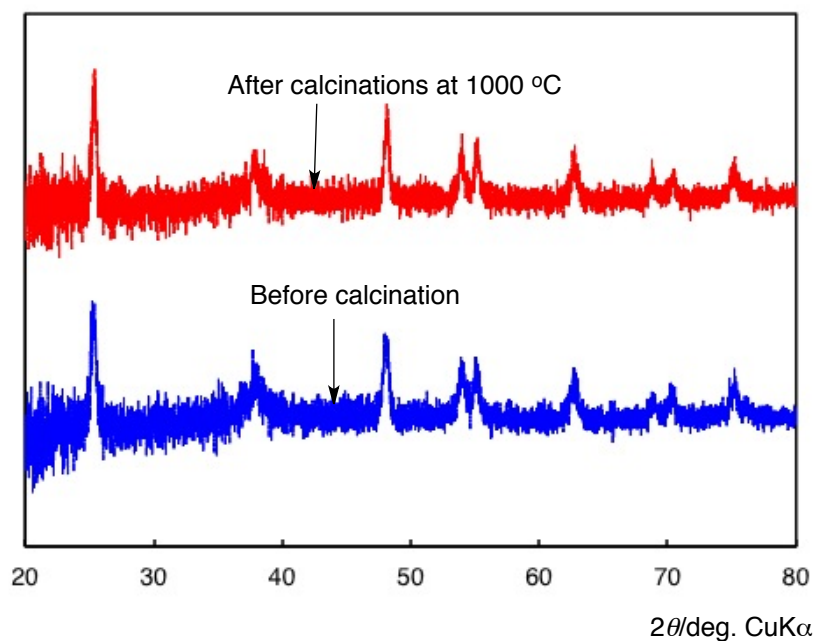


Fig. 2-21 X-ray diffraction patterns of $R_F-(VM-SiO_2)_n-R_F/an-TiO_2/BINOL$ nanocomposites (Run 4 in Table 2-1) before and after calcinations at 1000 °C.

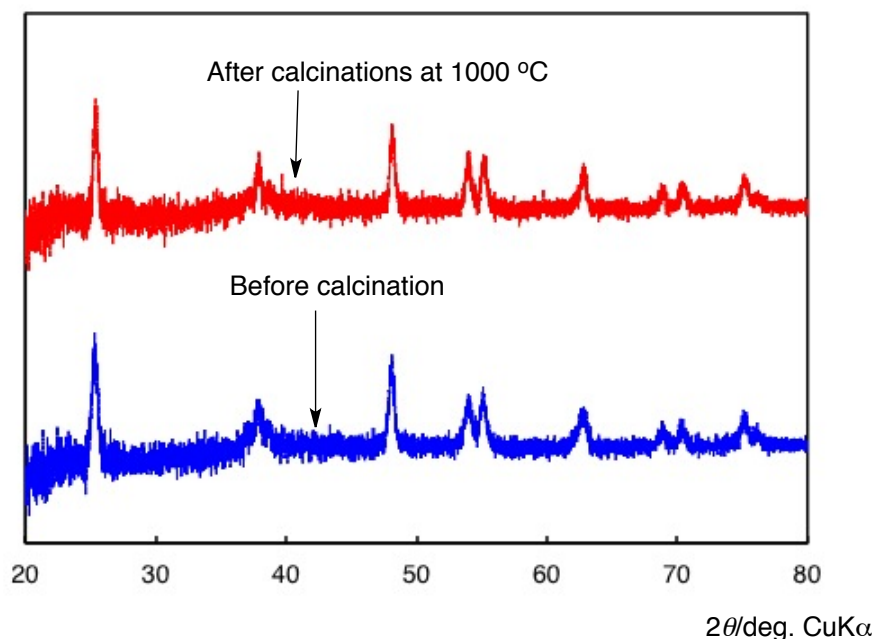


Fig. 2-22 X-ray diffraction patterns of $R_F-(VM-SiO_2)_n-R_F/an-TiO_2/C_{60}$ nanocomposites (Run 8 in Table 2-1) before and after calcinations at 1000 °C.

Figs. 2-20 ~ 22 show the XRD spectra of $R_F-(VM-SiO_2)_n-R_F/an-TiO_2/Ar-H$ nanocomposites (Runs 1, 4, and 8 in Table 2-1) before and after calcination at 1000 °C. The characteristic peaks of the nanocomposites before and after calcination were in completely agreement with those of the parent *an*-TiO₂ particles before calcination (Fig. 2-19), indicating that *an*-TiO₂ nanoparticles in the $R_F-(VM-SiO_2)_n-R_F/Ar-H$ nanocomposite cores can keep completely its structure without phase transformation into rutile even after calcination at 1000 °C. Usually, it is well-known that the phase transformation of titanium oxide from anatase to rutile is observed during calcination process from 600 to 750 °C.^{18~21)} However, titania-silica composite can keep the anatase structure at around 900 °C, although the rutile phase in this

composite appears at a calcination temperature of 1000 °C.^{31, 32)} This stabilization of anatase TiO₂ arises from the formation of Ti-O-Si interface to prevent the phase transformation to rutile.^{31, 32)} Thus, the present R_F-(VM-SiO₂)_n-R_F oligomeric nanocomposite lattice would lock the Ti-O species at the TiO₂ domains to prevent the phase transformation into rutile at 1000 °C.

2.3.2. Decolorization of methyl blue under UV light irradiation in the presence of fluoroalkyl end-capped vinyltrimethoxysilane oligomer/anatase titanium oxide nanocomposites - encapsulated ArH

The photocatalytic activity of R_F-(VM-SiO₂)_n-R_F/*an*-TiO₂/**Ar-H** nanocomposites before and after calcination at 1000 °C was evaluated in terms of the decolorization of methylene blue dye (MB) under UV light irradiation (λ_{max} 365 nm) in order to clarify the presence of *an*-TiO₂ in the present nanocomposites even after calcination at 1000 °C. The residual amounts of MB were estimated by the decrease of the absorbance at λ_{max} : 652 nm related to MB by UV light irradiation, and the results were summarized in Figs. 2-23 ~ 25.

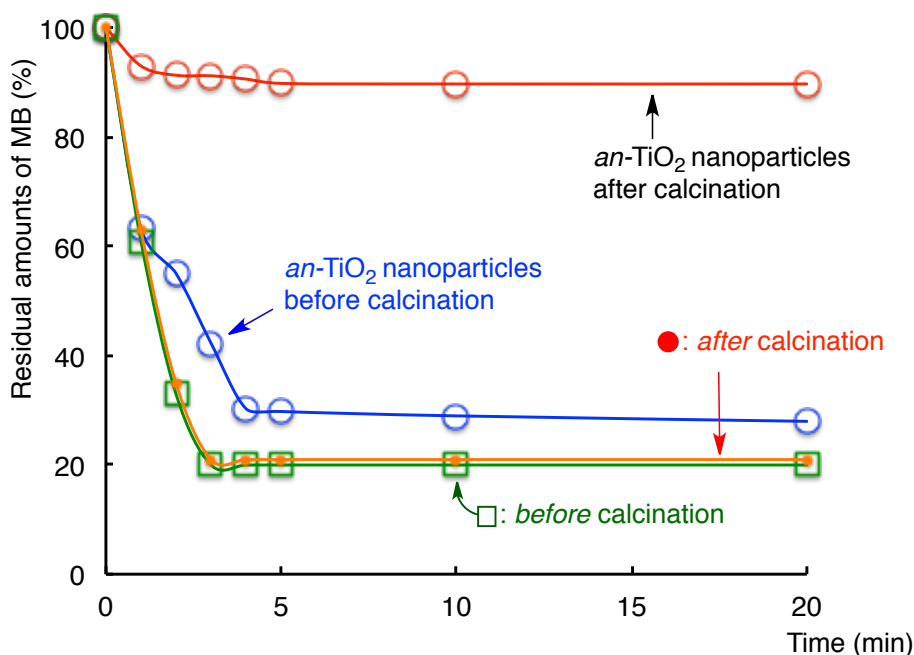


Fig. 2-23 Relationship between the residual amounts of MB and photoirradiation (λ_{\max} : 365 nm) time in the presence of $R_F-(VM-SiO_2)_n-R_F/an-TiO_2/BPA$ nanocomposites: Run 2 in Table 2-1 (or original $an-TiO_2$ nanoparticles) before and after calcination at 1000 °C : Concentration of MB: 2.5 mg/dm³; Concentration of nanocomposites (or original $an-TiO_2$ nanoparticles before and after calcination at 1000 °C): 25 mg/dm³.

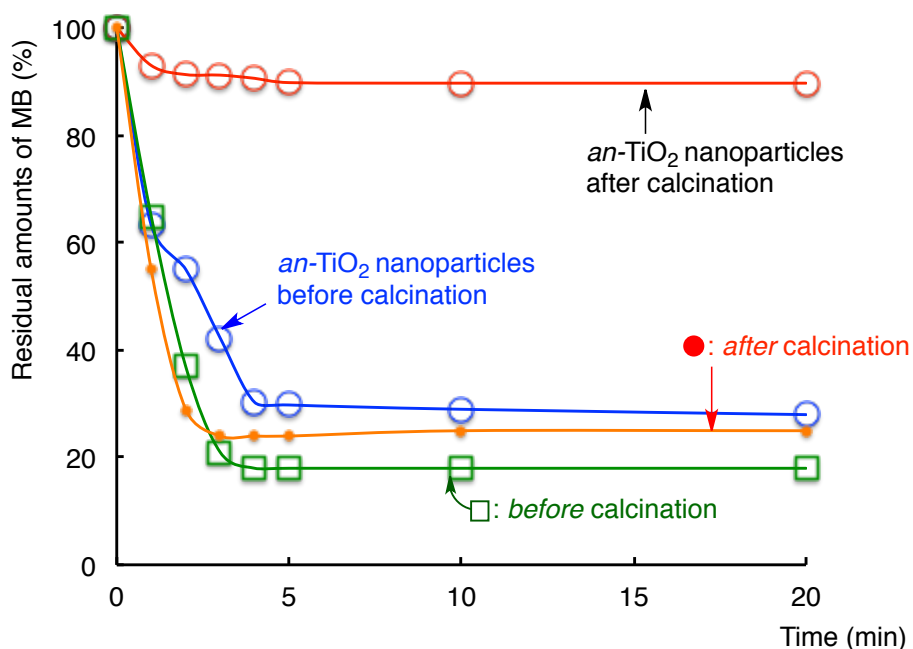


Fig. 2-24 Relationship between the residual amounts of MB and photoirradiation (λ_{\max} : 365 nm) time in the presence of $R_F-(VM-SiO_2)_n-R_F/an-TiO_2/BINOL$ nanocomposites: Run 4 in Table 2-1 (or original $an-TiO_2$ nanoparticles) before and after calcination at 1000 °C : Concentration of MB: 2.5 mg/dm³; Concentration of nanocomposites (or original $an-TiO_2$ nanoparticles before and after calcination at 1000 °C): 25 mg/dm³.

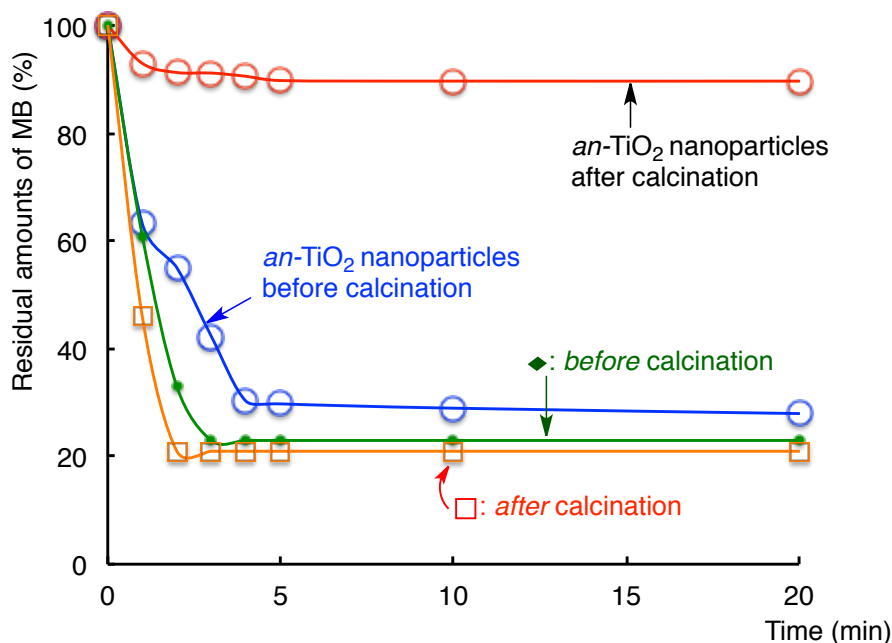


Fig. 2-25 Relationship between the residual amounts of MB and photoirradiation (λ_{max} : 365 nm) time in the presence of $R_F\text{-(VM-SiO}_2)_n\text{-}R_F/\text{an-TiO}_2/\text{C}_{60}$ nanocomposites: Run 7 in Table 2-1 (or original *an-TiO₂* nanoparticles) before and after calcination at 1000 °C : Concentration of MB: 2.5 mg/dm³; Concentration of nanocomposites (or original *an-TiO₂* nanoparticles before and after calcination at 1000 °C): 25 mg/dm³.

Original *an-TiO₂* nanoparticles before calcination can exhibit a good photocatalytic activity for the decolorization of MB, although the original *an-TiO₂* nanoparticles after calcination cannot give any photocatalytic activity even after 20 min-photoirradiation due to the phase transformation into rutile. However, interestingly, $R_F\text{-(VM-SiO}_2)_n\text{-}R_F/\text{an-TiO}_2/\text{Ar-H}$ nanocomposites before calcination were found to exhibit a higher photocatalytic activity for the decolorization of MB than that of the parent *an-TiO₂* nanoparticles before calcination under similar conditions. More interestingly, $R_F\text{-(VM-SiO}_2)_n\text{-}R_F/\text{an-TiO}_2/\text{Ar-H}$ nanocomposites after calcination were able to exhibit the same photocatalytic activity as that before calcination.

The contents (%) of TiO_2 in $\text{R}_F\text{-(VM-SiO}_2\text{)}_n\text{-R}_F\text{/an-TiO}_2\text{/Ar-H}$ nanocomposites before and after calcination at 1000 °C were estimated as followings by using EDX (Energy Dispersive X-ray) spectra measurements:

Run No*	Ar-H in $\text{R}_F\text{-(VM-SiO}_2\text{)}_n\text{-R}_F\text{/an-TiO}_2\text{/Ar-H}$ nanocomposites	before calcination	after calcination
Run 1	BPA	60 %	69 %
Run 2	BPA	65	67
Run 3	BPA	55	77
Run 4	BINOL	54	64
Run 5	BINOL	59	76
Run 6	BINOL	60	75
Run 7	C_{60}	69	74
Run 8	C_{60}	49	61
Run 9	C_{60}	50	67

*Each Run No corresponds to that of Table 2-1

The contents of TiO_2 in the composites before and after calcination were estimated to be

49 ~ 69 % and 61 ~ 77 %, respectively, indicating that the present $R_F-(VM-SiO_2)_n-R_F/an-TiO_2/Ar-H$ nanocomposites before and after calcination could give a superior photocatalytic activity to that of the original $an-TiO_2$ nanoparticles before calcination. Especially, the photocatalytic activity of $R_F-(VM-SiO_2)_n-R_F/an-TiO_2/Ar-H$ nanocomposites before and after calcination for the decoloring ability of MB under the initial UV light irradiation from 1 to 3 min were found to increase extremely compared with that of the parent $an-TiO_2$ nanoparticles or $R_F-(VM-SiO_2)_n-R_F/an-TiO_2$ nanocomposites as illustrated in Table 2-2.

Table 2-2 Relationship between the consumed amounts of MB (initial concentration: 2.5 mg/dm³) (%) and UV-light irradiation time (1 ~ 5 min) in the presence of $R_F-(VM-SiO_2)_n-R_F/an-TiO_2/Ar-H$ nanocomposites (25 mg/dm³).

Run*	Nanocomposites	Consumed MB (%)									
		UV light irradiation time									
		before calcination					after calcination at 1000 °C				
		1	2	3	4	5 (min)	1	2	3	4	5 (min)
	Original $an-TiO_2$ nanoparticles**	37	45	58	70	70	7	9	9	9	10
	$R_F-(VM-SiO_2)_n-R_F/an-TiO_2$ ***	21	34	45	57	71	20	32	43	54	64
1	$R_F-(VM-SiO_2)_n-R_F/an-TiO_2/BPA$	41	73	81	81	81	32	58	75	80	80
2		39	67	80	80	80	37	65	79	79	79
3		43	73	80	80	80	24	43	51	68	74
4	$R_F-(VM-SiO_2)_n-R_F/an-TiO_2/BINOL$	35	63	79	82	82	45	71	76	76	76
5		53	79	84	84	84	23	47	64	74	77
6		38	68	80	80	80	22	43	58	69	77
7	$R_F-(VM-SiO_2)_n-R_F/an-TiO_2/C_{60}$	34	66	76	76	76	70	78	78	78	78
8		39	67	77	77	77	54	79	79	79	79
9		38	65	74	76	76	45	75	80	80	80

*Run No corresponds to that of Table 2-1

**Concentration: 25 mg/dm³

***See Ref. 22

As shown in Table 2-2, the photocatalytic activity of $R_F-(VM-SiO_2)_n-R_F/an-TiO_2$ nanocomposites before and after calcination at 1000 °C at 1 ~ 3 min-photoirradiation for the decolorization of MB is not higher than that of original *an*-TiO₂ nanoparticles before calcination. However, interestingly, an extraordinarily higher photocatalytic activity for the decolorization of MB under the initial photoirradiation from 1 to 3 min was observed in $R_F-(VM-SiO_2)_n-R_F/an-TiO_2/Ar-H$ nanocomposites before and after calcination. In fact, the photocatalytic activity of $R_F-(VM-SiO_2)_n-R_F/an-TiO_2/BPA$ nanocomposites at 2 min-photoirradiation increased by about 2.1-fold, compared with that of $R_F-(VM-SiO_2)_n-R_F/an-TiO_2$ nanocomposites. A similar result was obtained in $R_F-(VM-SiO_2)_n-R_F/an-TiO_2/BINOL$ nanocomposites. More interestingly, the photocatalytic activity of $R_F-(VM-SiO_2)_n-R_F/an-TiO_2/C_{60}$ nanocomposites after calcination at 2 min-photoirradiation was found to increase by about 2.4-fold, compared with that of $R_F-(VM-SiO_2)_n-R_F/an-TiO_2$ nanocomposites under similar conditions. Previously, Wang, Zhao et al. reported the preparation of surface-fluorinated TiO₂ nanoparticles via the HF etching method.³³⁾ In this case, organic dyes such as Rhodamine B (RhB) preferentially anchors on pure TiO₂ surface through the carboxylic group in RhB, while its adsorption group is switched to the cationic moiety (-NEt₂ group) on surface-fluorinated TiO₂ through the electrostatic interaction between $F^{\delta-}-TiO_2$ and the cationic moiety in RhB.^{33, 34)}

Therefore, $R_F-(VM-SiO_2)_n-R_F/an-TiO_2$ nanocomposites should interact effectively with MB through the electrostatic interaction to give a good photocatalytic activity for the decolorization of MB. Especially, it was verified that the present $R_F-(VM-SiO_2)_n-R_F/an-TiO_2/Ar-H$ nanocomposites can exhibit an extraordinarily higher photocatalytic activity under the initial photoirradiation from 1 to 3 min than that of $R_F-(VM-SiO_2)_n-R_F/an-TiO_2$ nanocomposites. This finding would be due to the effective oleophilic-oleophilic interaction between the aromatic compounds in the fluorinated nanocomposites and MB. It was hitherto reported that fluorine-doped TiO_2 nanoparticles can enhance the photocatalytic activity, compared with that of original one, due to the formation of Ti-F species on the facets, especially surface terminating Ti-F bonds in the surface Ti-O-Ti networks.^{35 ~ 44)} Therefore, it is expected that the higher photocatalytic activity related to $R_F-(VM-SiO_2)_n-R_F/an-TiO_2/Ar-H$ nanocomposites even after calcination at 1000 °C would be partially due to the formation of Ti-F species in the nanocomposite matrices.

2.4. Conclusion

Fluoroalkyl end-capped vinyltrimethoxysilane oligomer/anatase titanium oxide nanocomposites - encapsulated low molecular weight aromatic compounds [**Ar-H**] such as

bisphenol A [BPA], 1,1'-bi(2-naphthol) [BINOL] and fullerene [R_F-(VM-SiO₂)_n-R_F/*an*-TiO₂/**Ar-H**] have been prepared by the sol-gel reactions of the corresponding oligomer in the presence of anatase TiO₂ nanoparticles (*an*-TiO₂) and **Ar-H** under alkaline conditions. These obtained composites were found to give a good dispersibility and stability for the traditional organic solvents such as methanol. FE-SEM and DLS measurements show that these composites before and after calcination at 1000 °C are nanometer size-controlled fine particles. TGA measurements show that encapsulated aromatic compounds such as BPA and BINOL, in which the theoretical contents in the composites are 25 ~ 32 %, can exhibit no weight loss corresponding to the contents of the aromatic compounds in the composites even after calcination at 800 °C. On the other hands, the encapsulated fullerene in the composites gave weight loss behavior related to the presence of fullerene in the composites after calcination at 800 °C; however, UV-vis spectra showed the presence of the residual fullerene in the composites even after calcination. XRD spectra of R_F-(VM-SiO₂)_n-R_F/*an*-TiO₂/**Ar-H** nanocomposites preserved completely its structure without phase transformation into rutile even after calcination at 1000 °C, although the parent anatase TiO₂ nanoparticles underwent a complete phase transformation into rutile under the same calcination conditions. Interestingly, an extremely higher photocatalytic activity for the decolorization of MB under the initial photoirradiation from 1 to 3 min, was observed in

$R_F-(VM-SiO_2)_n-R_F/an-TiO_2/Ar-H$ nanocomposites, compared with that of $R_F-(VM-SiO_2)_n-R_F/an-TiO_2$ nanocomposites under similar conditions. In fact, the photocatalytic activity of $R_F-(VM-SiO_2)_n-R_F/an-TiO_2/Ar-H$ nanocomposites before calcination were found to increase by about 2.0-fold at 2 min-photoirradiation, compared with that of $R_F-(VM-SiO_2)_n-R_F/an-TiO_2$ nanocomposites under similar conditions. Especially, $R_F-(VM-SiO_2)_n-R_F/an-TiO_2/fullerene$ nanocomposites after calcination enabled its photocatalytic activity to increase by about 2.5-fold at 2 min-photoirradiation, compared with that of $R_F-(VM-SiO_2)_n-R_F/an-TiO_2$ nanocomposites. In this way, the thermally stable $R_F-(VM-SiO_2)_n-R_F/an-TiO_2/Ar-H$ nanocomposites will have high potential for the applications to a variety of fields such as dye sensitized solar cell, because these nanocomposites can exhibit good photocatalytic activity relative to anatase titanium oxide even after calcinations appropriately at 1000 °C, and the encapsulated aromatic compounds such as BPA and BINOL in these nanocomposites can exhibit an extraordinarily thermal stable characteristic.

References

- 1) M. Arellano, I. Mickel-Haciski, D. L. Feke, and I. Manas-Zloczower, *J. Coat. Technol.*, **68**, 83 (1996).
- 2) P. A. Hartley, G. D. Parfitt, and L. B. Pollack, *Powder Technol.*, **42**, 35 (1985).
- 3) A. Millis and S.-K. Lee, *J. Photochem. Photobiol. A: Chem.*, **130**, 163 (2000).
- 4) A. Mills, G. Hill, S. Bhopal, I. P. Parkin, and S. A. O'Neill, *J. Photochem. Photobiol. A: Chem.*, **160**, 185 (2003).
- 5) Y. Zhu, L. Zhang, W. Yao, and L. Cao, *Appl. Surf. Sci.*, **158**, 32 (2000).
- 6) J. C. Yu, J. Yu, and J. Zhao, *Appl. Catal. B.*, **36**, 31 (2002).
- 7) J. S. Reddy and R. Kumar, *J. Catal.*, **130**, 440 (1991).
- 8) H. Sawada, E. Sawada, H. Kakehi, T. Kariya, M. Mugisawa, Y. Chounan, M. Miura, and N. Isu, *Polym. Compos.*, **30**, 1848 (2009).
- 9) E. Sawada, H. Kakehi, Y. Chounan, M. Miura, Y. Sato, N. Isu, and H. Sawada, *Compos. Part B*, **41**, 498 (2010).
- 10) A. L. Linsebigler, G. Q. Lu, and J. T. Yates, *Chem. Rev.*, **95**, 735 (1995).
- 11) M. A. Fox and M. T. Dulay, *Chem. Rev.*, **93**, 341 (1993).
- 12) K. E. Karakitsou and X. E. Verykios, *J. Phys. Chem.*, **97**, 1184 (1993).

- 13) M. R. Hoffmann, S. T. Martin, W. Choi, and D. W. Bahnemann, *Chem. Rev.*, **95**, 69 (1995).
- 14) M. Gratzel, *Nature*, **414**, 338 (2001).
- 15) B. O'Regan and M. Gratzel, *Nature*, **353**, 737 (1991).
- 16) A. L. Linsebigler, G. Q. Lu, and J. T. Yates, *Chem. Rev.*, **95**, 735 (1995).
- 17) S. Liu and A. Chen, *Langmuir*, **21**, 8409 (2005).
- 18) D. A. H. Hanaor and C. C. Sorrell, *J. Mater. Sci.*, **46**, 855 (2011).
- 19) X. Peng and A. Chen, *Adv. Funct. Mater.*, **16**, 1355 (2006).
- 20) G. Madras, B. J. McCoy, and A. Navrotsky, *J. Am. Ceram. Soc.*, **90**, 250 (2007).
- 21) G. Wu, J. Wang, D. F. Thoma, and A. Chen, *Langmuir*, **24**, 3503 (2008).
- 22) S. Guo, H. Yoshioka, H. Kakehi, Y. Kato, M. Miura, N. Isu, B. Ameduri, and H. Sawada, *J. Colloid Interface Sci.*, **387**, 141 (2012).
- 23) H. Sawada and M. Nakayama, *J. Chem. Soc., Chem. Commun.*, 677 (1991).
- 24) H. Sawada, Y. Matsuki, Y. Goto, S. Kodama, M. Sugiya, and Y. Nishiyama, *Bull. Chem. Soc. Jpn.*, **83**, 75 (2010).
- 25) H. Sawada, H. Kakehi, T. Tashima, Y. Nishiyama, M. Miura, and N. Isu, *J. Appl. Polym. Sci.*, **112**, 3482 (2009).
- 26) H. Sawada, T. Tashima, and S. Kodama, *Polym. Adv. Technol.*, **19**, 73 (2008).

- 27) H. Sawada, T. Narumi, S. Kodama, M. Kamijo, R. Ebara, M. Sugiya, and Y. Iwasaki, *Colloid Polym. Sci.*, **285**, 977 (2007).
- 28) H. Sawada, T. Tashima, H. Kakehi, Y. Nishiyama, M. Kikuchi, M. Miura, Y. Sato, and N. Isu, *Polym. J.*, **42**, 167 (2010).
- 29) H. Sawada, T. Tashima, Y. Nishiyama, M. Kikuchi, G. Kostov, Y. Goto, and B. Ameduri, *Macromolecules*, **44**, 1114 (2011).
- 30) H. Sawada, M. Kikuchi, and M. Nishida, *J. Polym. Sci. Part A: Polym. Chem.*, **49**, 1070 (2011).
- 31) A. Hilonga, J.-K. Kim, P. B. Sarawade, and H. T. Kim, *J. Mater. Sci.*, **45**, 1255 (2010).
- 32) A. Hilonga, J.-K. Kim, P. B. Sarawade, and H. T. Kim, *J. Mater. Sci.*, **45**, 1264 (2010).
- 33) Q. Wang, C. Chen, D. Zhao, W. Ma, and J. Zhao, *Langmuir*, **24**, 7338 (2008).
- 34) S. Liu, J. Yu, B. Cheng, and M. Jaroniec, *Adv. Colloid Interface Sci.*, **173**, 35 (2012).
- 35) G. Liu, C. Sun, H. G. Yang, S. C. Smith, L. Wang, G. Q. Lu, and H.-M. Cheng, *Chem. Commun.*, **46**, 755 (2010).
- 36) W. Ho, J. C. Yu, and S. Lee, *Chem. Commun.*, 1115 (2006).
- 37) H. Zhang, P. Liu, P. F. Li, H. Liu, Y. Qang, S. Zhang, M. Guo, H. Cheng, and H. Zhao, *Chem. Eur. J.*, **17**, 5949 (2011).
- 38) D. Zhang, G. Li, X. Yang, and J. C. Yu, *Chem. Commun.*, 4381 (2009).

- 39) G. Wu, J. Wang, D. F. Thomas, and A. Chen, *Langmuir*, **24**, 3503 (2008).
- 40) M. Liu, L. Zhao, S. Ju, Z. Yan, T. He, C. Zhou, and W. Wang, *Chem. Commun.*, **46**, 1664 (2010).
- 41) X. Han, Q. Kuang, M. Jin, Z. Xie, and L. Zheng, *J. Am. Chem. Soc.*, **131**, 3152 (2009).
- 42) G. H. Yang, G. Liu, S. Z. Qiao, C. H. Sun, Y. G. Jin, S. C. Smith, J. Zou, H. M. Cheng, and G. Q. Lu, *J. Am. Chem. Soc.*, **131**, 4078 (2009).
- 43) D. Li, H. Haneda, N. K. Labhsetwar, S. Hishita, and N. Ohashi, *Chem. Phys. Lett.*, **401**, 579 (2005).
- 44) J. C. Yu, J. Yu, W. Ho, Z. Jiang, and L. Zhang, *Chem. Mater.*, **14**, 3808 (2002).

CHAPTER 3

Photocatalytic Activity of Vinylidene Fluoride - containing Copolymers/Anatase Titanium Oxide/Silica Nanocomposites

3.1. Introduction

Titanium oxide (TiO_2) is the most important white pigment involved in coating and plastic industry because of the high refractive index of TiO_2 nanoparticles ($n_D \sim 2.6$), which enables it to produce high gloss composites.¹⁾ It is widely used because it efficiently scatters visible light, thereby imparting whiteness, brightness, and opacity when incorporated in coatings, as well as in cosmetics and toothpastes. It has been utilized in many applications ranging from photocatalysis,²⁾ catalyst supports,³⁾ dye-sensitized solar cells,⁴⁾ semiconductors and capacitors,⁵⁾ photovoltaics,⁶⁾ ductile ceramics,⁷⁾ lithium ion batteries (LIB)⁸⁾ (especially anatase, rutile, and brookite polymorphs are promising structures for anode materials in LIB), and to gas sensors.⁹⁾ In addition, organic polymer matrices containing dispersed TiO_2 oxide nanoparticles have found a practical use for mediating photochemical process in membranes, catalytic sensors, and photosensitive materials and for stimulating numerous biochemical and biophysical process.^{10, 11)} However, the dispersion of the nanoparticles uniformly throughout organic polymeric matrices is an issue, because the nanoparticles can easily agglomerate or coalesce forming large particles which result in a reversed effect on the catalyst efficiency.^{12,}
¹³⁾ In their comprehensive review, Fröschl *et al.*⁵⁾ reported selective synthetic methods towards TiO_2 nano-materials and these authors mentioned that TiO_2 displays various phases: amorphous, rutile, anatase and brookite. The last one has been involved in various

applications, especially for electrochemical Lithium insertion.¹⁴⁾ A few polymer/TiO₂ composites have been reported in the literature, for example by Thomas *et al.*^{15 ~ 18)} who used isotactic polystyrene,¹⁵⁾ natural rubber-EPDM,¹⁶⁾ nitrile rubber,¹⁷⁾ and also synthesized natural rubber/nano SiO₂/TiO₂ composites.¹⁸⁾ In addition, Chu *et al.*¹⁹⁾ described original PEO-*b*-PPO-*b*-PEO triblock copolymer/TiO₂ composites. As a matter of fact, fluorinated polysoaps are well-known to exhibit a superior surface active property than that of the corresponding non-fluorinated homologues.^{20 ~ 21)} Thus, it was of particular interest to develop fluorinated polymers/TiO₂ nanocomposites that possess satisfactory dispersibility and stability. Actually, only a few publications focus on the fluoropolymers/TiO₂ composites based on poly(tetrafluoroethylene), PTFE,²²⁾ poly(vinylidene fluoride), PVDF,²³⁾ poly(fluoroacrylate)s,²⁴⁾ fluoroalkyl end capped polymers (that displayed good dispersibility and stability in various solvents),²⁵⁾ poly(TFE-*co*-HFP) copolymer,²⁶⁾ and poly(VDF-*co*-TrFE) copolymer²⁷⁾ (where HFP and TrFE stand for hexafluoropropylene and trifluoroethylene, respectively). In addition, anatase titanium oxide (*an*-TiO₂) seems to behave as a more efficient photocatalyst than the rutile one. However, *an*-TiO₂ can be irreversibly modified into rutile *an*-TiO₂ at elevated temperatures.^{28 ~ 30)} Concerning the thermally stable TiO₂ nanocomposites for various applications, it was worth exploring new fluorinated (co)polymers/*an*-TiO₂ nanocomposites that possess not only a good dispersibility in solvents

as well as satisfactory chemical and thermal stabilities but also a higher photocatalytic activity without any phase transformation into rutile under higher temperature conditions. It has been hitherto reported that the fluorination of TiO_2 , involving either fluorine adsorption or lattice fluorine-doping, is effective for the enhancement of the photocatalytic activity of TiO_2 ,^{31 ~ 35)} compared to that of the original TiO_2 . Therefore, it is expected that reactions of *an*- TiO_2 nanoparticles with fluorinated polymers to generate original composites should enhance the photocatalytic property of *an*- TiO_2 in the resulting fluorinated copolymers/ TiO_2 composites. The present study attempts to investigate if fluorinated copolymers may enhance not only the photocatalytic ability of *an*- TiO_2 but also the thermal stability of these fluorinated copolymers through reactions of these corresponding copolymers with *an*- TiO_2 nanoparticles and SiO_2 nanoparticles. In particular, it was of interest to investigate if original resulting fluorinated copolymers/silica/*an*- TiO_2 nanocomposites could enable to preserve the *an*- TiO_2 structure after calcination at 1000 °C and display a good photocatalytic activity imparted by such a nanofiller within the composites. These are the objectives of this present study.

3.2. Experimental

3.2.1 Measurements

Molecular weights of VDF copolymers were assessed at 40 °C by using SEC with columns 2HR5E and 1HR2E types with DMF/LiBr in 0.1 mol.l⁻¹ as the eluent with an isocratic pump and PMMA standards. Dynamic light-scattering (DLS) measurements were carried out using Otsuka Electronics DLS-7000 HL (Tokyo, Japan). Field emission scanning electron micrographs (FE-SEM) and energy dispersive X-ray (EDX) spectra were obtained using JEOL JSM-7000F (Tokyo, Japan). X-ray diffraction (XRD) measurements were performed by the use of Mac Science M18XHF-SRA (Tokyo, Japan). ¹H NMR spectra were recorded using JEOL JNM-400 (400 MHz) FT NMR SYSTEM (Tokyo, Japan). ¹⁹F NMR spectra were recorded on Bruker AC 400 instruments in DMF- *d*₇ with CFCl₃ as the reference. The experimental conditions for recording ¹H (or ¹⁹F) NMR spectra were as follows: flip angle 90° (or 30°), acquisition time 4.5 s (or 0.7 s), pulse delay 2 s (or 2 s), number of scans 128 (or 512, and 1024 for ¹³C NMR), and a pulse width of 5 μs for ¹⁹F NMR.

Thermal analyses were carried out by raising the temperature up to around 800 °C, at a heating rate of 10 °C.min⁻¹, under air atmospheric conditions, by the use of Bruker axs

TG-DTA2000SA differential thermobalance (Kanagawa, Japan).

3.2.2. Materials

Titanium oxide nanoparticles (average particle size: 20 nm) were received from Ishihara Sangyo Kaisha Ltd. (Osaka, Japan). Vinylidene fluoride (VDF) copolymers, poly(VDF-*co*-CF₂CFCO₂CH₃)³⁶⁾, poly(VDF-*co*-CFHCFCO₂H)³⁷⁾, and poly(VDF-*co*-CF₂CF(CH₂)₃OCOCH₃)³⁸⁾ copolymers were prepared by reported methods of conventional free radical copolymerizations of vinylidene fluoride (VDF) with F₂C=CO₂CH₃, FCH=CFCO₂H, and F₂C=CF(CH₂)₃OCOCH₃ comonomers, respectively. Their molecular weights (assessed by size exclusion chromatography) were ca. 50,000 g.mol⁻¹ (with poly(methyl methacrylate), PMMA standards) while their microstructures (i.e. the mol. contents of VDF and fluorinated functional comonomers in the copolymers) were determined by ¹⁹F NMR spectroscopy.

3.2.3. Preparation of poly(VDF-*co*-M₂) copolymer/silica/anatase titanium oxide nanocomposites

A typical procedure for the preparation of fluorinated copolymers/silica/anatase TiO₂ nanocomposites is as follows: to a methanol solution (20 ml) of a fluorinated copolymer (number average molecular weight, $M_n = 50.000 \text{ g.mol}^{-1}$, 250 mg) were added 250 mg of *an*-TiO₂ nanoparticles, 0.25 ml of tetraethoxysilane (TEOS), silica nanoparticles average particle size of 11 nm (wt.) 30 %, THF [1.60 g; (Methanol Silica-sol (TR))], and 0.25 ml of 25 % aqueous ammonia solution. The mixture was stirred with a magnetic stirring bar at room temperature for 5 h, and then was centrifuged for 30 min. The fluorinated copolymer/TiO₂ nanocomposites were easily separated from the methanol solution. Methanol (20 mL) was added to the obtained total product mixture and the methanol solution was stirred at room temperature for 1 day. After centrifugal separation of the mixture, the obtained product was dried under vacuum at 50 °C for 2 days to produce purified white fluorinated composite powders (560 mg). The different weights of reactants, yields, and particles sizes of other FP/TiO₂ and FP/SiO₂/TiO₂ composites are listed in Table 1.

3.2.4. Discoloration of methylene blue under UV light irradiation in the presence of fluorinated copolymers/silica/anatase titanium oxide nanocomposites

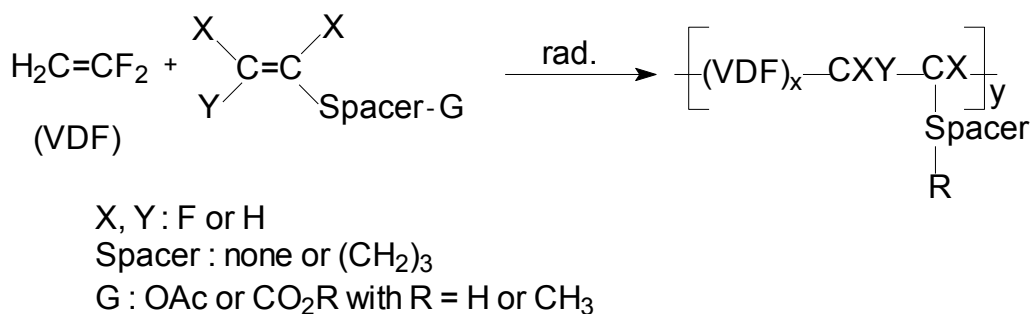
Methanol or DMF solution (0.8 mL) of methylene blue (10 mg.dm^{-3}) and well-dispersed

fluorocopolymer/silica/*an*-TiO₂ nanocomposites (200 mg.dm⁻³) methanol (or DMF) solution (0.4 mL) were added in 2 mL THF solution. UV-vis spectra of the suspension methanol solution thus obtained exhibited absorption bands around 652 nm assigned to methylene blue dye. The discoloration of methylene blue dye was examined by irradiating this suspension solution with UV lamp (λ_{max} : 365 nm) for 20 min at room temperature.

3.3. Results and discussion

3.3.1. Preparation of poly(VDF-*co*-M) Copolymer/*an*-TiO₂ Nanocomposites and poly(VDF-*co*-M) Copolymer/SiO₂/*an*-TiO₂ Nanocomposites

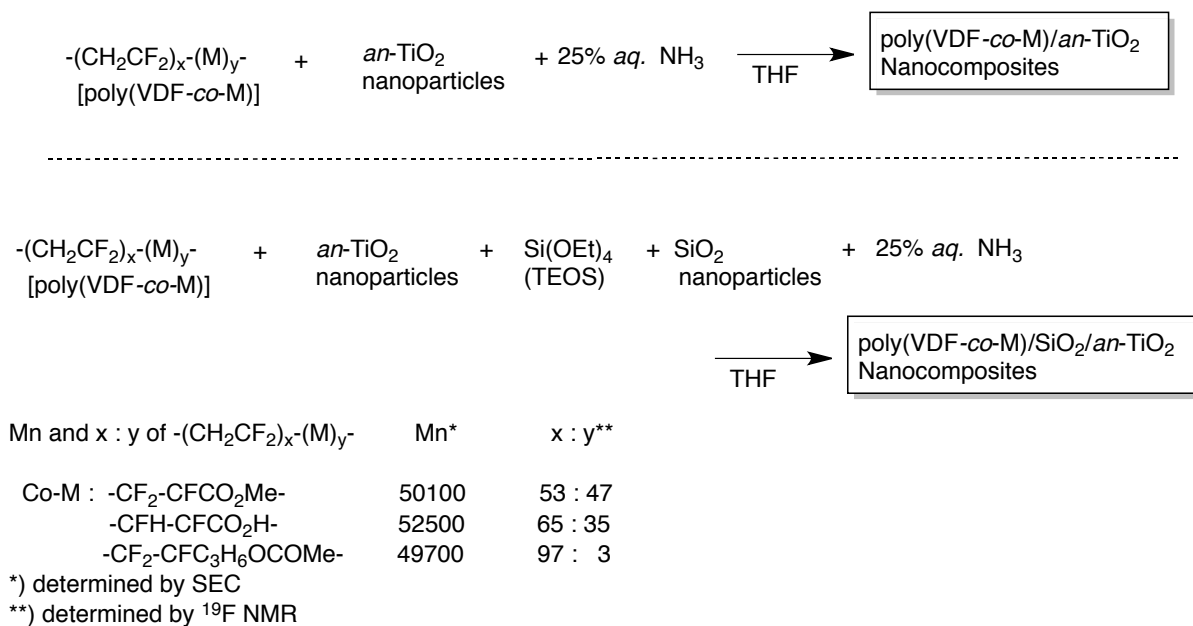
The radical copolymerizations of vinylidene fluoride (VDF) with various functional comonomers, F₂C=CFCO₂CH₃, FCH=CFCO₂H, and F₂C=CF(CH₂)₃OCOCH₃ were initiated by *t*-butyl peroxyvalate at 70 °C, and led to statistical poly(VDF-*co*-CF₂CFCO₂CH₃)³⁶⁾, poly(VDF-*co*-FCHCFCO₂H)³⁷⁾, and poly(VDF-*co*-CF₂CFC₃H₆OCOCH₃) copolymers³⁸⁾ in satisfactory yields (> 60 %) (see Scheme 3-1).



Scheme 3-1 Free radical copolymerization of vinylidene fluoride (VDF) with functional fluorinated XYC=CX-spacer-G comonomer.

After reaction and precipitation in cold pentane (or water), the molecular weights of the resulting poly(VDF-*co*-M) copolymers were ca. 50,000 g.mol⁻¹ (assessed by size exclusion chromatography with PMMA standards).^{36~38)} The ratios of the integrals of the ¹⁹F NMR signals corresponding to both comonomers enabled to determine the molar percentages of these fluorinated comonomers in each VDF-containing copolymer.

Then, VDF copolymers/*an*-TiO₂ nanocomposites and VDF copolymers/SiO₂/*an*-TiO₂ nanocomposites were prepared under slightly basic conditions that enable crosslinking³⁹⁾ in mild conditions enough to avoid any dehydrofluorination of VDF units (see Scheme 3-2). The results are presented in Table 3-1.



Scheme 3-2 Preparation of poly(VDF-*co*-M)/an-TiO₂ nanocomposites and poly(VDF-*co*-M)/SiO₂/an-TiO₂ nanocomposites.

Nanocomposite formations involving poly(VDF-*co*-M) copolymers were found to proceed under slightly alkaline conditions to give the expected poly(VDF-*co*-M)/an-TiO₂ and poly(VDF-*co*-M)/SiO₂/an-TiO₂ nanocomposites in 31-68 % isolated yields (see Scheme 3-2 and Table 3-1).

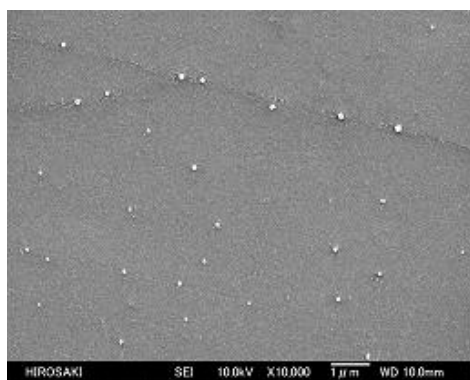
Table 3-1 Preparation of poly(VDF-*co*-M)/*an*-TiO₂ nanocomposites and poly(VDF-*co*-M)/SiO₂/*an*-TiO₂ nanocomposites.

Run	poly(VDF- <i>co</i> -M) (mg)	<i>an</i> -TiO ₂ (mg)	TEOS (ml)	SiO ₂ (mg)	aq. NH ₃ (ml)	Product yield ^{a)} (%)	Size of composites ^{b)} (after calcination) (nm) ± STD
M: CF ₂ =CFCO ₂ Me							
1	400	500	-	-	0.25	57	27.9 ± 5.8 (30.2 ± 7.3)
2	250	250	0.25	480	0.25	31	23.4 ± 5.5 (46.3 ± 10.3)
M: CHF=CFCO ₂ H							
3	400	500	-	-	0.25	59	39.1 ± 8.7 (24.9 ± 6.3)
4	250	250	0.25	480	0.25	36	143.2 ± 30.6 (143.8 ± 32.7)
M: CF ₂ =CFC ₃ H ₆ OCOMe							
5	400	500	-	-	0.25	68	26.1 ± 5.6 (32.8 ± 5.4)
6	250	250	0.25	480	0.25	40	21.8 ± 5.3 (18.1 ± 4.4)

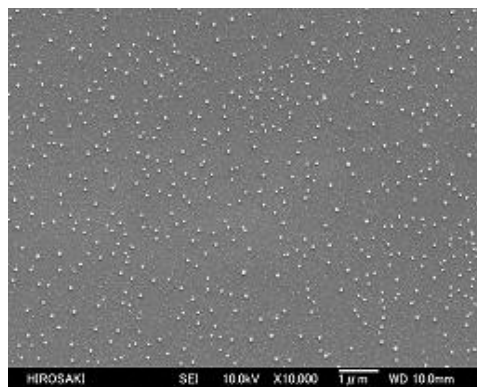
a) Yield based on poly(VDF-*co*-M) and TiO₂ (or TEOS or SiO₂ nanoparticles).

b) Determined by DLS (dynamic light scattering) measurements in methanol solutions.

Interestingly, under these mild conditions, poly(VDF-*co*-functional comonomer) copolymers did not undergo any dehydrofluorination as reported in a previous work ⁴⁰⁾ and these obtained nanocomposites exhibited good dispersibility and stability in methanol, ethanol and tetrahydrofuran. The sizes of the obtained composites before and after calcination at 1000 °C assessed by DLS were nanometer size-controlled (18-144 nm). FE-SEM images of poly(VDF-*co*-CF₂CFCO₂Me) copolymer/SiO₂/*an*-TiO₂ composites (Run 2 in Table 3-1) also show the formation of fine nanoparticles with the almost same sizes before (90 nm) and after (54 nm) calcination (see Fig. 3-1). Interestingly, the white color of the nanocomposite powders did not change before and after calcination at 1000 °C.



a) Before calcination
mean of particle size: 90 nm



b) After calcination
mean of particle size: 54 nm

Fig. 3-1 FE-SEM (Field Emission-Scanning Electron Microscopy) images of methanol solutions of poly(VDF-*co*-CF₂CFCO₂Me)/SiO₂/*an*-TiO₂ nanocomposites before and after calcination at 1000 °C (used sample: Run 2 in Table 3-1).

The XRD spectra of poly(VDF-*co*-M) copolymers/*an*-TiO₂ nanocomposites (Figs. 3-2, 3-3 and Fig. 3-4) and poly(VDF-*co*-M) copolymer/SiO₂/*an*-TiO₂ nanocomposites (Figs. 3-5 ~ 3-7) before and after calcination at 1000 °C (Table 3-1) were compared to those of pristine *an*-TiO₂ nanoparticles.

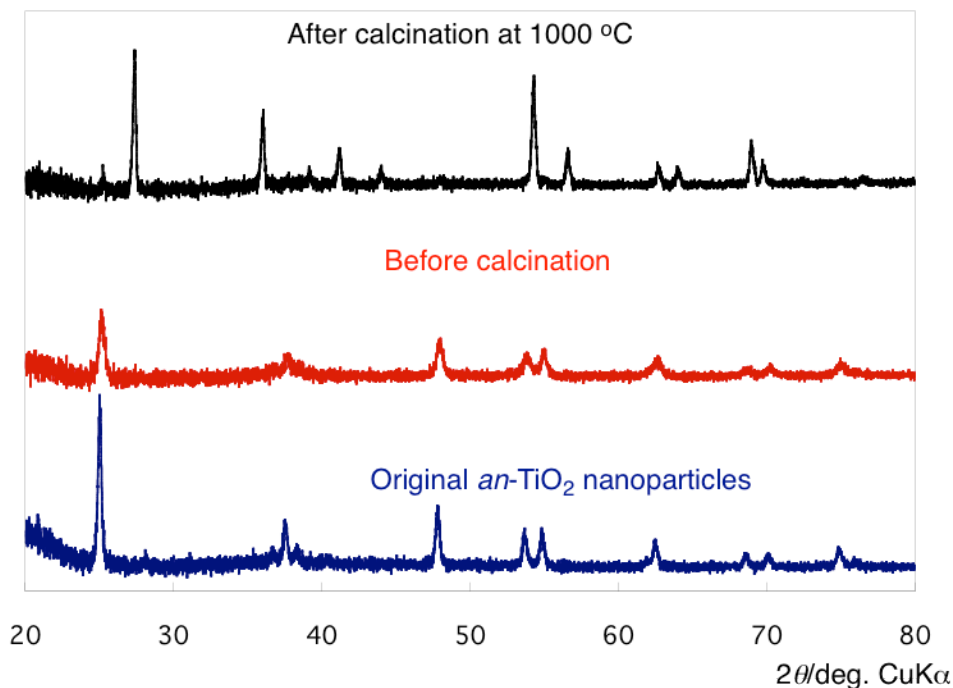


Fig. 3-2 X-ray diffraction patterns of original *an*- TiO_2 nanoparticles (bottom spectrum) and poly(VDF-*co*- $\text{CF}_2\text{CFCO}_2\text{Me}$)/*an*- TiO_2 nanocomposites (Run 1 in Table 3-1) before (middle) and after (top) calcinations at 1000 °C.

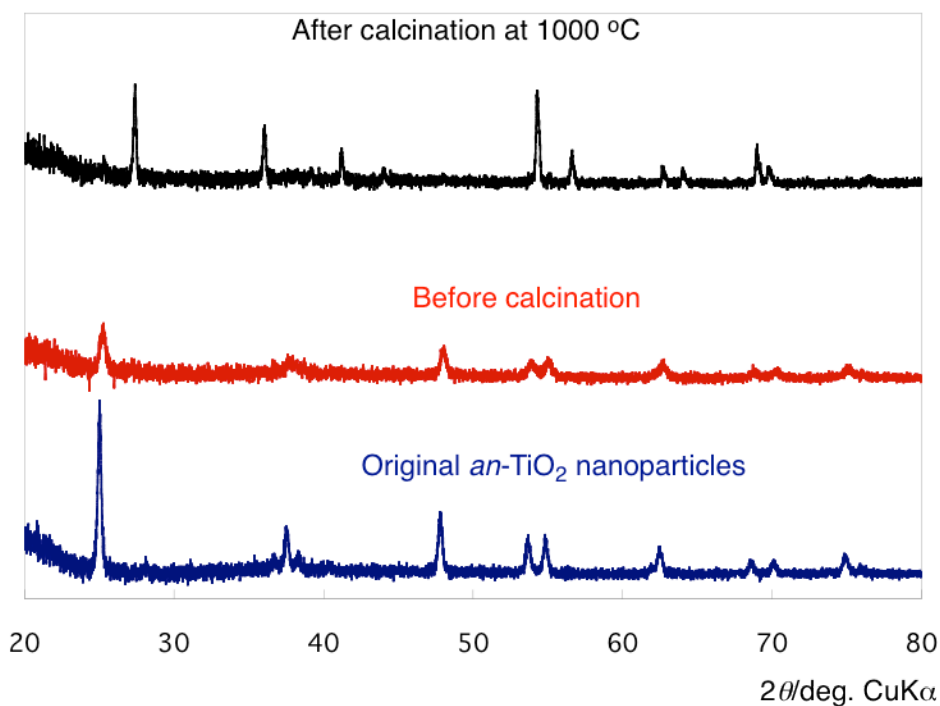


Fig. 3-3 X-ray diffraction patterns of original *an*- TiO_2 nanoparticles (bottom spectrum) and poly(VDF-*co*- $\text{CHFCFCO}_2\text{H}$)/*an*- TiO_2 nanocomposites (Run 3 in Table 3-1) before (middle) and after (top) calcinations at 1000 °C.

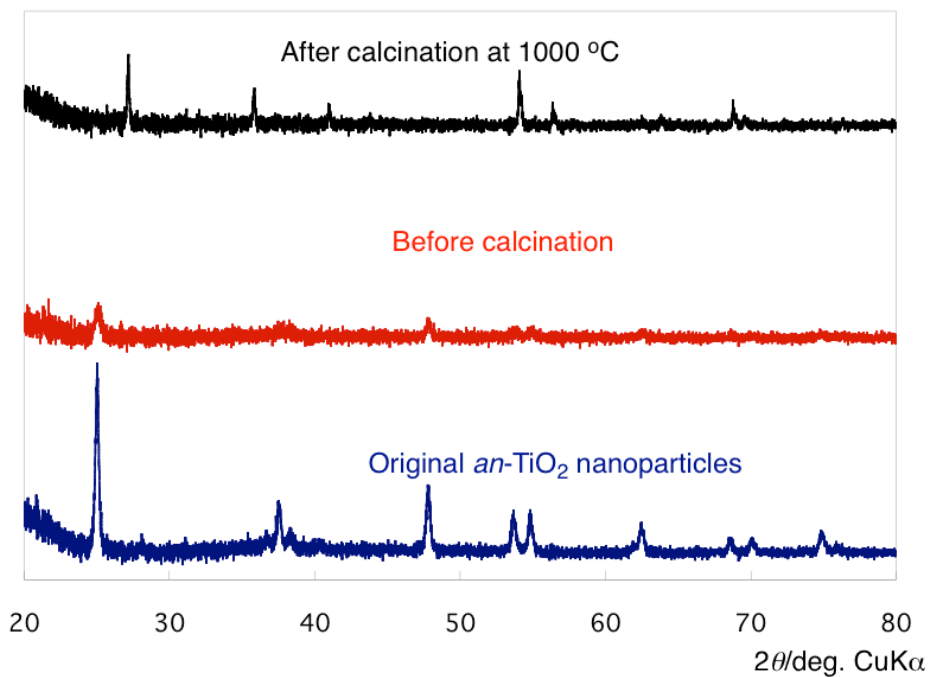


Fig. 3-4 X-ray diffraction patterns of original *an*-TiO₂ nanoparticles (bottom spectrum) and poly(VDF-*co*-CF₂CFC₃H₆OCOME)/*an*-TiO₂ nanocomposites (Run 5 in Table 3-1) before (middle) and after (top) calcinations at 1000 °C.

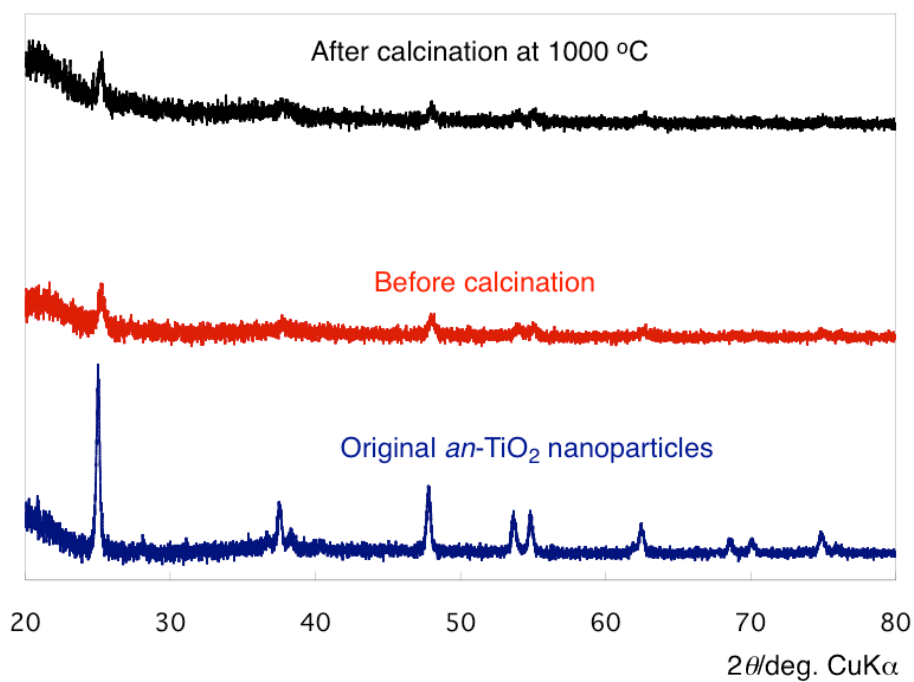


Fig. 3-5 X-ray diffraction patterns of original *an*-TiO₂ nanoparticles (bottom spectrum) and poly(VDF-*co*-CF₂CFCO₂Me)/SiO₂/*an*-TiO₂ nanocomposites (Run 2 in Table 3-1) before (middle) and after (top) calcinations at 1000 °C.

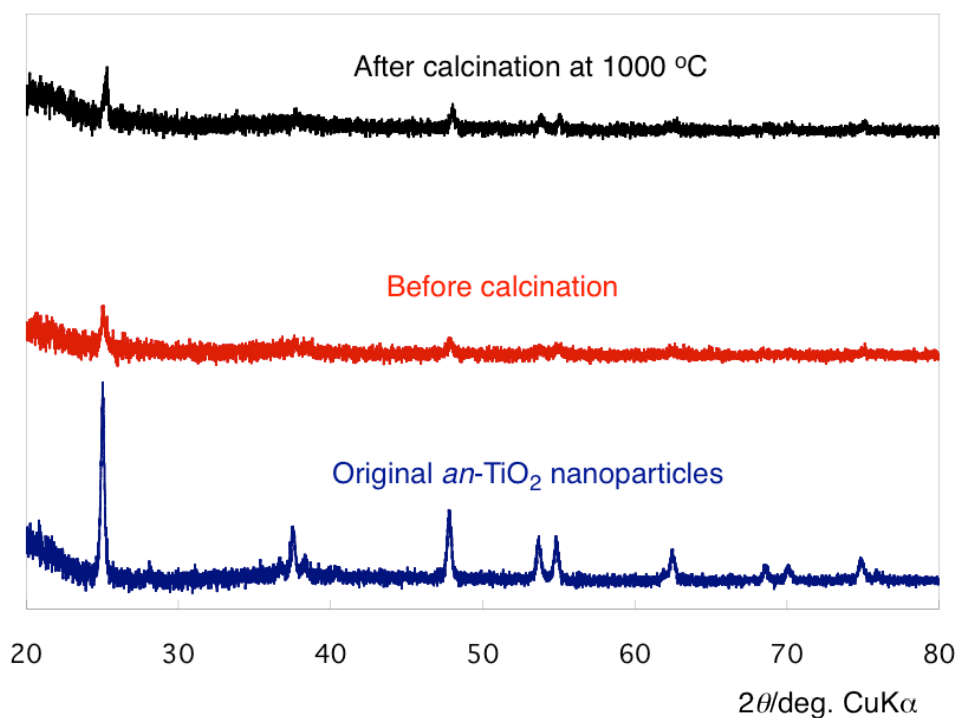


Fig. 3-6 X-ray diffraction patterns of original *an*-TiO₂ nanoparticles (bottom spectrum) and poly(VDF-*co*-CHFCFCO₂H)/SiO₂/*an*-TiO₂ nanocomposites (Run 4 in Table 3-1) before (middle) and after (top) calcinations at 1000 °C.

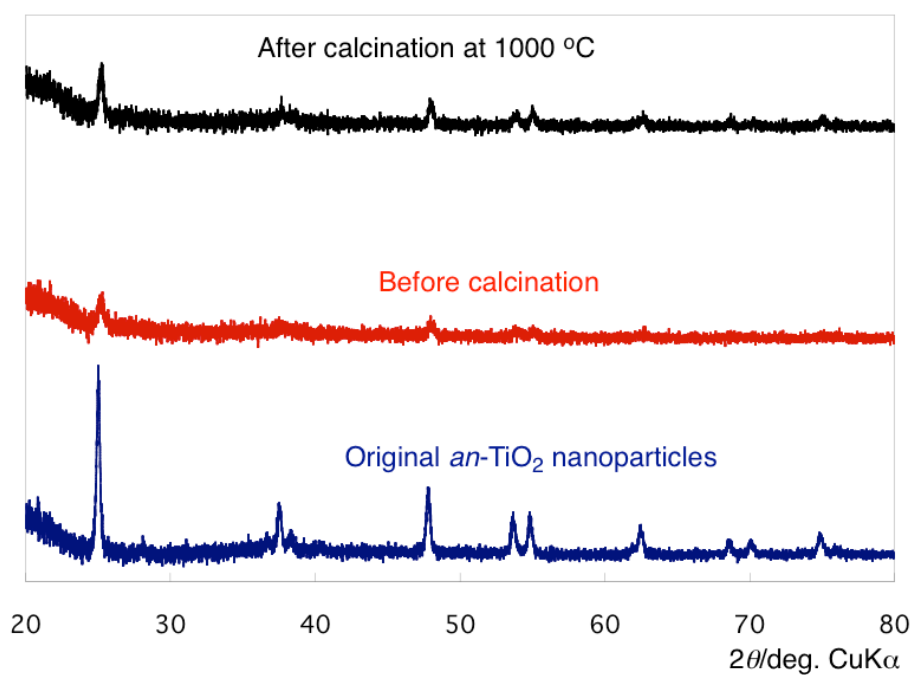


Fig. 3-7 X-ray diffraction patterns of original *an*-TiO₂ nanoparticles (bottom spectrum) and poly(VDF-*co*-CF₂CFC₃H₆OCOMe)/SiO₂/*an*-TiO₂ nanocomposites (Run 6 in Table 3-1) before (middle) and after (top) calcinations at 1000 °C.

Poly(VDF-*co*-M)/*an*-TiO₂ nanocomposites before calcination (Runs 1, 3 and 5 in Table 3-1) displayed almost the same XRD characteristic peaks (Figs. 3-2, 3-3 and Fig. 3-4) as those of original *an*-TiO₂ nanoparticles (Figure 3-8). However, TiO₂ in the nanocomposites underwent a complete phase transformation into rutile after calcination at 1000 °C (Figs. 3-2, 3-3 and 3-4) as well as that of pristine *an*-TiO₂ nanoparticles (Figure 3-8). On the other hand, poly(VDF-*co*-M) copolymers/SiO₂/*an*-TiO₂ nanocomposites (Runs 2, 4 and 6 in Table 3-1), which were prepared by the composite formations of the corresponding copolymers with *an*-TiO₂ nanoparticles, SiO₂ nanoparticles and TEOS, were found to preserve their crystalline anatase structure even after calcination at 1000 °C (Figs. 3-5, 3-6 and 3-7).

These obtained poly(VDF-*co*-M)/SiO₂/*an*-TiO₂ nanocomposites exhibited a good dispersibility and stability in methanol, ethanol and tetrahydrofuran illustrated in Scheme 3-2 and Table 3-1. Dynamic light scattering (DLS) technique was a suitable tool to assess the sizes of these composites before and after calcination and evidenced that the sizes of these composites were nanometer size-controlled (18 ~ 141 nm). The white color of poly(VDF-*co*-M)_y/SiO₂/*an*-TiO₂ nanocomposite powders did not change before and after calcination at 1000 °C.

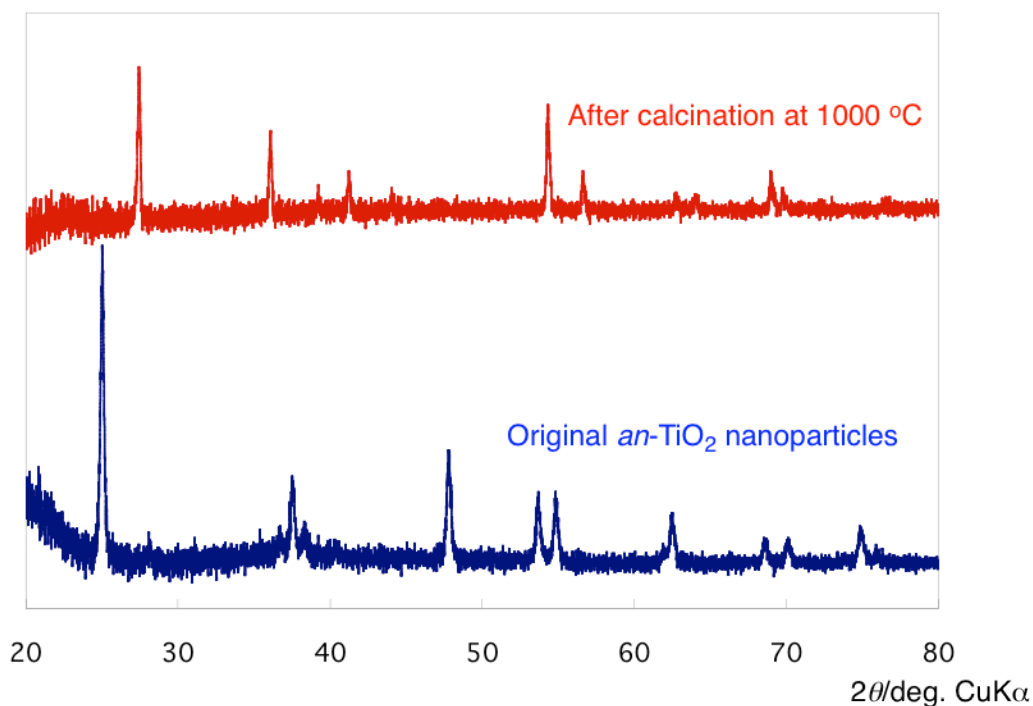


Fig. 3-8 X-ray diffraction patterns of original *an*-TiO₂ nanoparticles before (bottom spectrum) and after (top) calcination at 1000 °C.

However, no transformation into rutile after calcination at 1000 °C was interestingly observed in poly(VDF-*co*-M)/SiO₂/*an*-TiO₂ nanocomposites (Runs 2, 4 and 6 in Table 3-1).

In this way, poly(VDF-*co*-M)/*an*-TiO₂ nanocomposites were able to effectively modify their crystalline structure from anatase into rutile after calcination at 1000 °C. However, it was demonstrated that the incorporation of silica moieties into these above nanocomposites cores *via* the sol-gel processes involving TEOS and SiO₂ nanoparticles under alkaline conditions preserved their crystalline anatase structure completely without any phase modification into rutile, even after calcination at 1000 °C.

3.3.2. Photocatalytic activity of fluorinated copolymers/*an*-TiO₂ and fluorinated copolymers/SiO₂/*an*-TiO₂ nanocomposites

Anatase titanium oxide is known to irreversibly undergo a phase transformation into rutile at elevated temperatures ⁴¹⁾ in air (ranging between 600 and 750 °C). ^{5, 28, 29)} Actually, the incorporation of silica moieties into TiO₂ enabled to prevent the phase transformation into rutile. ⁴²⁾ In fact, Hilonga *et al.* ⁴³⁾ reported that titania-silica composite, which was prepared by the sol-gel reaction of titanium oxychloride and sodium silicate, can preserve anatase structure at ca. 600-900 °C, although the phase transformation from anatase into rutile was partly observed in this nanocomposites after calcination at 1000 °C.

Therefore, it is presumed that the synergistic interaction between silicon and fluorine atoms in such fluorinated polymers/SiO₂/*an*-TiO₂ nanocomposites should enhance the thermal stability of *an*-TiO₂ in the resulting nanocomposites. Actually, fluorinated polymers/SiO₂/*an*-TiO₂ nanocomposites lattice lock the Ti-O species at the interface of the TiO₂ domains through the formation of Ti-O-Si species and Ti-F species, preventing from the nucleation that is necessary for the phase transformation into rutile at 1000 °C. In fact, Gao *et al.* ⁴⁴⁾ reported that Ti-O-Si species were formed in TiO₂-SiO₂ mixed oxides, while Ti-F species can be obtained by a simple ligand exchange reaction between surface hydroxyl

groups on TiO_2 (Ti-OH) and fluoride anion (F^-).^{45, 46)} In addition, Ti-F species have been generated through the fluoride doping ($\text{TiO}_{2-x}\text{F}_x$) technique.⁴⁷⁾ Especially, fluoride doping has been found to enhance the crystallization of the anatase phase and the photocatalytic activity.^{33, 48 ~ 49)} Surface-fluorinated TiO_2 can also show enhanced photocatalytic ability.^{50 ~ 59)} From these results, it is suggested that thermally stable anatase structure in these present fluorinated polymers/ SiO_2 /*an*- TiO_2 nanocomposites would arise from the presence of not only silica nanoparticles but also from fluorine moieties in the nanocomposites cores.

Indeed, fluorine counterparts in polymers are expected to interact efficiently with *an*- TiO_2 in the nanocomposites to enhance the photocatalytic activity of fluorinated polymer nanocomposites related to the presence of *an*- TiO_2 . First, the photocatalytic activity of poly(VDF-*co*- $\text{CF}_2\text{CFCO}_2\text{Me}$) copolymer/ SiO_2 /*an*- TiO_2 nanocomposites (Run 2 in Table 3-1) before and after calcination at 1000 °C was evaluated in terms of discoloration of methylene blue dye (MB) under UV light irradiation. The residual amounts of MB *versus* time were estimated by the decrease of the absorption band at 652 nm related to MB by UV light irradiation, and the results are shown in Fig. 3-9.

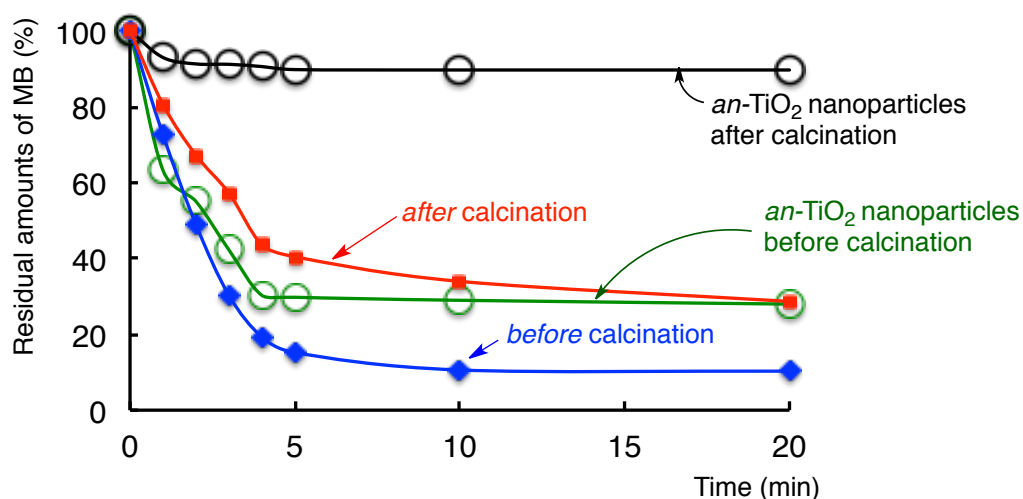


Fig. 3-9 Residual amounts of methylene blue dye (MB) versus photoirradiation (λ_{max} : 365 nm) time in the presence of poly(VDF-*co*-CF₂CFCO₂Me)/SiO₂/*an*-TiO₂ nanocomposites: diamonds and full squares (or original *an*-TiO₂ nanoparticles: open circles) before and after calcination at 1000 °C (used sample: Run 2 in Table 1).
 Concentration of methylene blue dye: 2.5 mg/dm³;
 Concentration of nanocomposites (or original *an*-TiO₂ nanoparticles before and after calcination at 1000 °C): 25 mg/dm³.

The photocatalytic activity is linked to the residual amounts of MB, and as shown in Fig. 3-9, original *an*-TiO₂ nanoparticles display a photocatalytic activity toward MB, although the corresponding TiO₂ nanoparticles with a complete phase transformation from anatase to rutile after calcination at 1000 °C did show any photocatalytic property, even after 20 min-photoirradiation.

Actually, this resulting rutile TiO₂ displayed 90 % residual MB after 20 min in contrast to initial *an*-TiO₂ that induced 29 %. This indicates that original *an*-TiO₂ nanoparticles can possess no photocatalytic activity after calcination at 1000 °C. Interestingly, poly(VDF-*co*-CF₂CFCO₂Me) copolymer/SiO₂/*an*-TiO₂ nanocomposites before calcination at

1000 °C exhibited a higher photocatalytic activity for the discoloration of MB than that of original *an*-TiO₂ nanoparticles. It is also worth noting that, after calcination at 1000 °C, these poly(VDF-*co*-CF₂CFCO₂Me) copolymer/SiO₂/*an*-TiO₂ nanocomposites exhibit the same photocatalytic activity as that of original *an*-TiO₂ nanoparticles after 20 min-photoirradiation.

The photocatalytic activity of other poly(VDF-*co*-M) copolymers/SiO₂/*an*-TiO₂ nanocomposites have also been studied for 20 min-UV light irradiation before and after calcination at 1000 °C under the same conditions as those of the case above (Fig. 3-9), and the results are summarized in Fig. 3-10.

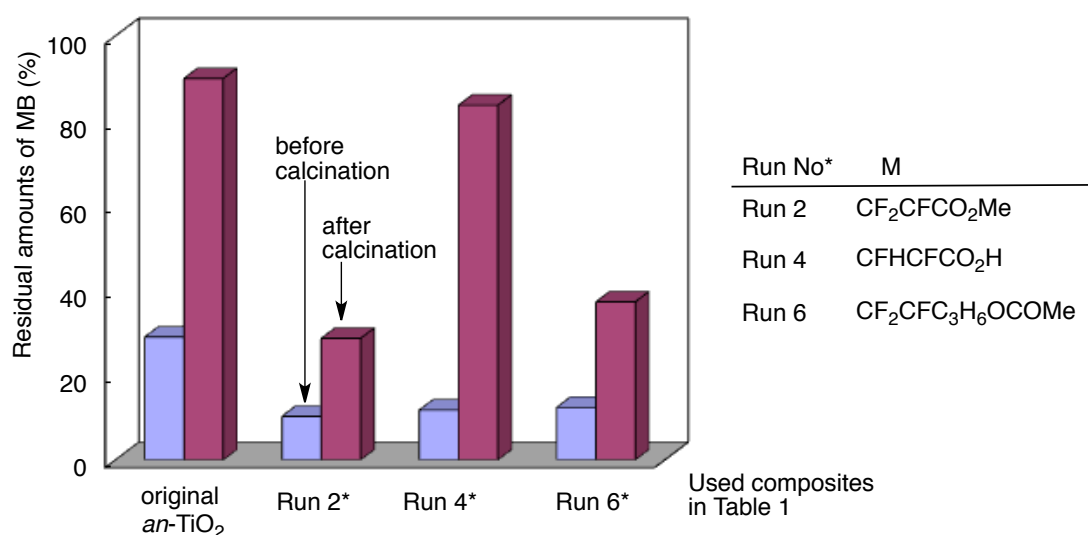


Fig. 3-10 Photo-decoloration of methylene blue dye in methanol solutions of poly(VDF-*co*-M)/SiO₂/*an*-TiO₂ nanocomposites in Table 3-1 before (gray scale) and after (black scale) calcination at 1000 °C.

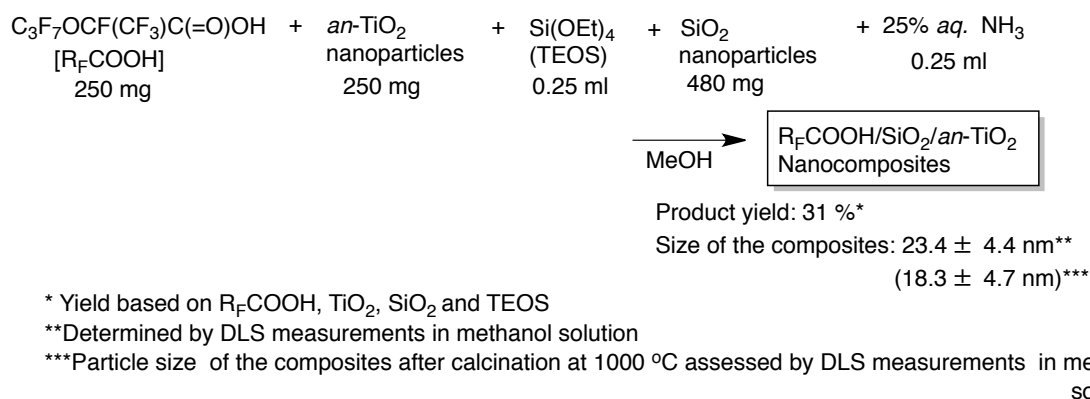
Concentration of poly(VDF-*co*-M)/SiO₂/*an*-TiO₂ nanocomposites (or original *an*-TiO₂ nanoparticles): 25 mg/dm³

Concentration of methylene blue dye: 2.5 mg/dm³

UV irradiation (λ_{max} : 365 nm) time: 20 min

Figure 3-10 shows that the photocatalytic activity of poly(VDF-*co*-M)/SiO₂/*an*-TiO₂ nanocomposites before calcination were found to increase more than twice, compared to that of original *an*-TiO₂ nanoparticles before calcination. After calcination, poly(VDF-*co*-M)/SiO₂/*an*-TiO₂ nanocomposites also induced a photocatalytic activity higher than that of original TiO₂ nanoparticles after calcination. In the poly(VDF-*co*-CF₂CFCO₂Me)/SiO₂/*an*-TiO₂ nanocomposite, a higher photocatalytic activity was observed before and after calcination (Run 2 in Table 3-1). Unexpectedly, fluorinated nanocomposites that possess COOH units (Run 4 in Table 3-1) after calcination displayed a photocatalytic activity lower than that of other nanocomposites. This observation can arise from the presence of higher acidic carboxyl groups since they are adjacent to electron-withdrawing CF-CHF groups in the composites.

To clarify the effect of carboxyl groups for the photocatalytic activity of such fluorinated nanocomposites, fluorinated derivative that bears a higher acidic carboxylic acid, C₃F₇OCF(CF₃)COOH [R_F-COOH], was involved in a nanocomposite reaction (Scheme 3-3). This structure was chosen since it is more simple than that of carboxylic acid-containing fluorinated polymers in poly(VDF-*co*-CFHCFCO₂H)/SiO₂/*an*-TiO₂ nanocomposites.



Scheme 3-3 Preparation of R_FCOOH/SiO₂/an-TiO₂ nanocomposites from R_FCOOH (where R_F stand for C₃F₇OCF₃).

Even after calcinations, R_F-COOH/SiO₂/an-TiO₂ nanocomposites (see Scheme 3-3) did not undergo any phase transformation into rutile at all, as well as those of the present fluorinated polymers/SiO₂/an-TiO₂ nanocomposites (see Fig. 3-11). As above, photocatalytic activity of R_F-COOH/SiO₂/an-TiO₂ nanocomposites was evaluated in terms of discoloration of MB under UV light irradiation under similar conditions as those of Fig. 3-9, and the results are displayed in Fig. 3-12.

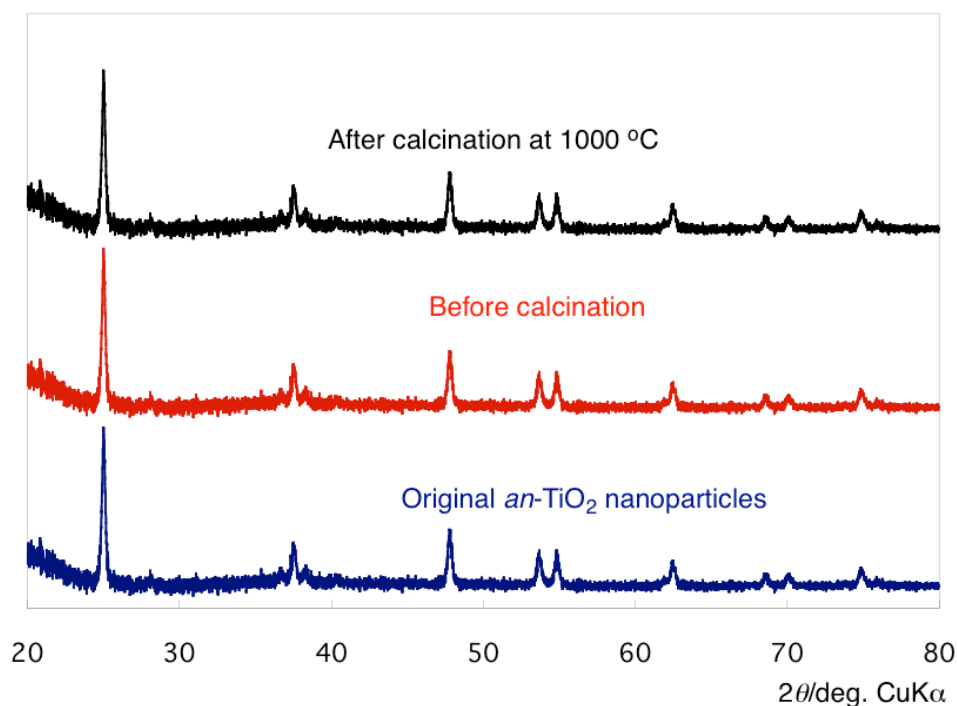


Fig. 3-11 X-ray diffraction patterns of original *an*-TiO₂ nanoparticles (bottom spectrum) and C₃F₇OCF(CF₃)COOH/SiO₂/*an*-TiO₂ nanocomposites (Scheme 3-3) before (middle) and after (after) calcinations at 1000 °C.

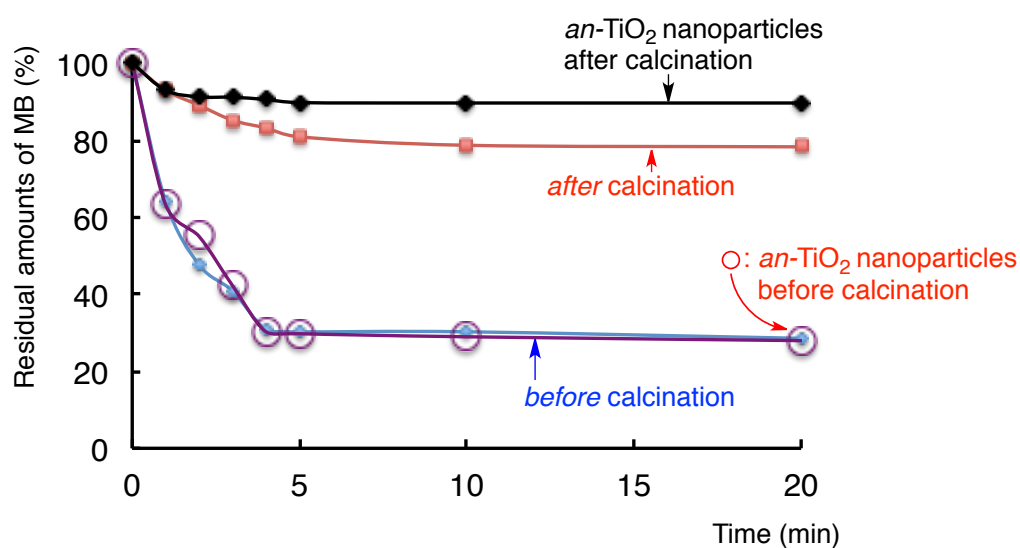


Fig. 3-12 Relationship between the residual amounts of methylene blue dye and photoirradiation (λ_{max} : 365 nm) time in the presence of R_FCOOH/SiO₂/*an*-TiO₂ nanocomposites: open circles and full diamonds and squares (or original *an*-TiO₂ nanoparticles: open circles and full diamonds) before and after calcination at 1000 °C. Concentration of methylene blue dye: 2.5 mg/dm³; Concentration of nanocomposites (or original *an*-TiO₂ nanoparticles before and after calcination at 1000 °C): 25 mg/dm³.

Figure 3-12 reveals that $R_F\text{COOH}/\text{SiO}_2/\text{an-TiO}_2$ nanocomposites before calcination exhibit the same photocatalytic activity as that of parent *an-TiO*₂ nanoparticles. However, after calcination, they displayed a quite poor photocatalytic activity. This result suggests that higher acidic carboxylic groups in the nanocomposites would reduce the photocatalytic ability in the nanocomposites after calcination, as well as that of poly(VDF-*co*-CHF₂CF₂CO₂H) copolymer/*SiO*₂/*an-TiO*₂ nanocomposites after calcination (Run 4 in Table 3-1).

In this way, poly(VDF-*co*-M) copolymer/*SiO*₂/*an-TiO*₂ nanocomposites before calcination displayed a higher photocatalytic activity for the discoloration of methylene blue dye under UV light irradiation, compared to that of original *an-TiO*₂ nanoparticles under similar conditions. Poly(VDF-*co*-CF₂CF₂CO₂Me)/*SiO*₂/*an-TiO*₂ nanocomposites exhibited a higher photocatalytic activity before and after calcination. In contrast, poly(VDF-*co*-CHF₂CF₂CO₂H)/*SiO*₂/*an-TiO*₂ nanocomposites after calcination reduced their photocatalytic activity. The contents of *TiO*₂ and *SiO*₂ in poly(VDF-*co*-CF₂CF₂CO₂Me)/*SiO*₂/*an-TiO*₂ and poly(VDF-*co*-CHF₂CF₂CO₂H)/*SiO*₂/*an-TiO*₂ nanocomposites before and after calcination at 1000 °C by energy dispersive X-ray (EDX) spectra measurements were estimated as follows:

	TiO ₂ (%)	SiO ₂ (%)
poly(VDF- <i>co</i> -CF ₂ CFCO ₂ Me)/SiO ₂ / <i>an</i> -TiO ₂	16 (13*)	64 (77*)
poly(VDF- <i>co</i> -CFHCFCOOH)/SiO ₂ / <i>an</i> -TiO ₂	11 (11*)	23 (51*)

*) After calcination

EDX spectra show that the contents of TiO₂ in the composites before and after calcination are estimated to be 11-16 % and 11-13 %, respectively. Thus, it should be said that the present fluorinated nanocomposites can possess a better photocatalytic activity than that of original *an*-TiO₂ nanoparticles.

In addition, the thermal stabilities of poly(VDF-*co*-M)/SiO₂/*an*-TiO₂ nanocomposites (where M stands for CF₂=CFCO₂Me, CFH=CFCOOH, and CF₂=CF(CH₂)₃OCOMe) were assessed under air and the corresponding thermograms are displayed in Figs. 3-13, 14 and 15. These thermograms show the following weight losses (%) corresponding to the contents of fluorinated polymers in the nanocomposites at 800 °C, as follows:

Weight Loss (%) at 800 °C

poly(VDF-*co*-CF₂CFCO₂Me) copolymer/SiO₂/*an*-TiO₂ 2

poly(VDF-*co*-CF₂CF(CH₂)₃OCOMe) copolymer/SiO₂/*an*-TiO₂ 17

poly(VDF-*co*-CFHCFCOOH) copolymer/SiO₂/*an*-TiO₂ 20

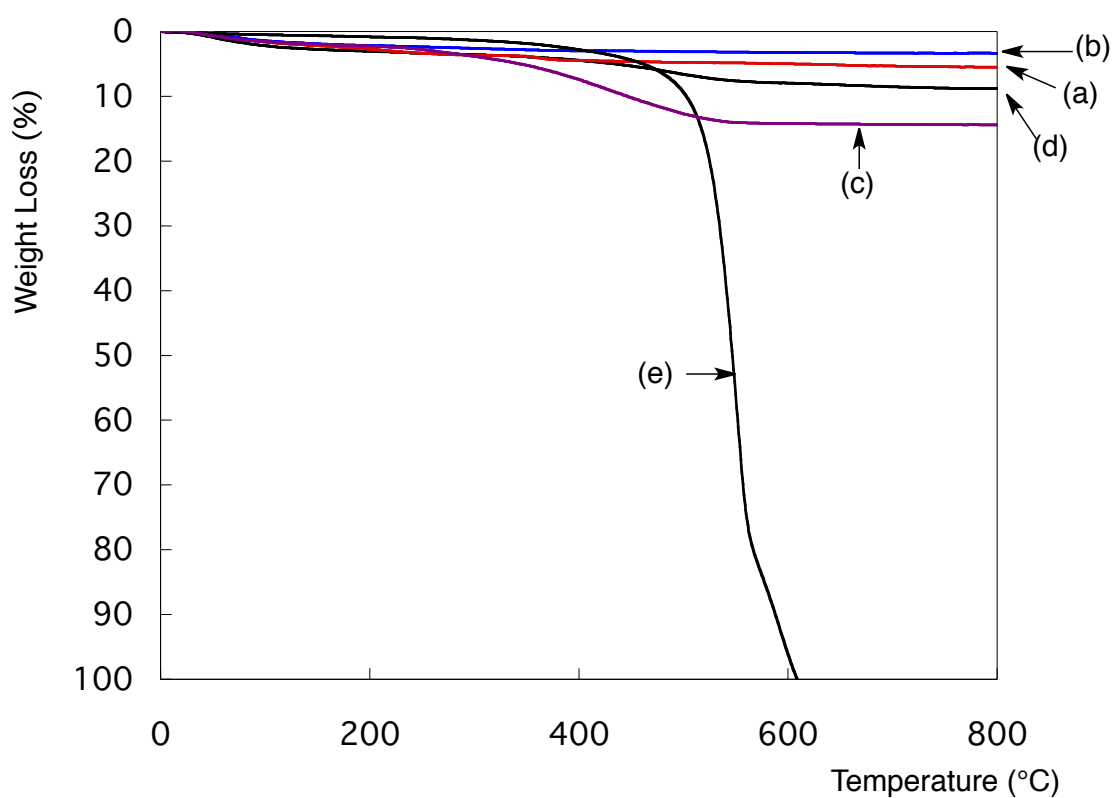


Fig. 3-13 Thermogravimetric curves of original SiO₂ nanoparticles (a), which were prepared from TEOS and silica nanoparticles, *an*-TiO₂ nanoparticles (b), poly(VDF-*co*-CF₂CFCO₂Me)/*an*-TiO₂ nanocomposites (Run 1 in Table 3-1) (c), poly(VDF-*co*-CF₂CFCO₂Me)/SiO₂/*an*-TiO₂ nanocomposites (Run 2 in Table 3-1) (d), and poly(VDF-*co*-CF₂CFCO₂Me) copolymer (e).

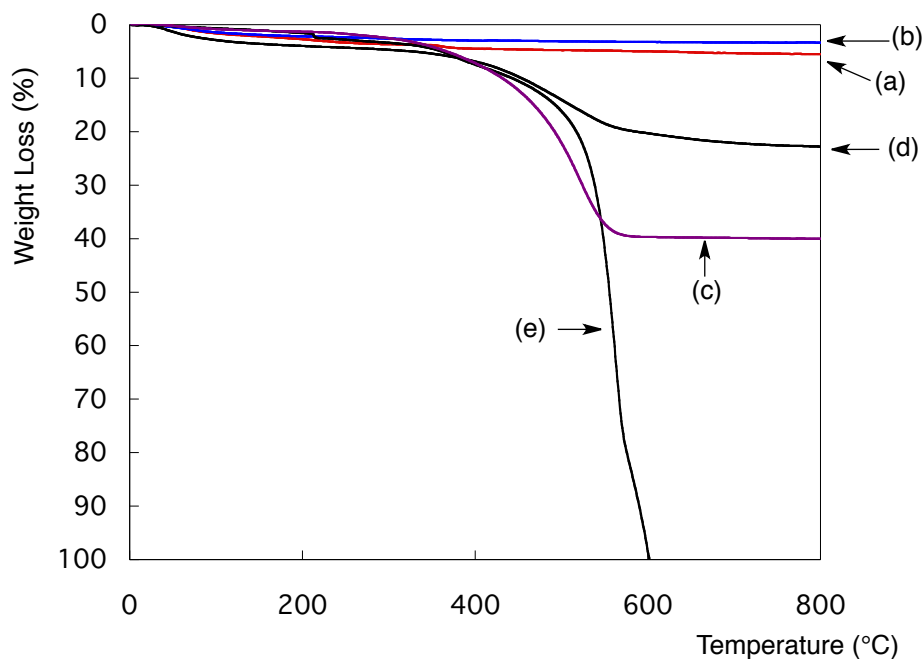


Fig. 3-14 Thermogravimetric curves of original SiO_2 nanoparticles (a), which were prepared from TEOS and silica nanoparticles, $an\text{-TiO}_2$ nanoparticles (b), poly(VDF-*co*-CFHCFCOOH)_y/ $an\text{-TiO}_2$ nanocomposites (Run 3 in Table 3-1) (c), poly(VDF-*co*-CFHCFCOOH)/ SiO_2 / $an\text{-TiO}_2$ nanocomposites (Run 4 in Table 3-1) (d), and poly(VDF-*co*-CFHCFCOOH) copolymer (e).

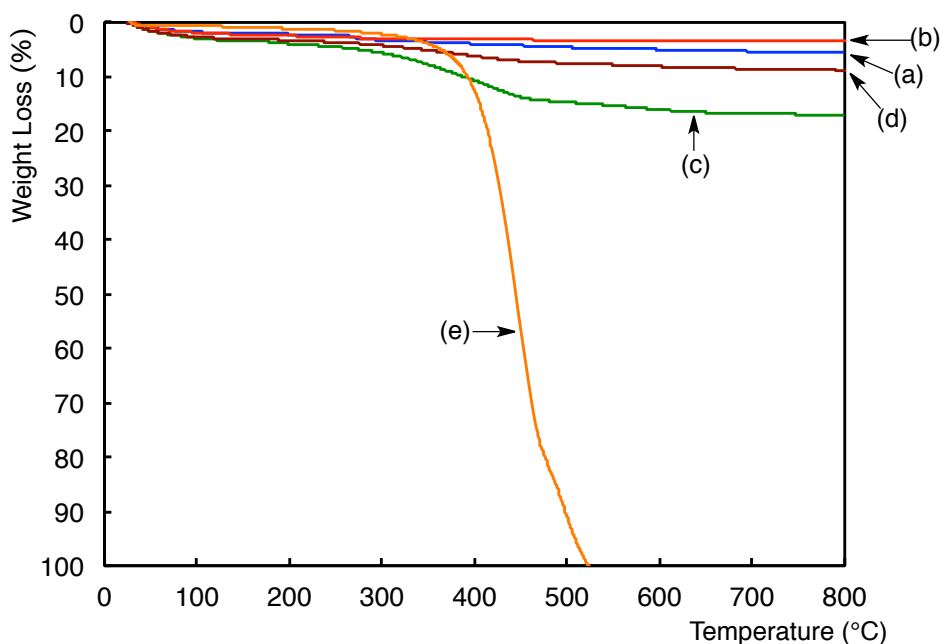


Fig. 3-15 Thermogravimetric curves of original SiO_2 nanoparticles (a), which were prepared from TEOS and silica nanoparticles, $an\text{-TiO}_2$ nanoparticles (b), poly(VDF-*co*-CF₂CFC₃H₆OCOMe)/ $an\text{-TiO}_2$ nanocomposites (Run 5 in Table 3-1) (c), poly(VDF-*co*-CF₂CFC₃H₆OCOMe)/ SiO_2 / $an\text{-TiO}_2$ nanocomposites (Run 6 in Table 3-1) (d), and poly(VDF-*co*-CF₂CFC₃H₆OCOMe) copolymer (e).

It was previously reported that fluoroalkyl end-capped *N*-(1,1-dimethyl-3-oxobutyl)acrylamide oligomers/silica nanocomposites⁶⁰⁾ and poly(VDF-*ter*-TFMA-*ter*-HFP) terpolymers/silica nanocomposites (where TFMA and HFP stand for 2-trifluoromethacrylic acid and hexafluoropropylene, respectively)⁴⁰⁾ can exhibit almost no weight loss even after calcination at 800 °C through a dehydrofluorination process that released hexafluorosilicate anions. Thus, poly(VDF-*co*-CF₂CFCO₂Me)/SiO₂/*an*-TiO₂ nanocomposites, the weight loss of which is 2 %, are likely to give hydrogen fluoride through the calcination process to interact with *an*-TiO₂ nanoparticles. Such *an*-TiO₂ nanoparticles interacted with hydrogen fluoride and could enhance the photocatalytic activity in the composites.

3.4. Conclusion

For the first time, poly(VDF-*co*-fluorofunctional M) copolymers have been utilized with *an*-TiO₂ nanoparticles under slightly alkaline conditions to obtain fluorinated copolymers/*an*-TiO₂ nanocomposites. Similarly, successful syntheses of fluorinated copolymers/SiO₂/*an*-TiO₂ nanocomposites by using silica nanoparticles and TEOS were achieved under such above conditions. These fluorinated copolymers/*an*-TiO₂ composites

underwent a complete phase transformation from anatase into rutile TiO_2 after calcination at 1000 °C. A similar phase transformation into rutile was observed from original (or pristine) *an*- TiO_2 nanoparticles in these conditions that confirm the literature.³⁵⁾ However, nanocomposite formations from these fluorinated copolymers with *an*- TiO_2 nanoparticles, SiO_2 nanoparticles and TEOS under alkaline conditions, enabled to obtain fluorinated copolymers/ SiO_2 /*an*- TiO_2 nanocomposites that completely preserved the crystalline anatase structure without any phase transformation into rutile, even after calcination at 1000 °C. Before calcinations, these fluorinated copolymers/ SiO_2 /*an*- TiO_2 nanocomposites exhibited a good photocatalytic activity as evidenced by the discoloration of methylene blue dye under UV light irradiation, as well as that of original *an*- TiO_2 nanoparticles. After calcinations, fluorinated poly(VDF-*co*- $\text{CF}_2\text{CFCO}_2\text{Me}$)/ SiO_2 /*an*- TiO_2 nanocomposites led to similar photocatalytic activity as that of original *an*- TiO_2 nanoparticles before calcinations, and much higher than both other F-copolymers/ TiO_2 / SiO_2 composites.

In addition, these nanocomposites display a high thermal stability (for example at 800 °C, 2 wt.% only was lost for poly(VDF-*co*- $\text{CF}_2\text{CFCO}_2\text{Me}$)/ SiO_2 /*an*- TiO_2 composites). Therefore, these present fluorinated copolymers/ SiO_2 /*an*- TiO_2 nanocomposites exhibit a high potential for specific applications such as dye sensitized solar cell, or binders and electrodes for Lithium ion batteries since these original fluorinated polymer nanocomposites are

thermostable and have demonstrated a good photocatalytic ability relative to anatase titanium oxide even after calcination at 1000 °C.

References

- 1) a) M. Arellano, I. Mickel-Haciski, D. L. Feke, and I. Manas-Zloczower, *J. Coat. Technol.*, **68**, 83 (1996);
b) L. B. Beecroff and C. K. Ober, *Chem. Mater.*, **9**, 1302 (1997);
c) J. M. Macak, H. Tsuchiya, and P. Schmuki, *Angew. Chem. Int. Ed.*, **44**, 2100 (2005).
- 2) a) Z. Zhang, C.-C. Wang, R. Zakaria, and J. Y. Ying, *J. Phys. Chem. B*, **102** 10871 (1998);
b) J. Geserick, T. Froeschl, N. Huesing, G. Kucerova, M. Makosch, T. Diemant, R. Eckle and R. J. Behm, *Dalton Trans.*, **40**, 3269 (2011).
- 3) a) M. Haruta, J. Kobayashi, H. Sano, and N. Yamada, *Chem. Lett.*, 405 (1987);
b) M. M. Schubert, V. Plzak, J. Garche, and R. J. Behm, *Catal. Lett.*, **76**, 143 (2001);
c) Y. Shao, Y. Liu, Y. Wang, and Y. Lin, *J. Mater. Chem.*, **19**, 46 (2009).
- 4) a) B. O'Regan and M. Gratzel, *Nature*, **353**, 737 (1991);
b) M. Gratzel, *Inorg. Chem.*, **44**, 6841 (2005);
c) D. Zhang, T. Yoshida, T. Oekermann, K. Furuta, and H. Minoura, *Adv. Funct. Mater.*, **16**, 1228 (2006).
- 5) a) A. L. Linsebigler, G. Q. Lu, and J. T. Yates, *Chem. Rev.*, **95**, 735 (1995);
b) T. Froeschl, U. Hormann, P. Kubiak, G. Kucerova, M. Pfanzelt, C. K. Weiss, R. J.

- Behm, N. Huesing, U. Kaiser, K. Landfester, and M. Wohlfahrt-Mehrens, *Chem. Soc. Rev.*, **41**, 5313 (2012).
- 6) N. G. Park, J. van de Lagemaat, and A. J. Frank, *J. Phys. Chem. B*, **104**, 8989 (2000).
- 7) M. S. Hoffmann, T. Martin, W. Choi, and D. W. Bahnemann, *Chem. Rev.*, **95**, 69 (1995).
- 8) a) L. Kavan, M. Graetzel, J. Rathousky, and A. J. Zukalb, *Electrochem. Soc.*, **143**, 394 (1996);
- b) D. Dambournet, I. Belharouak, and K. Amine, *Chem. Mater.*, **22**, 1173 (2010);
- c) P. Kubiak, T. Froeschl, N. Huesing, U. Hoermann, U. Kaiser, R. Schiller, C. K. Weiss, K. Landfester, and M. Wohlfahrt-Mehrens, *Small*, **7**, 1690 (2011);
- d) L. Kavan, *Chem. Rec.*, **12**, 131 (2012);
- e) M. Mancini, F. Nobili, R. Tossici, and R. Marassi, *Electrochimica Acta*, **85**, 566 (2012).
- 9) M. A. Fox and M. T. Dulay, *Chem. Rev.*, **93**, 341 (1993).
- 10) F. Croce, R. Curini, A. Martinelli, L. Persi, F. Ronci, B. Scrosati, and R. Caminiti, *J. Phys. Chem. B*, **103**, 10632 (1999).
- 11) G. B. Appetecchi, F. Croce, L. Persi, F. Ronci, and B. Scrosati, *Electrochim. Acta.*, **45**, 1481 (2000).
- 12) C. H. M. Caris, R. P. M. Kujipers, A. M. van Herk, and A. L. German, *Macromol. Chem. Macromol. Symp.*, **35/36**, 535 (1990).

- 13) P. A. Hartley, G. D. Parfitt, and L. B. Pollack, *Powder Technol.*, **42**, 35 (1985).
- 14) a) R. Van de Krol, A. Goossens, and E. A. Meulenkamp, *J. Electrochem. Soc.*, **146**, 3150 (1999);
- b) M. A. Reddy, M. S. Kishore, V. Pralong, U. V. Varadaraju, and B. Raveau, *Electrochem. Solid-State Lett.*, **10**, A29 (2007).
- 15) S. P. Thomas, S. Thomas, and S. Bandyopadhyay, *Composites Part A: Appl. Sci. Manufact.*, **40A**, 36 (2009).
- 16) T. E. Motaung, A. S. Luyt, and S. Thomas, *Polym. Composites*, **32**, 1289 (2011).
- 17) P. C. Thomas, S. P. Thomas, G. George, S. Thomas, and J. Kuruvilla, *J. Polym. Res.*, **18**, 2367 (2011).
- 18) A. P. Meera, S. Said, Y. Grohens, A. S. Luyt, and S. Thomas, *Indus. Eng. Chem. Res.*, **48**, 3410 (2009).
- 19) H. Q. Chu, C. Yu, Y. Wan, and D. Zhao, *J. Mater. Chem.*, **19**, 8610 (2009).
- 20) B. Ameduri and B. Boutevin, "Well-Architected Fluoropolymers: Synthesis, Properties and Applications", Elsevier, Amsterdam, pp. 231 (2004).
- 21) a) J.- F. Berret, D. Calvet, A. Collet, and M. Viguier, *Curr. Opinion Colloid Interface Sci.*, **8**, 296 (2003);
- b) T. Imae, *Curr. Opinion Colloid Interface Sci.*, **8**, 307 (2003);

- c) H. Sawada, *J. Fluorine Chem.*, **105**, 219 (2000);
- d) H. Sawada, *Prog. Polym. Sci.*, **32**, 509 (2007);
- e) H. Sawada, *Polym. Chem.*, **3**, 46 (2012).
- 22) a) T. Kamegawa, Y. Shimizu, and H. Yamashita, *Adv. Mater.*, **24**, 3697 (2012);
- b) M. Senna, V. Sepelak, J. Shi, B. Bauer, A. Feldhoff, V. Laporte, and K.-D. Becker, *J. Solid State Chem.*, **187**, 51 (2012).
- 23) a) T. He, Z. Zhou, W. Xu, F. Ren, H. Ma, and J. Wang, *Polymer*, **50**, 3031 (2009);
- b) N. L. An, H. Z. Liu, Y. C. Ding, M. Zhang, and Y. P. Tang, *Appl. Surf. Sci.*, **257**, 3831 (2011);
- c) F. Shi, Y. Ma, J. Ma, P. Wang, and W. Sun, *J. Membr. Sci.*, **389**, 522 (2012);
- d) F. Shi, Y. Ma, J. Ma, P. Wang, and W. Sun, *J. Membr. Sci.*, **427**, 259 (2013) ;
- e) R. S. Rocha, R. M. Reis, M. R. V. Lanza, and R. Bertazzoli, *Electrochim. Acta*, **87**, 606 (2013);
- f) J. G. Lee, S. H. Kim, H. C. Kang, and S. H. Park, *Macromol. Res.*, **21**, 349 (2013).
- 24) S. Fu, M. Zhang, and D. Yao, *Machines, Technologies, Materials*, **10**, 46 (2011).
- 25) a) H. Sawada, E. Sawada, H. Kakehi, T. Kariya, M. Mugisawa, Y. Chounan, M. Miura, and N. Isu, *Polym. Composites*, **30**, 1848 (2009);
- b) E. Sawada, H. Kakehi, Y. Chounan, M. Miura, Y. Sato, N. Isu, and H. Sawada,

- Composites Part B*, **41**, 498 (2010).
- 26) L. Sisti, L. Cruciani, G. Totaro, M. Vannini, C. Berti, D. M. Tobaldi, A. Tucci, L. Aloisio, D. Di Gioia, and S. Commereuc, *Thin Solid Films*, **520**, 2824 (2012).
- 27) S. Lin, X. Kuang, F. Wang, and H. Zhu, *Physica Status Solidi; Rapid Research Lett.*, **6**, 352 (2012).
- 28) X. S. Peng and A. Chen, *Adv. Funct. Mater.*, **16**, 1355 (2006).
- 29) G. Madras, B. McCoy, and A. Navtotsky, *J. Am. Ceram. Soc.*, **90**, 250 (2007).
- 30) a) H. Zhang and J. F. Banfield, *Am. Mineral.*, **84**, 528 (1999);
b) H. Zhang and J. F. Banfield, *J. Mater. Res.*, **15**, 437 (2000).
- 31) S. Liu, J. Yu, B. Cheng, and M. Jaroniec, *Adv. Colloid Interface Sci.*, **173**, 35 (2012).
- 32) C. Minero, G. Mariella, V. Maurino, and E. Pelizzetti, *Langmuir*, **16**, 2632 (2000).
- 33) J. C. Yu, G. Yu, W. Ho, Z. Jiang, and L. Zhang, *Chem. Mater.*, **14**, 3808 (2002).
- 34) G. Wu, J. Wang, D. F. Thomas, and A. Chen, *Langmuir*, **24**, 3503 (2008).
- 35) W. Ho, J. C. Yu, and S. Lee, *Chem. Commun.*, **10**, 1115 (2006).
- 36) R. Souzy, J. Guiot, B. Ameduri, B. Boutevin, and O. Paleta, *Macromolecules*, **36**, 9390 (2003).
- 37) F. Boschet, J.-M. Cracowski, V. Montembault, and B. Ameduri, *Macromolecules*, **43**, 4879 (2010).

- 38) B. Ameduri, B. Boutevin, G. Kostov, and P. Petrova, *Macromolecules*, **32**, 4544 (1999).
- 39) a) F. Mammeri, E. Le Bourhis, L. Rozes, and C. Sanchez, *J Mater. Chem.*, **15**, 3787 (2005);
- b) G. Tillet, B. Boutevin, and B. Ameduri, *Prog. Polym. Sci.*, **36**, 191 (2011).
- 40) H. Sawada, T. Tashima, Y. Nishiyama, M. Kikuchi, Y. Goto, G. Kostov, and B. Ameduri, *Macromolecules*, **44**, 1114 (2011).
- 41) D. A. H. Hanaor and C. C. Sorrell, *J. Mater. Sci.*, **46**, 855 (2011).
- 42) L. Sikong, J. Damchan, K. Kooptarnond, and S. Niyomwas, *Songklanakarin J. Sci. Technol.*, **30**, 385 (2008).
- 43) a) A. Hilonga, J.-K. Kim, P. B. Sarawade, and H. T. Kim, *J. Mater. Sci.*, **45**, 1255 (2010);
- b) A. Hilonga, J.-K. Kim, P. B. Sarawade, and H. T. Kim, *J. Mater. Sci.*, **45**, 1264 (2010).
- 44) X. Gao and I. E. Wachs, *Catalysis Today*, **51**, 233 (1999).
- 45) M. S. Vohra, S. Kim, and W. Choi, *J. Photochem. Photobiol.*, **160**, 55 (2003).
- 46) K. Lv, X. Li, K. Deng, J. Sun, X. Li, and M. Li, *Appl. Catal. B: Environ.*, **95**, 383 (2010).
- 47) H. Park and W. Choi, *J. Phys. Chem. B*, **108**, 4086 (2004).
- 48) a) A. Hattori, M. Yamamoto, H. Tada, and S. Ito, *Chem. Lett.*, 707 (1998);
- b) A. Hattori, K. Shimoda, H. Tada, and S. Ito, *Langmuir*, **15**, 5422 (1999).
- 49) J. G. Yu, J. C. Yu, B. Cheng, S. K. Hark, and K. Iu, *J. Solid State Chem.*, **174**, 372 (2003).

- 50) a) J. C. Yu, W. Ho, J. Yu, S. K. Hark, and K. Iu, *Langmuir*, **19**, 3889 (2003);
- b) J. Yu and L. Shi, *J. Mol. Catal. A: Chem.*, **326**, 8 (2010).
- 51) Y. M. Wu, J. L. Zhang, L. Xiao, and F. Chen, *Appl. Catal. B: Environ.*, **88**, 525 (2009).
- 52) J. Kim, J. Lee, and W. Y. Choi, *Chem. Commun.*, 756 (2008).
- 53) X. Yang, Y. H. Wang, L. L. Xu, X. D. Yu, and Y. H. Guo, *J. Phys. Chem. C*, **112**, 11481 (2008).
- 54) G. Lin, C. Sun, H. Yang, S. C. Gui Smith, L. Wang, G. Q. Lu, and H.-M. Cheng, *Chem. Commun.*, **46**, 755 (2010).
- 55) H. Zhang, P. Liu, F. Li, H. Liu, Y. Wang, S. Zhang, M. Guo, H. Cheng, and H. Zhao, *Chem. Eur. J.*, **17**, 5949 (2011).
- 56) D. Zhang, G. Li, X. Yang, and J. C. Yu, *Chem. Commun.*, 4381 (2009).
- 57) J.-G. Yu, H.-G. Yu, B. Cheng, X.-J. Zhao, J. C. Yu, and W.-K. Ho, *J. Phys. Chem. B*, **107**, 13871 (2003).
- 58) M. Liu, L. Piao, L. Zhao, S. Ju, Z. Yan, T. He, C. Zhou, and W. Wang, *Chem. Commun.*, **46**, 1664 (2010).
- 59) a) J. Tang, H. Quan, and J. Ye, *Chem. Mater.*, **19**, 116 (2007);
- b) X. Han, Q. Kuang, M. Jin, Z. Xie, and L. J. Zheng, *Am. Chem. Soc.*, **131**, 3152 (2009);
- c) H. G. Yang, G. Liu, S. Z. Qiao, C. H. Sun, Y. G. Jin, S. C. Smith, J. Zou, H. M. Cheng,

and G. Q. Lu, *J. Am. Chem. Soc.*, **131**, 4078 (2009);

d) J. Yu, W. Wang, B. Cheng, and B.-L. Su, *Phys. Chem. C*, **113**, 6743 (2009).

60) H. Sawada, T. Narumi, S. Kodama, M. Kamijo, R. Ebara, M. Sugiya, and Y. Iwasaki, *Colloid Polym. Sci.*, **285**, 977 (2007).

CHAPTER 4

Preparation and Properties of Fluorinated Aliphatic Alcohols/Silica Nanocomposites-Application to the Encapsulation of Anatase Titanium Oxide Nanoparticles into These Composite Cores

4.1. Introduction

Partially fluoroalkylated polymers, especially two fluoroalkyl end-capped oligomers $[R_F-(M)_n-R_F]$; R_F = fluoroalkyl groups; M = radical polymerizable monomers] are attractive functional materials, because they can exhibit a wide variety of unique properties such as high solubility, surface active properties and nanometer size-controlled molecular aggregates through the aggregation of terminal fluoroalkyl groups, which cannot be achieved by the corresponding non-fluorinated, randomly or block-type fluoroalkylated polymers.^{1 ~ 22)}

From the developmental viewpoints of new functional materials possessing unique characteristics imparted by fluorine, it is in particular interest to explore novel fluorinated polymers/inorganic nanocomposites, because of exhibiting a large variety of extraordinary characteristic deriving from the synergism between the properties of each individual material.^{24 ~ 27)}

In fact, it has been already reported on the preparation of new fluoroalkyl end-capped oligomer/silica nanocomposites through the encapsulation of silica nanoparticles as guest molecules into fluoroalkyl end-capped oligomeric nanoparticle cores, and fluoroalkyl end-capped oligomers containing higher acidic protons such as sulfo groups formed by the nanocomposite reactions in the presence of tetraethoxysilane (TEOS) and silica nanoparticles under alkaline conditions afforded no weight loss behavior at 800 °C; although the

corresponding oligomer containing carboxyl groups can exhibit a usual weight loss after calcination corresponding to the content of the oligomer in the composite matrices.²⁸⁾ Low molecular weight fluorinated surfactants such as perfluoro-1,3-propanedisulfonic acid (PFPS) were also applied to the nanocomposite reactions with TEOS in the presence of silica nanoparticles under alkaline conditions to give no weight loss corresponding to the content of PFPS in the silica nanocomposite cores even after calcination at 800 °C.^{29, 30)} It was suggested that the smooth dehydrofluorination between the sulfonic acid protons (higher acidic protons) and fluorines in fluorinated oligomers catalyzed by both ammonia and silica nanoparticles should proceed to give hydrogen fluoride, and this hydrogen fluoride can react with silica nanoparticles to afford ammonium hexafluorosilicate.^{31 ~ 33)} The obtained hexafluorosilicate anions should afford a nonflammable characteristic toward fluorinated oligomers in the nanocomposite matrices.^{31 ~ 33)} Therefore, from the developmental viewpoint of nonflammable fluorinated functional materials, it is deeply desirable to explore other fluorinated materials possessing a nonflammable property in the silica matrices. This chapter shows that a variety of fluorinated aliphatic alcohols can give a nonflammable characteristic in the silica nanocomposite cores even after calcination at 800 °C, and these nanocomposites are applicable to the surface modification of glass to exhibit a superoleophobic characteristic with a superhydrophilicity on the modified surface. Moreover, it has been found that anatase

titanium oxide nanoparticles are effectively encapsulated into fluorinated alcohol/silica nanocomposite cores to give the corresponding fluorinated alcohol/silica/anatase TiO_2 nanocomposites, and these fluorinated nanocomposites before and even after calcination can afford a higher photocatalytic activity than that of original anatase TiO_2 nanoparticles under similar conditions. These results will be also described herein.

4.2. Experimental

4.2.1 Measurements

Size [number - average diameter (average hydrodynamic diameter)] of nanocomposites was measured by using Otsuka Electronics DLS-7000 HL (Tokyo, Japan). Field emission scanning electron micrographs (FE-SEM) and energy dispersive X-ray (EDX) spectra were obtained using JEOL JSM-7000F (Tokyo, Japan). Thermal analyses were recorded on Bruker axs TG-DTA2000SA differential thermobalance (Kanagawa, Japan). Ultraviolet-visible (UV-vis) spectra were carried out using Shimadzu UV-1600 UV-vis spectrophotometer (Kyoto, Japan). Contact angles were measured using a Kyowa Interface Science Drop Master 300 (Saitama, Japan). Dynamic force microscope (DFM) was measured by using SII NanoTechnology Inc. E-sweep (Chiba Japan). X-ray diffraction (XRD) measurements were performed by the use of Rigaku MiniFlex 600 (Tokyo, Japan).

4.2.2. Materials

1*H*, 1*H*, 2*H*, 2*H*-nonafluoro-1-hexanol (**FA4**), 1*H*, 1*H*, 2*H*, 2*H*-tridecafluoro-1-*n*-octanol

(**FA6**), 1*H*, 1*H*, 2*H*, 2*H*-heptadecafluoro-1-decanol (**FA8**) and 1*H*, 1*H*, 2*H*, 2*H*, 6*H*, 6*H*-nonadecafluoro-1-undecanol (**DTFA**) were received from Unimatic Co., Ltd., respectively. Anatase titanium oxide nanoparticles (average particle size: 20 nm) were received from Ishihara Sangyo Kaisha Ltd. (Osaka, Japan). Tetraethoxysilane (TEOS), bisphenol A (BPA), 1,1'-bi(2-naphthol) [BINOL] and fullerene were purchased from Tokyo Chemical Industry Co., Ltd. (Tokyo, Japan). Silica-nanoparticle methanol solution [30 % (wt.): average particle size: 11 nm (Methanol Silica-sol^{TR})] was supplied by Nissan Chemical Industrials Ltd. (Tokyo, Japan). Aqueous ammonia was purchased from Wako Pure Chemical Industries, Ltd. (Osaka, Japan).

4.2.3. Preparation of 1*H*, 1*H*, 2*H*, 2*H*-tridecafluoro-1-*n*-octanol (FA6**)/SiO₂ nanocomposites**

To a methanol solution (20 ml) of 1*H*, 1*H*, 2*H*, 2*H*-tridecafluoro-1-*n*-octanol (**FA6**) [C₆F₁₃CH₂CH₂OH: 250 mg] were added tetraethoxysilane (TEOS: 0.25 ml), silica-nanoparticle methanol solution [30 % (wt.): 1.67 g] and 25 % aqueous ammonia solution (0.25 ml). The mixture was stirred with a magnetic stirring bar at room temperature for 5 hr. After the solvent was evaporated off, to the obtained crude products was added methanol (15

ml). The methanol solution was stirred with magnetic stirring bar at room temperature for 1 day, and then was centrifuged for 30 min. The expected fluorinated nanocomposites were easily separated from the methanol solution, and then was washed with methanol in several times. Fluorinated nanocomposites powders thus obtained were dried in vacuo at 50 °C for 2 days to afford purified particle powders (581 mg). Other fluorinated aliphatic alcohols/silica nanocomposites were also prepared under similar conditions.

4.2.4. Preparation of 1*H*, 1*H*, 2*H*, 2*H*-tridecafluoro-1-*n*-octanol (FA6)/SiO₂/anatase TiO₂ nanocomposites

To a methanol solution (20 ml) containing **FA6** (250 mg) were added tetraethoxysilane (TEOS: 0.25 ml), silica-nanoparticle methanol solution [30 % (wt.): 833 mg], anatase TiO₂ nanoparticles [*an*-TiO₂ (250 mg)], and 25 % aqueous ammonia solution (0.50 ml). The mixture was stirred with a magnetic stirring bar at room temperature for 2 hr, and then was centrifuged for 30 min. The expected fluorinated nanocomposites were easily separated from the methanol solution. Methanol (20 ml) was added to the obtained crude product. The methanol solution was stirred with magnetic stirring bar at room temperature for 1 day. After centrifugal separation of this solution, the obtained product was dried in vacuum at 50

°C for 2 days to produce purified fluorinated composite white colored powders (548 mg).

4.2.5. Preparation of 1*H*, 1*H*, 2*H*, 2*H*-tridecafluoro-1-*n*-octanol (FA6)/SiO₂/anatase TiO₂ nanocomposites - encapsulated bisphenol A

To a methanol solution (20 ml) containing **FA6** (250 mg) were added tetraethoxysilane (TEOS: 0.25 ml), silica-nanoparticle methanol solution [30 % (wt.): 833 mg], anatase TiO₂ nanoparticles [*an*-TiO₂ (250 mg)], bisphenol A (BPA: 100 mg), and 25 % aqueous ammonia solution (0.50 ml). The mixture was stirred with a magnetic stirring bar at room temperature for 2 hr, and then was centrifuged for 30 min. The expected fluorinated nanocomposites – encapsulated bisphenol A (BPA) were easily separated from the methanol solution. Methanol (20 ml) was added to the obtained crude product. The methanol solution was stirred with magnetic stirring bar at room temperature for 1 day. After centrifugal separation of this solution, the obtained product was dried in vacuum at 50 °C for 2 days to produce purified fluorinated nanocomposites - encapsulated bisphenol A as white colored powders (578 mg). Fluorinated nanocomposites – encapsulated other aromatic compounds such as 1,1'-bi(2-naphthol) (BINOL) and fullerene were also prepared under similar conditions.

4.2.6. Preparation of modified glass treated with fluorinated aliphatic alcohols/silica nanocomposites by dipping method

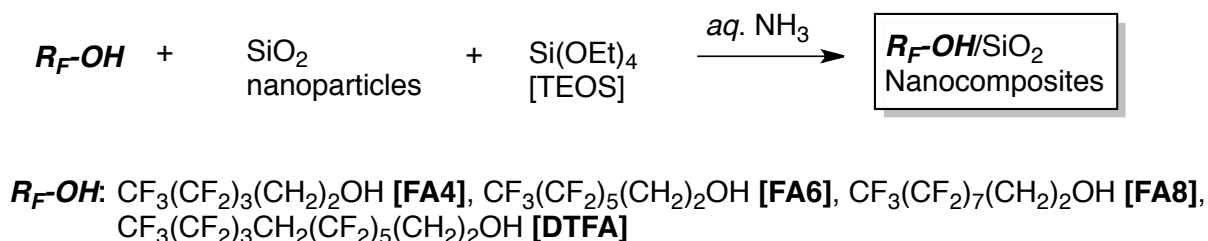
To a methanol solution (20 ml) containing **FA8** (250 mg) were added tetraethoxysilane (0.25 ml), silica-nanoparticle methanol solution [30 % (wt.): 1.67 g], and 25 wt% aqueous ammonia solution (0.40 ml). The mixture was stirred with a magnetic stirring bar at room temperature for 5 hr. The glass plate ($18 \times 18 \text{ mm}^2$ pieces) was dipped into the methanol solution of fluorinated nanocomposites at room temperature and left for 1 min. This was lifted from the solution at constant rate and dried at room temperature for 1 day under vacuum to afford the modified glass.

4.3. Results and discussion

4.3.1. Preparation of a variety of fluorinated aliphatic alcohols/SiO₂ nanocomposites and

Application to the surface modification of glass treated with these nanocomposites

Tetraethoxysilane (TEOS) underwent the sol-gel reaction in the presence of silica nanoparticles and a variety of fluorinated aliphatic alcohols under alkaline conditions to give the corresponding fluorinated alcohols/silica composites (**R_F-OH/SiO₂**) in 55 ~ 76 % isolated yields. These results are demonstrated in Scheme 4-1 and Table 4-1.



Scheme 4-1 Preparation of **R_F-OH/SiO₂** nanocomposites.

Table 4-1 Preparation of $R_F\text{-OH}/\text{SiO}_2$ nanocomposites.

Run	$R_F\text{-OH}$ (mg)	SiO_2 (mg)	TEOS (mL)	aq. 25 % NH_3 (mL)	Yield (%) ^{a)}	Size of the composites (nm) ^{b)}	Weight loss (%) ^{d)}
FA4							
1	250	500	0.25	0.25	71	36.8 ± 9.9 (39.0 ± 3.1) ^{c)}	7
2	250	500	0.25	0.50	72	30.1 ± 7.3 (39.5 ± 9.9)	7
3	250	500	0.25	1.0	46	69.1 ± 13.9 (45.3 ± 10.9)	7
4	250	500	0.25	2.0	55	41.5 ± 10.2 (42.6 ± 9.2)	7
5	250	500	0.25	4.0	76	34.0 ± 7.6 (139.8 ± 25.5)	7
FA6							
6	250	500	0.25	0.25	61	35.3 ± 8.3 (53.3 ± 11.4)	8
7	250	500	0.25	0.50	71	40.5 ± 11.3 (40.5 ± 12.0)	6
8	250	500	0.25	1.0	71	40.5 ± 13.0 (62.3 ± 18.5)	6
9	250	500	0.25	2.0	59	105.3 ± 19.0 (97.5 ± 30.2)	7
10	250	500	0.25	4.0	52	45.4 ± 13.2 (60.9 ± 17.1)	6
FA8							
11	250	500	0.25	0.25	63	41.7 ± 13.7 (81.7 ± 21.6)	7
12	250	500	0.25	0.50	59	28.2 ± 6.0 (32.2 ± 9.8)	6
13	250	500	0.25	1.0	58	56.6 ± 11.5 (53.7 ± 10.2)	6
14	250	500	0.25	2.0	63	53.6 ± 11.4 (55.1 ± 14.5)	6
15	250	500	0.25	4.0	69	39.7 ± 9.2 (35.4 ± 12.8)	7
DTFA							
16	250	500	0.25	0.25	71	54.5 ± 19.3 (71.9 ± 15.3)	7
17	250	500	0.25	0.50	73	44.3 ± 13.8 (46.2 ± 10.4)	7
18	250	500	0.25	1.0	64	55.6 ± 12.3 (53.1 ± 14.7)	8
19	250	500	0.25	2.0	61	53.6 ± 10.3 (54.0 ± 12.9)	6
20	250	500	0.25	4.0	70	63.6 ± 14.1 (72.0 ± 15.5)	6

a) Yields based on $R_F\text{-OH}$, SiO_2 and TEOS

b) Determined by dynamic light scattering (DLS) measurements

c) After calcination at 800 °C

d) Determined by thermogravimetric analysis (TGA)

As shown in Table 4-1, the yields of the expected composites are in general dependent

upon the feed ratios of ***R_F-OH*** and *aq.* NH₃ employed, increasing with greater feed ratios of *aq.* NH₃ in *aq.* NH₃ – ***R_F-OH*** except for **FA6/SiO₂** and **DTAF/SiO₂** composites. This finding suggests that the relatively higher feed amounts of *aq.* ammonia is essential for the smooth sol-gel reactions in Scheme 4-1.

These obtained composites were found to exhibit a good dispersibility and stability for not only water but also the traditional organic solvents such as methanol, ethanol, 1,2-dichloroethane and tetrahydrofuran. Thus, the size of ***R_F-OH***/SiO₂ composites in Table 4-1 before and after calcination at 800 °C in methanol has been measured by dynamic light-scattering (DLS) measurements at 25 °C. Each size of these obtained fluorinated SiO₂ composites before and after calcination at 800 °C is nanometer size-controlled fine particles: 28 ~ 105 nm and 32 ~ 140 nm (number-average diameter), respectively (see Table 4-1).

The field-emission scanning electron micrograph (FE-SEM) of well-dispersed methanol solutions of nanocomposites (Runs 1 and 20 in Table 4-1) before and after calcination at 800 °C has been measured, and the results were shown in Figs. 4-1 and 4-2.

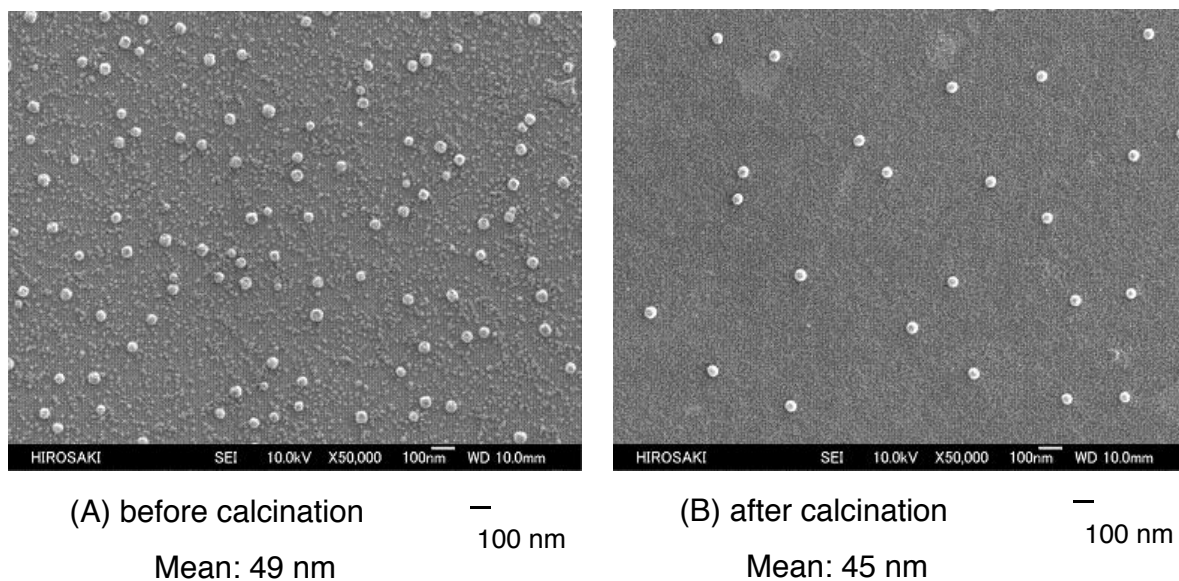


Fig. 4-1 FE-SEM (Field Emission Scanning Electron Microscopy) images of methanol solutions of FA4/SiO₂ nanocomposites (Run 1 in Table 4-1).

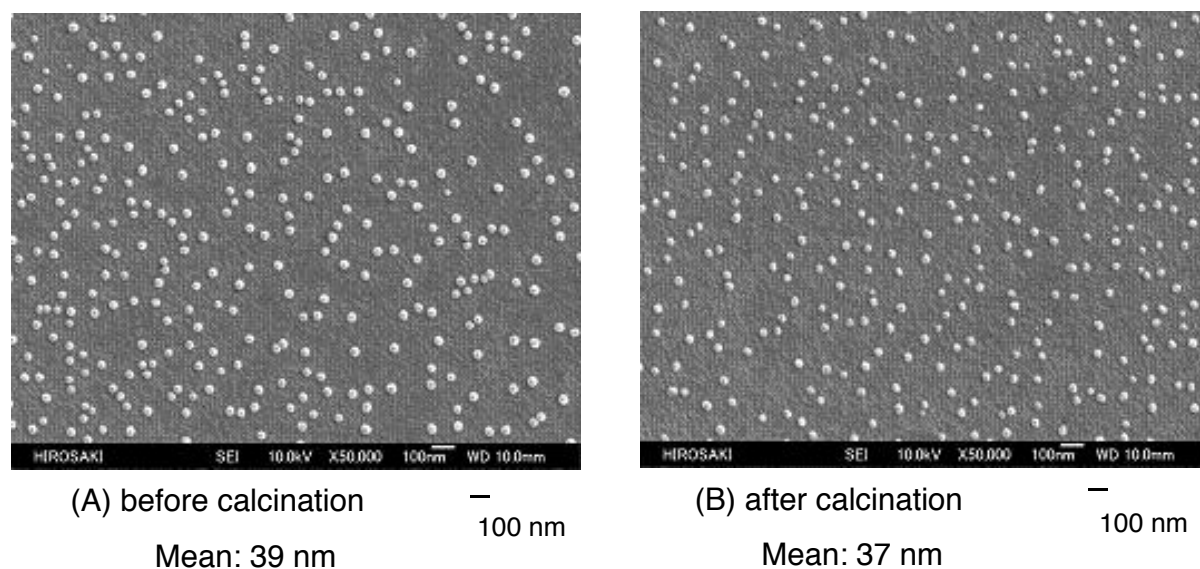


Fig. 4-2 FE-SEM (Field Emission Scanning Electron Microscopy) images of methanol solutions of DTFA/SiO₂ nanocomposites (Run 20 in Table 4-1).

FE-SEM pictures of these nanocomposites before and after calcination at 800 °C also showed the formation of composite fine particles with an average diameter of 39 ~ 49 nm and

37 ~ 45 nm, respectively, and the composite particles of the almost same size were obtained before (37 ~ 64 nm) and after (39 ~ 72 nm) calcination.

The thermal stability of $R_F\text{-OH/SiO}_2$ nanocomposites has been studied by the use of thermogravimetric analyses (TGA), in which the weight loss of the nanocomposites was measured by raising the temperature around 800 °C at 10 °C/min heating ratio under air atmospheric conditions, and the results were shown in Fig. 4-3. The weight loss value at 800 °C of each nanocomposite was also illustrated in Table 4-1.

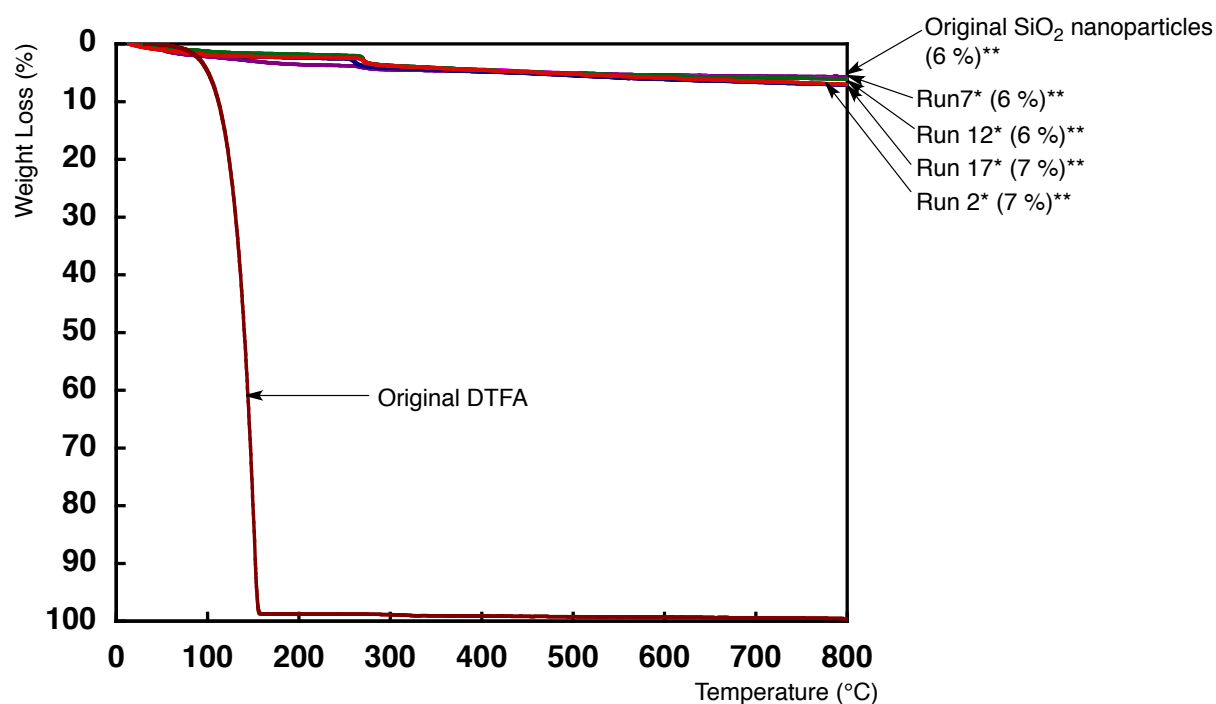


Fig. 4-3 Thermogravimetric analyses of $R_F\text{-OH/SiO}_2$ nanocomposites.

*) Each Run No. corresponds to that of Table 4-1

**)Weight loss at 800 °C

Boiling points of parent fluorinated alcohols: **FA4**, **FA6** and **FA8** are 76 °C/56 mmHg, 87

$^{\circ}\text{C}/20\text{ mmHg}$ and $115\text{ }^{\circ}\text{C}/20\text{ mmHg}$, respectively. Fig. 4-3 shows that original **DTFA** markedly dropped around $100\text{ }^{\circ}\text{C}$ to give a perfect weight loss ($\sim 100\%$) around $160\text{ }^{\circ}\text{C}$. On the other hand, **FA4/SiO₂** nanocomposites, **FA6/SiO₂** nanocomposites, **FA8/SiO₂** nanocomposites, and **DTFA/SiO₂** nanocomposites were found to exhibit no weight loss corresponding to the contents of fluorinated alcohols in the composites even after calcination, and the weight loss ($6 \sim 7\%$) at $800\text{ }^{\circ}\text{C}$ of each nanocomposite was quite similar to that (6%) of the parent silica nanoparticles, although the theoretical contents of these fluorinated alcohols in the composites is 31% . Other fluorinated silica nanocomposites illustrated in Table 4-1 gave the similar weight loss ($6 \sim 8\%$) at $800\text{ }^{\circ}\text{C}$, and the fluorinated alcohols exhibited no weight loss behavior even after calcination at $800\text{ }^{\circ}\text{C}$.

The energy dispersive X-ray analyses (EDX) of **FA4/SiO₂** nanocomposites (Run 2 in Table 4-1) and **DTFA/SiO₂** nanocomposites (Run 20 in Table 4-1) have been measured to verify the presence of organic segments in the nanocomposites before and after calcination, and the results are as follows:

Atomic contents (atm, %)				
	C	O	F	Si
FA4/SiO₂ nanocomposites				
Before calcination	18.99	53.45	0.10	27.46
After calcination	26.01	47.45	0.04	26.49

DTFA/SiO₂ nanocomposites				
Before calcination	22.23	60.22	0.76	16.80
After calcination	28.58	56.77	0.69	13.96

Interestingly, each fluorinated nanocomposite after calcination at 800 °C exhibited the similar atomic content values (carbon and fluorine) to that before calcination, indicating that the fluorinated alcohols should exhibit a nonflammable characteristic even after calcination at 800 °C.

It was previously reported that fluoroalkyl end-capped *N*-(1,1-dimethyl-3-oxobutyl)acrylamide oligomer [R_F-(DOBAA)_n-R_F] and 2-methacryloyloxyethanesulfonic acid oligomer [R_F-(CH₂CMeCO₂CH₂CH₂SO₃H)_n-R_F: R_F-(MES)_n-R_F] can exhibit no weight loss characteristic in the silica nanocomposite matrices

even after calcination.^{28, 34 ~ 36)} It is suggested that ammonium hexafluosilicate is formed through the dehydrofluorination between the amido protons (or higher acidic sulfo protons) and fluorines in oligomers during the nanocomposite reactions in the presence of aqueous ammonia, and the effective interaction between ammonium hexafluorosilicate and $R_F-(DOBAA)_n-R_F$ oligomer (or $R_F-(MES)_n-R_F$ oligomer) in the silica gel matrices should afford a nonflammable characteristic toward these oligomers.^{28, 34 ~ 36)} Thus, dehydrofluorination between fluorines and protons in R_F-OH should proceed under alkaline conditions (aqueous ammonia) in the presence of silica nanoparticles as a co-catalyst to give tetrafluorosilane, and finally, ammonium hexafluorosilicate. The formation of ammonium hexafluorosilicate enables R_F-OH in the silica composite cores to give a nonflammable behavior even after calcination at 800 °C.

Some R_F-OH /silica nanocomposites in Table 4-1 were applied to the surface modification of glass, and the contact angles of dodecane and water for the glass plate were measured by depositing a droplet of dodecane or water (2 μ l) on the modified glass surface. The results were shown in Table 4-2.

Table 4-2 Contact angles of water and dodecane on the modified glass treated with ***R_F-OH***/SiO₂ nanocomposites.

Run*	Contact angle (Degree)							
	Dodecane							
		0 min	5 min	10 min	15 min	20 min	25 min	30 min
5	35	21	10	0	0	0	0	0
10	49	28	0	0	0	0	0	0
15	127	91	18	4	0	0	0	0
19	80	95	75	63	57	50	47	42

*) Each Run No. corresponds to that of Table 4-1

As shown in Table 4-2, the contact angles of dodecane and water on the modified glass surfaces treated with ***R_F-OH***/silica nanocomposites are 35 ~ 127° and 21 ~ 95°, respectively, compared with those (0 and 51°) of nontreated glass. A steep time dependence of contact angle of water was observed in the ***R_F-OH*** (**FA4**, **FA6** and **FA8**)/silica nanocomposites, although such time dependence was not observed in the dodecane contact angle measurements at all. The contact angles decreased dramatically from 21 ~ 91° to 0° over 5 ~ 15 min to give a superhydrophilicity on the modified surfaces, although such time dependence was not observed in the **DTAF**/SiO₂ nanocomposites. This finding suggests that at the interface with water, hydrophobic fluoroalkyl segments are replaced by the strongly hydrophilic hydroxyl groups in ***R_F-OH***. The hydroxyl segments in ***R_F-OH*** are also likely to be arranged more regularly at the interface. It takes about 5 ~ 15 min to replace the fluoroalkyl segments by hydroxyl groups when the environment is changed from air to water.

In contrast, since **DTFA** possesses the methylene unit $[-(\text{CH}_2)_2-]$ introduced into the inside of the longer fluoroalkyl group, the smooth flip-flop motion between such partly fluoroalkylated units and the hydroxyl groups in the **DTFA** would be restricted on the modified surface to give the superhydrophilic characteristic (water contact angle value: 0°), compared with that of perfectly fluoroalkylated ones.

On the other hand, dodecane contact angle values were found to increase from 19° to 127° with the increase of the carbon chain of fluoroalkyl groups from $\text{CF}_3(\text{CF}_2)_3-$ to $\text{CF}_3(\text{CF}_2)_7-$. Interestingly, **FA8/SiO₂** nanocomposites afforded the superoleophobic surface (dodecane contact angle: 127°). In general, highly oleophobic (superoleophobic) surface are realized by achieving low surface energy and high surface roughness.^{37 ~ 39)} The fabrication of superoleophobic surfaces is difficult due to the lower surface tension of oils than that of water.^{40, 41)} However, the superhydrophobic and superoleophobic (superamphiphobic) microtextured surface have been prepared by spray coating a blend of poly(methyl methacrylate) and the low surface energy molecule *1H, 1H, 2H, 2H*-heptadecafluorodecyl polyhedral oligomeric silsesquioxane.⁴²⁾

The surface roughness is very important for the wetting properties for liquids. Thus, we have studied on the surface roughness of the modified glasses with **FA4/SiO₂** nanocomposites and **FA8/SiO₂** nanocomposites, which exhibit the relatively higher oleophobicity (dodecane

contact angle: 49°) and the superoleophobicity (dodecane contact angle value: 127°), respectively, by the use of DFM (dynamic force microscopy), and the results are shown in Fig. 4-4.

As shown in Fig. 4-4, DFM measurements show that the topographical image of each surface show a roughness characteristic, and the roughness average: Ra (77 nm) of the modified glass possessing superoleophobic characteristic (A) is higher than that (Ra: 63 nm) of the modified glass possessing the relatively higher oleophobic characteristic (B).

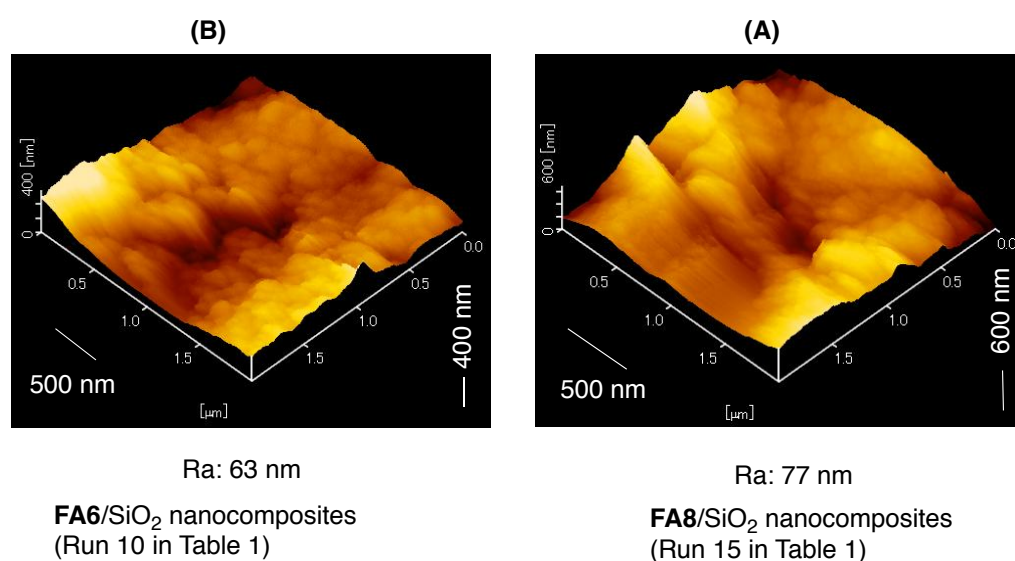


Fig. 4-4 DFM (Dynamic Force Microscopy) topographic images of the modified glass surface treated with **FA6/SiO₂** nanocomposites and **FA8/SiO₂** nanocomposites.

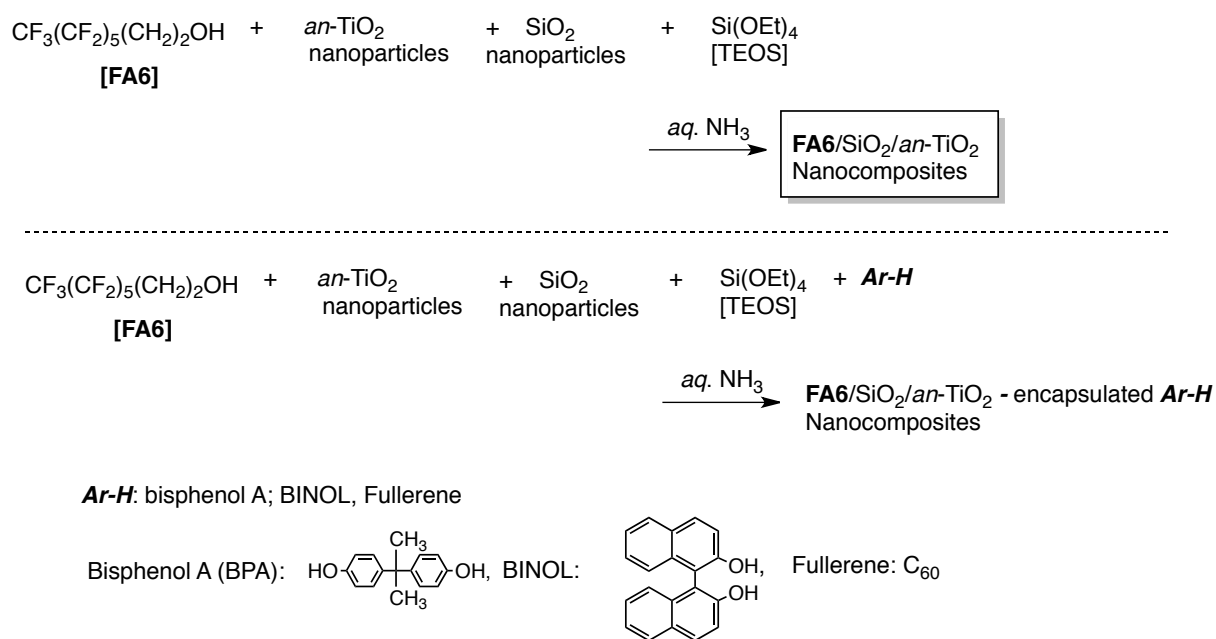
In this way, the present **FA8/SiO₂** nanocomposites are essential to the architecture of rough surface, and are effective for the architecture of the superhydrophilic and superoleophobic fractal surface by combination of appropriate surface roughness with longer

perfluoroalkyl groups possessing both hydrophilic and oleophobic properties in the composites.

4.3.2. Preparation and photocatalytic activity of 1*H*, 1*H*, 2*H*, 2*H*-tridecafloro-1-*n*-octanol (FA6)/SiO₂/anatase TiO₂ nanocomposites and 1*H*, 1*H*, 2*H*, 2*H*-tridecafloro-1-*n*-octanol (FA6)/SiO₂/anatase TiO₂ nanocomposites encapsulaed *Ar-H*

It has been very recently reported that fluoroalkyl end-capped vinyltrimethoxysilane oligomer $[R_F-CH_2CHSi(OMe)_3]_n-R_F$; $n = 2, 3$; $R_F = CF(CF_3)OC_3F_7$] undergoes the sol-gel reactions in the presence of anatase TiO₂ nanoparticle (*an*-TiO₂) under alkaline conditions to give the corresponding fluorinated oligomeric silica nanocomposites - encapsulated *an*-TiO₂ nanoparticles.⁴³⁾ Interestingly, the fluorinated nanocomposits - encapsulated *an*-TiO₂ nanoparticles before and even after calciantion can give a higher photocatalytic activity than that of original *an*-TiO₂ nanoparticles under similar conditions. It was suggested that such higher photocatalytic activity is due to the formation of Ti-F units in the composites. From the developmental viewpoints of new fluorinated functional material, especially new fluorinated materials possessing a higher photocatalytic activity, it is of particular interest to explore the fluorinated aliphatic alcohol/SiO₂/*an*-TiO₂ nanocomposites. Thus, new fluorinated aliphatic

alcohol/SiO₂/*an*-TiO₂ nanocomposites were prepared. In addition, the fluorinated aliphatic alcohol/SiO₂/*an*-TiO₂ nanocomposites – encapsulated aromatic compounds (***Ar-H***) such as bisphenol A (BPA), 1,1'-bi(2-naphthol) [BINOL] and fullerene were also prepared under similar conditions. These results were shown in Scheme 4-2 and Table 4-3.



Scheme 4-2 Preparation of **FA6/SiO₂/*an*-TiO₂** nanocomposites and **FA6/SiO₂/*an*-TiO₂** - encapsulated ***Ar-H*** nanocomposites.

Table 4-3 Preparation of **FA6**/SiO₂/*an*-TiO₂/**Ar-H** nanocomposites.

Run	FA6 (mg)	<i>an</i> -TiO ₂ (mg)	SiO ₂ (mg)	TEOS (ml)	NH ₃ (ml)	Ar-H (mg)	Product yield *	Size of composites ** (after calcination) (nm) ± STD
1	250	250	250	0.25	0.50	—	73	22.5 ± 5.4 (22.4 ± 5.1)***
						BPA		
2	250	250	250	0.25	0.50	100	68	17.4 ± 3.8 (21.8 ± 6.2)
3	250	250	250	0.25	0.50	250	58	19.8 ± 5.0 (17.6 ± 3.8)
4	250	250	250	0.25	0.50	500	47	19.5 ± 3.8 (20.5 ± 4.1)
						BINOL		
5	250	250	250	0.25	0.50	100	66	27.3 ± 5.9 (31.9 ± 6.3)
6	250	250	250	0.25	0.50	250	58	23.8 ± 4.0 (25.8 ± 4.3)
7	250	250	250	0.25	0.50	500	48	77.1 ± 17.3 (82.8 ± 15.8)
						C ₆₀		
8	250	250	250	0.25	0.50	5	84	35.8 ± 8.7 (45.3 ± 7.2)
9	250	250	250	0.25	0.50	25	63	27.7 ± 6.8 (36.8 ± 7.7)
10	250	250	250	0.25	0.50	50	63	56.4 ± 15.3 (27.5 ± 6.8)

* Yield based on **FA6**, TiO₂, SiO₂, TEOS and **Ar-H**

** Determined by DLS (dynamic light scattering) measurements in methanol solutions

*** After calcination at 1000°C

As shown in Scheme 4-2 and Table 4-3, the expected **FA6**/SiO₂/*an*-TiO₂ composites and **FA6**/SiO₂/*an*-TiO₂ nanocomposites - encapsulated aromatic compounds were obtained in 47 ~ 84 % isolated yields by the sol-gel reactions under alkaline conditions. These obtained composites afforded a good dispersibility and stability for not only water but also the traditional organic solvents such as methanol, ethanol, 1,2-dichloroethane and tetrahydrofuran. Thus, the size of these composites illustrated in Table 4-1 before and after calcination at 1000 °C in methanol have been measured by dynamic light-scattering (DLS) measurements at 25 °C. Each size of these obtained fluorinated composites before and after calcination at 1000 °C is nanometer size-controlled fine particles: 17 ~ 77 nm and 18 ~ 82 nm (number-average

diameter), respectively (see Table 4-1).

The field-emission scanning electron micrograph (FE-SEM) of well-dispersed methanol solutions of **FA6**/SiO₂/*an*-TiO₂ nanocomposites – encapsulated fullerene (Run 9 in Table 4-3) before and after calcination at 1000 °C have been measured, and the results were shown in Fig. 4-5.

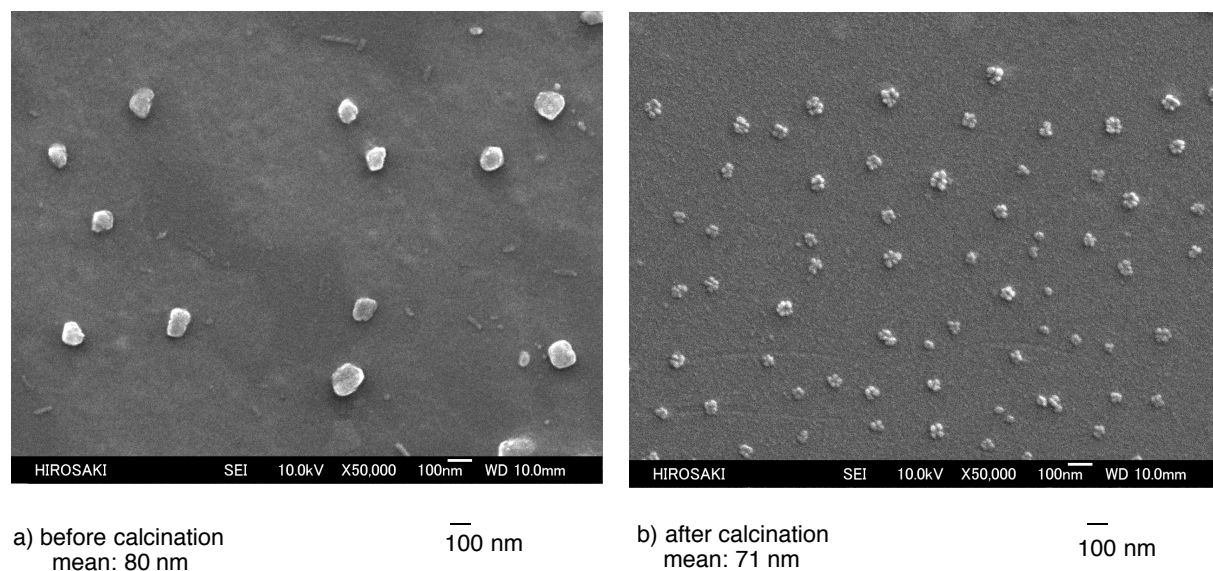


Fig. 4-5 FE-SEM (Fuel Emission-Scanning Electron Microscopy) images of **FA6**/SiO₂/*an*-TiO₂ nanocomposites - encapsulated C₆₀ (Run 9 in Table 4-3) before and after calcination at 1000 °C.

FE-SEM pictures of the nanocomposites before and after calcination at 1000 °C also showed the formation of composite fine particles with an average diameter of 80 nm and 71 nm, respectively, and the composite particles of the almost same size were obtained before and after calcination.

The thermal stability of **FA6**/SiO₂/*an*-TiO₂ nanocomposites and **FA6**/SiO₂/*an*-TiO₂

nanocomposites - encapsulated BPA has been studied by the use of thermogravimetric analyses (TGA), in which the weight loss of these nanocomposites was measured by raising the temperature around 800 °C at 10 °C/min heating ratio under air atmospheric conditions, and the results were shown in Fig. 4-6.

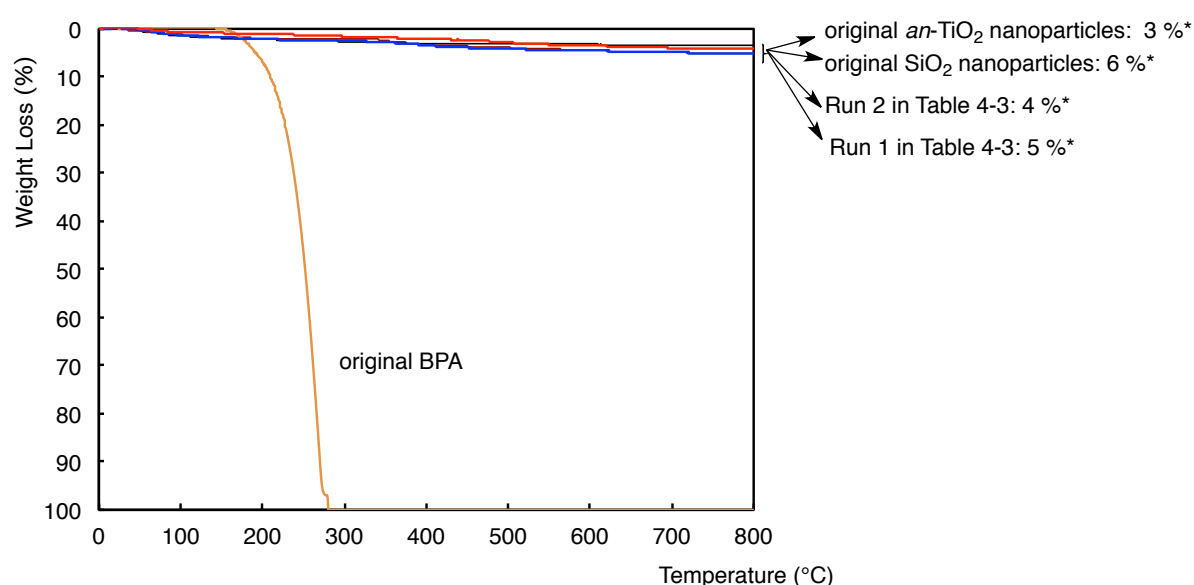


Fig. 4-6 Thermogravimetric analysis of original BPA, *an*-TiO₂ nanoparticles, SiO₂ nanoparticles, **FA6**/SiO₂/*an*-TiO₂ nanocomposites (Run 1 in Table 4-3), and **FA6**/SiO₂/*an*-TiO₂ nanocomposites-encapsulated BPA (Run 2 in Table 4-3).
*) Weight loss at 800 °C.

As shown in Fig. 4-6, **FA6**/SiO₂/*an*-TiO₂ nanocomposites (Run 1 in Table 4-3) exhibited no weight loss even after calcination at 800 °C, of whose behavior is similar to that of **FA6**/SiO₂ nanocomposites illustrated in Fig. 4-3. Interestingly, **FA6**/SiO₂/*an*-TiO₂ - encapsulated BPA (Run 2 in Table 4-3), in which the theoretical content of BPA in the composites is 11 %, were found to exhibit no weight loss behavior corresponding to the

contents of encapsulated BPA in the composites even after calcination at 800 °C, although the original BPA decomposed completely around 280 °C (see Fig. 4-6). Similar results were obtained in **FA6**/SiO₂/*an*-TiO₂ nanocomposites - encapsulated BINOL [theoretical content of BINOL in the composites: 11 % (Run 5 in Table 4-3)] and **FA6**/SiO₂/*an*-TiO₂ nanocomposites – encapsulated fullerene [theoretical content of fullerene in the composites: 1 % (Run 8 in Table 4-3)] (see Figs. 4-7 and 4-8).

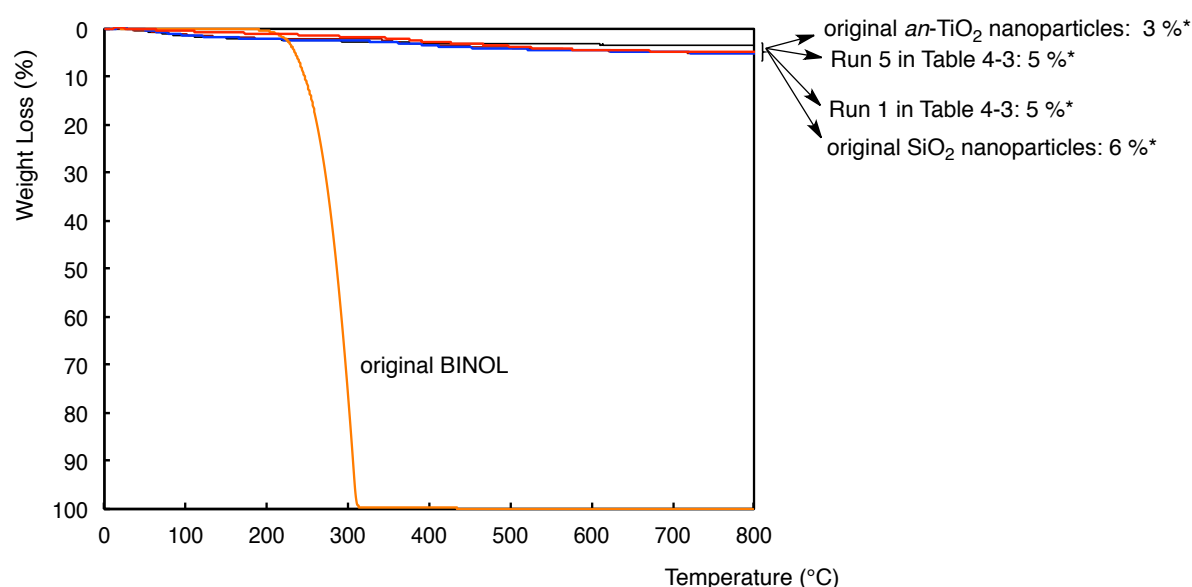


Fig. 4-7 Thermogravimetric analysis of original BINOL, *an*-TiO₂ nanoparticles, SiO₂ nanoparticles, **FA6**/SiO₂/*an*-TiO₂ nanocomposites (Run 1 in Table 4-3), and **FA6**/SiO₂/*an*-TiO₂ nanocomposites - encapsulated BINOL (Run 5 in Table 4-3).

*) Weight loss at 800 °C

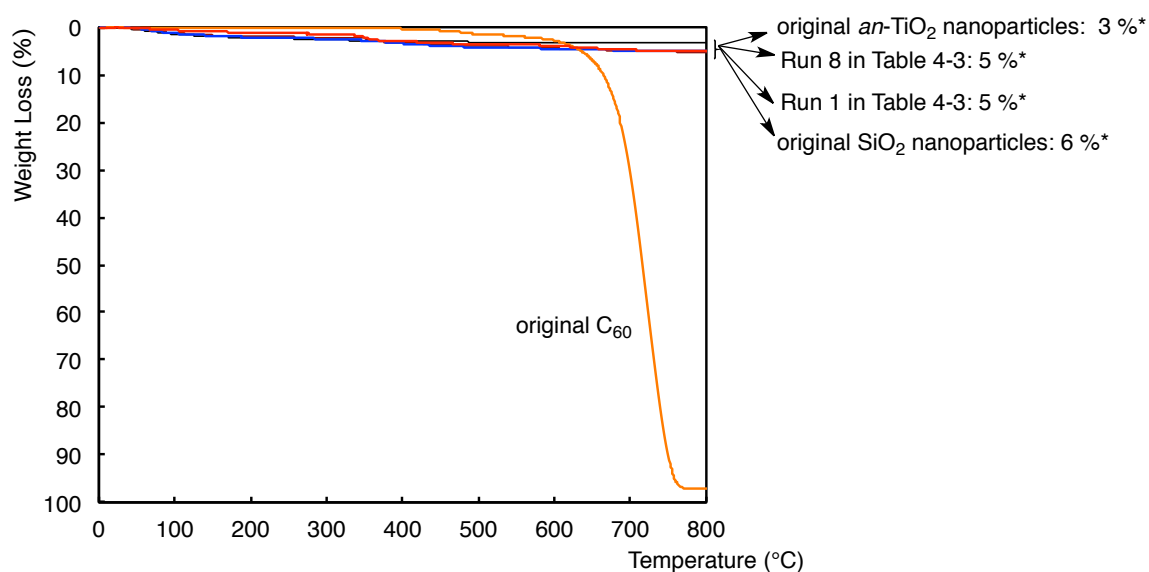


Fig. 4-8 Thermogravimetric analysis of original fullerene, *an*-TiO₂ nanoparticles, SiO₂ nanoparticles, **FA6**/SiO₂/*an*-TiO₂ nanocomposites (Run 1 in Table 4-3), and **FA6**/SiO₂/*an*-TiO₂ nanocomposites-encapsulated C₆₀ (Run 8 in Table 4-3).
*) Weight loss at 800 °C

More interestingly, **FA6**/SiO₂/*an*-TiO₂ - encapsulated BPA nanocomposites (Runs 3 and 4 in Table 4-3) and **FA6**/SiO₂/*an*-TiO₂ - encapsulated BINOL nanocomposites (Runs 6 and 7 in Table 4-3), which were prepared under the greater feed ratios of BPA (or BINOL) (250 mg and 500 mg) in BPA (or BINOL) - **FA6**, were also found to exhibit no weight loss corresponding to the contents of BPA or BINOL in the composites even after calcination at 800 °C (see Figs. 4-9 ~ 4-12).

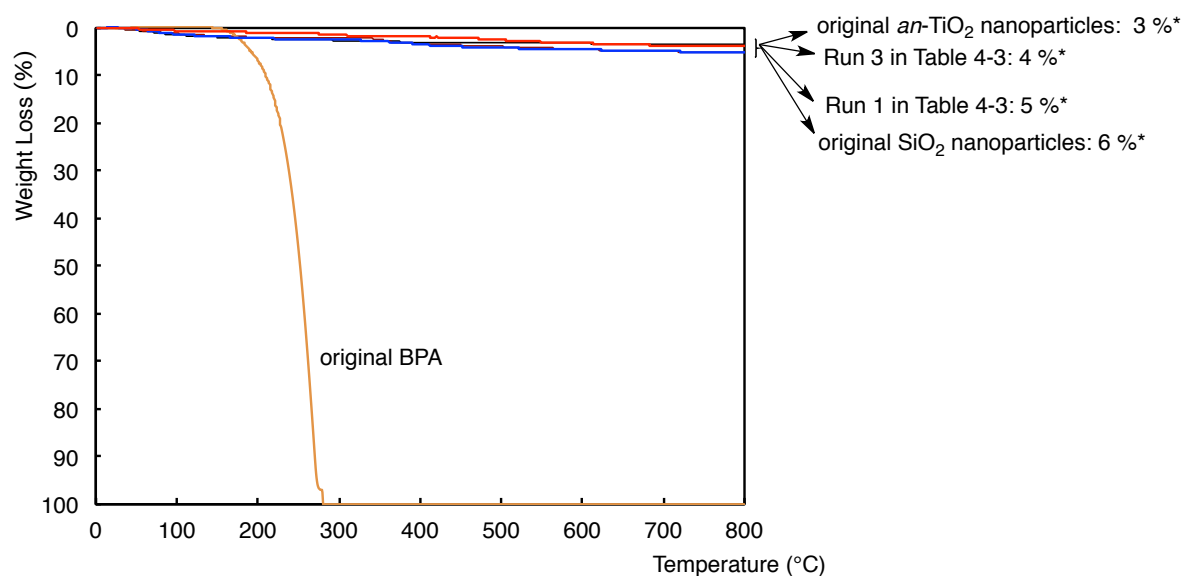


Fig. 4-9 Thermogravimetric analysis of original BPA, $an\text{-TiO}_2$ nanoparticles, SiO_2 nanoparticles, **FA6**/ SiO_2 / $an\text{-TiO}_2$ nanocomposites (Run 1 in Table 4-3), and **FA6**/ SiO_2 / $an\text{-TiO}_2$ nanocomposites - encapsulated BPA (Run 3 in Table 4-3).
*) Weight loss at 800 °C

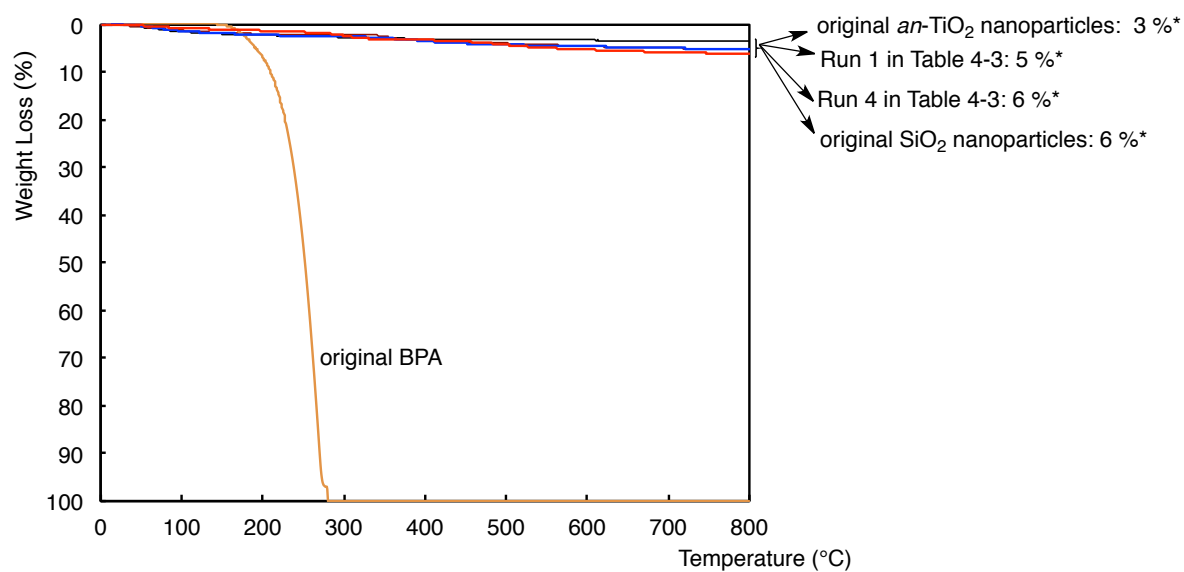


Fig. 4-10 Thermogravimetric analysis of original BPA, $an\text{-TiO}_2$ nanoparticles, SiO_2 nanoparticles, **FA6**/ SiO_2 / $an\text{-TiO}_2$ nanocomposites (Run 1 in Table 4-3), and **FA6**/ SiO_2 / $an\text{-TiO}_2$ nanocomposites - encapsulated BPA (Run 4 in Table 4-3).
*) Weight loss at 800 °C

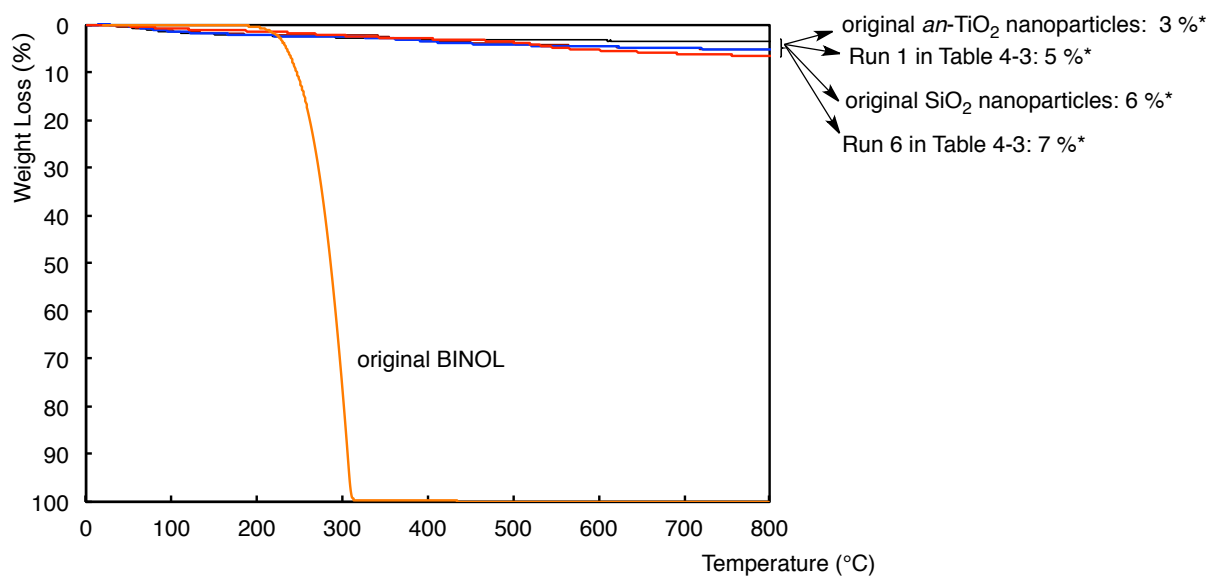


Fig. 4-11 Thermogravimetric analysis of original BINOL, *an*-TiO₂ nanoparticles, SiO₂ nanoparticles, **FA6**/SiO₂/*an*-TiO₂ nanocomposites (Run 1 in Table 4-3), and **FA6**/SiO₂/*an*-TiO₂ nanocomposites - encapsulated BINOL (Run 6 in Table 4-3).

*) Weight loss at 800 °C

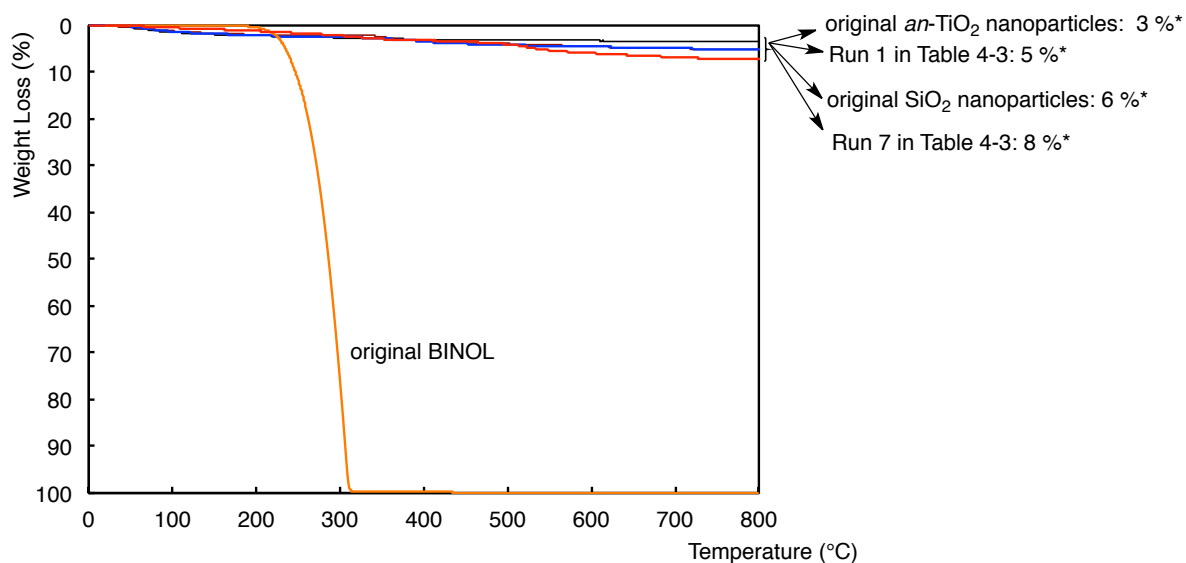


Fig. 4-12 Thermogravimetric analysis of original BINOL, *an*-TiO₂ nanoparticles, SiO₂ nanoparticles, **FA6**/SiO₂/*an*-TiO₂ nanocomposites (Run 1 in Table 4-3), and **FA6**/SiO₂/*an*-TiO₂ nanocomposites - encapsulated BINOL (Run 7 in Table 4-3).

*) Weight loss at 800 °C

On the other hand, **FA6**/SiO₂/*an*-TiO₂ - encapsulated fullerene (Runs 9 and 10 in Table 4-3), which were prepared under the feed ratios (25 mg and 50 mg) of fullerene in fullerene –

FA6, were found to exhibit a clear weight loss at 800 °C in each nanocomposite (see Figs. 4-13 and 4-14).

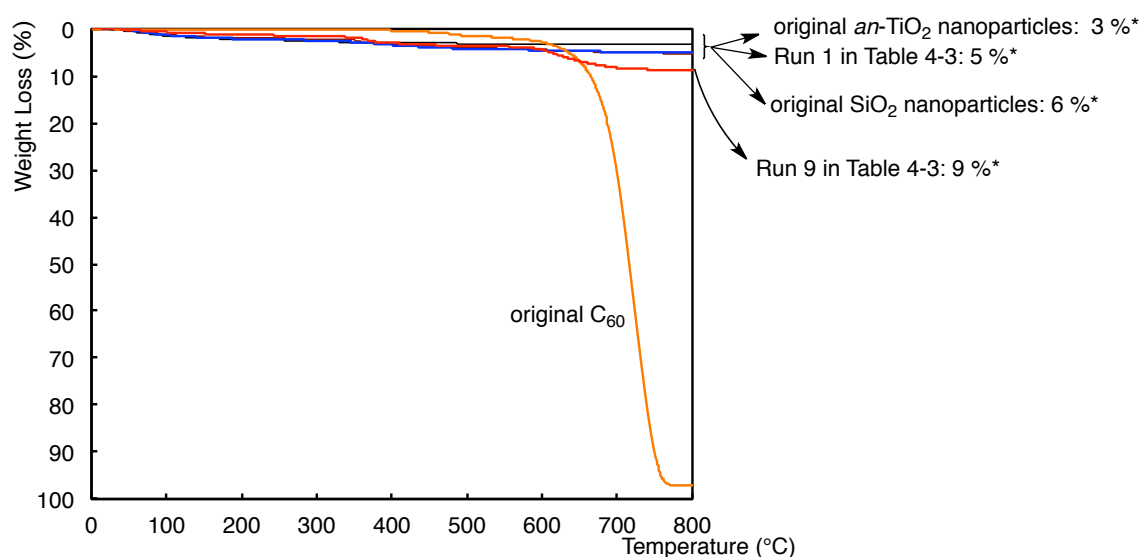


Fig. 4-13 Thermogravimetric analysis of original fullerene, *an*-TiO₂ nanoparticles, SiO₂ nanoparticles, **FA6**/SiO₂/*an*-TiO₂ nanocomposites (Run 1 in Table 4-3), and **FA6**/SiO₂/*an*-TiO₂ nanocomposites - encapsulated C₆₀ (Run 9 in Table 4-3).
*) Weight loss at 800 °C

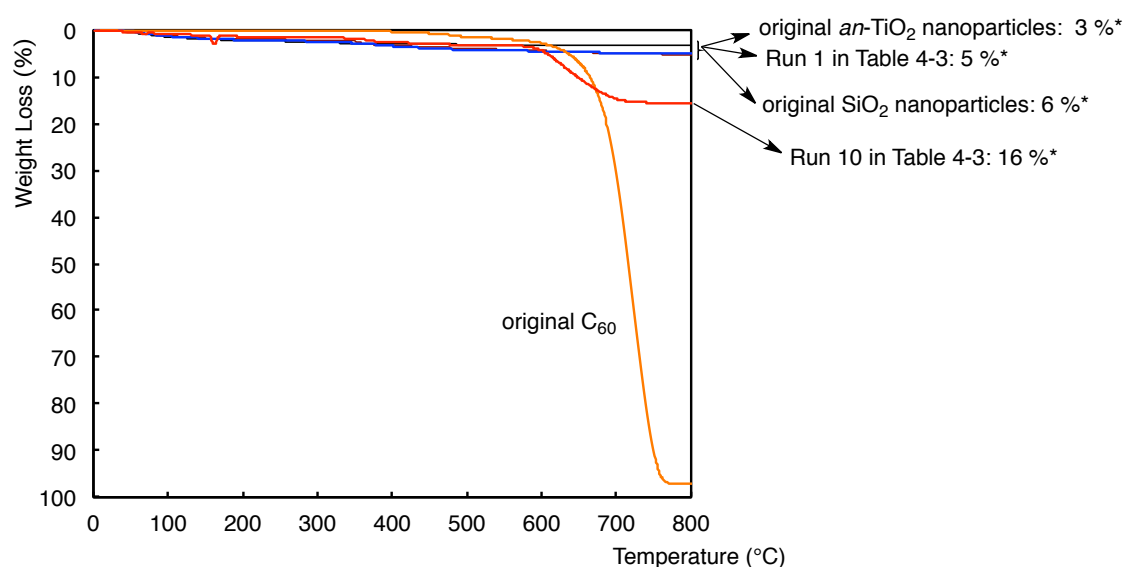


Fig. 4-14 Thermogravimetric analysis of original fullerene, *an*-TiO₂ nanoparticles, SiO₂ nanoparticles, **FA6**/SiO₂/*an*-TiO₂ nanocomposites (Run 1 in Table 4-3), and **FA6**/SiO₂/*an*-TiO₂ nanocomposites - encapsulated C₆₀ (Run 10 in Table 4-3).
*) Weight loss at 800 °C

It was previously reported that encapsulated aromatic compounds possessing acidic hydroxyl groups such as BPA in fluoroalkyl end-capped acrylic acid oligomer $[R_F-(CH_2CHCOOH)_n-R_F]$; $R_F = CF(CF_3)OC_3F_7$ /silica nanocomposite matrices can exhibit a non-flammable characteristic due to the formation of hexafluorosilicate anions in the composite matrices through the dehydrofluorination of phenol-type acidic protons and fluorines in the composites catalyzed by both ammonia and silica nanoparticles.³²⁾ Therefore, encapsulated fullerenes in the nanocomposites, which were prepared under such greater feed ratios of fullerene, should exhibit a clear weight loss after calcination at 800 °C.

It has been reported that $R_F-(VM-SiO_2)_n-R_F/an-TiO_2$ nanocomposites can keep the anatase TiO_2 structure even after calcination at 1000 °C, although the parent *an*- TiO_2 nanoparticles give a perfect phase transformation into the rutile under similar conditions (see Fig. 4-15).⁴³⁾

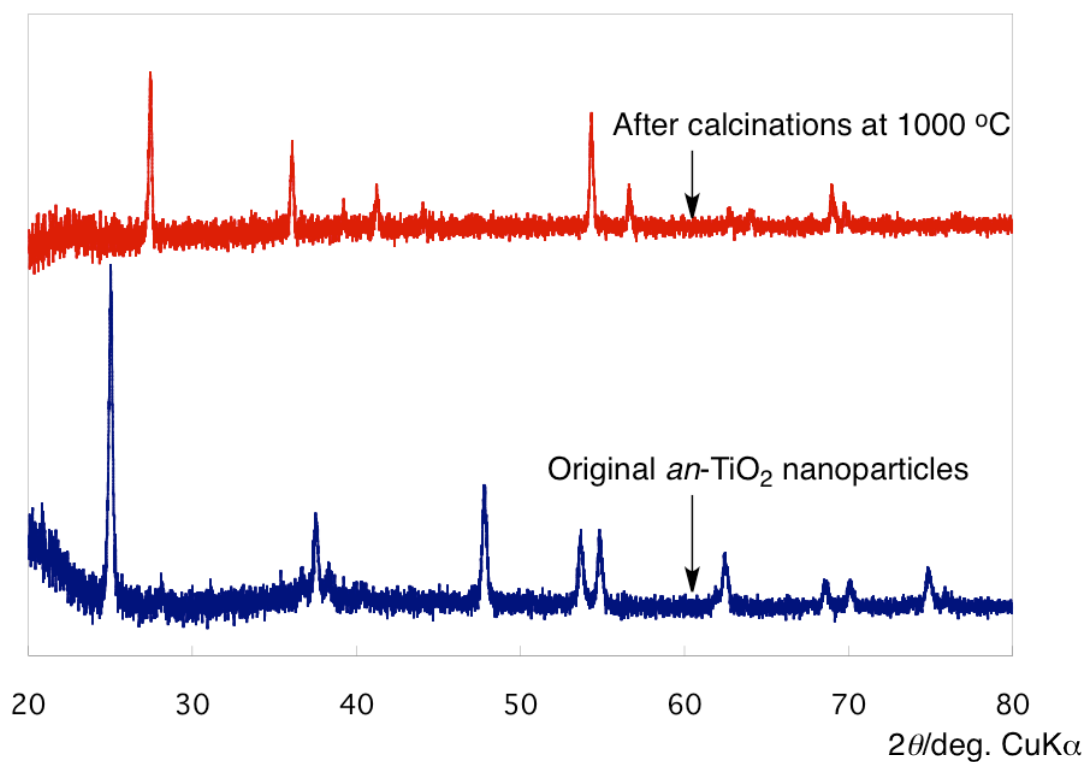


Fig. 4-15 X-ray diffraction patterns of original *an*-TiO₂ nanoparticles before and after calcinations at 1000 °C.

Thus, the XRD spectra of **FA6**/SiO₂/*an*-TiO₂ nanocomposites (Run 1 in Table 4-3) have been studied, and the results were shown in Fig. 4-16.

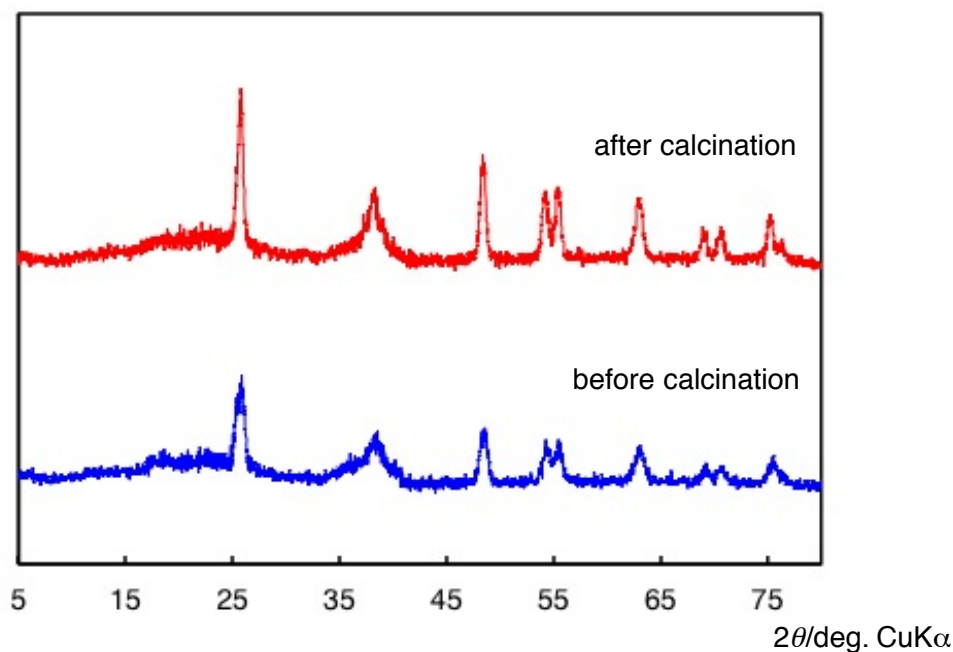


Fig. 4-16 X-ray Diffraction Patterns of **FA6**/SiO₂/*an*-TiO₂ nanocomposites (Run 1 in Table 4-3) before and after calcination at 1000 °C.

Fig. 4-16 shows the XRD spectra of **FA6**/SiO₂/*an*-TiO₂ nanocomposites before and after calcination at 1000 °C. The characteristic peaks of the nanocomposites before and after calcination were completely agreement with those of the parent *an*-TiO₂ particles before calcination (Fig. 4-15), indicating that *an*-TiO₂ nanoparticles in the nanocomposite cores can keep completely its structure without phase transformation into the rutile even after calcination at 1000 °C. Usually, it is well-known that the phase transformation of titanium oxide from anatase to rutile is observed during the calcination process from 600 to 750 °C.^{44~}

⁴⁷⁾ However, titania-silica composite can keep the anatase structure at around 900 °C, although the rutile phase in this composite appears at a calcination temperature of 1000 °C.^{48,}

⁴⁹⁾ This stabilization of anatase TiO₂ arises from the formation of Ti-O-Si interface to prevent the phase transformation to rutile. ^{48, 49)} Thus, the present **FA6**/SiO₂/*an*-TiO₂ nanocomposite lattice would lock the Ti-O species at the TiO₂ domains to prevent the phase transformation to rutile at 1000 °C.

FA6/SiO₂/*an*-TiO₂ nanocomposite – encapsulated BPA were also found to prevent the phase transformation to rutile after calcination at 1000 °C as shown in Fig. 4-17. Similarly, **FA6**/SiO₂/*an*-TiO₂ nanocomposite – encapsulated BINOL (or fullerene) were able to prevent perfectly the phase transformation to rutile after calcination at 1000 °C (data not shown).

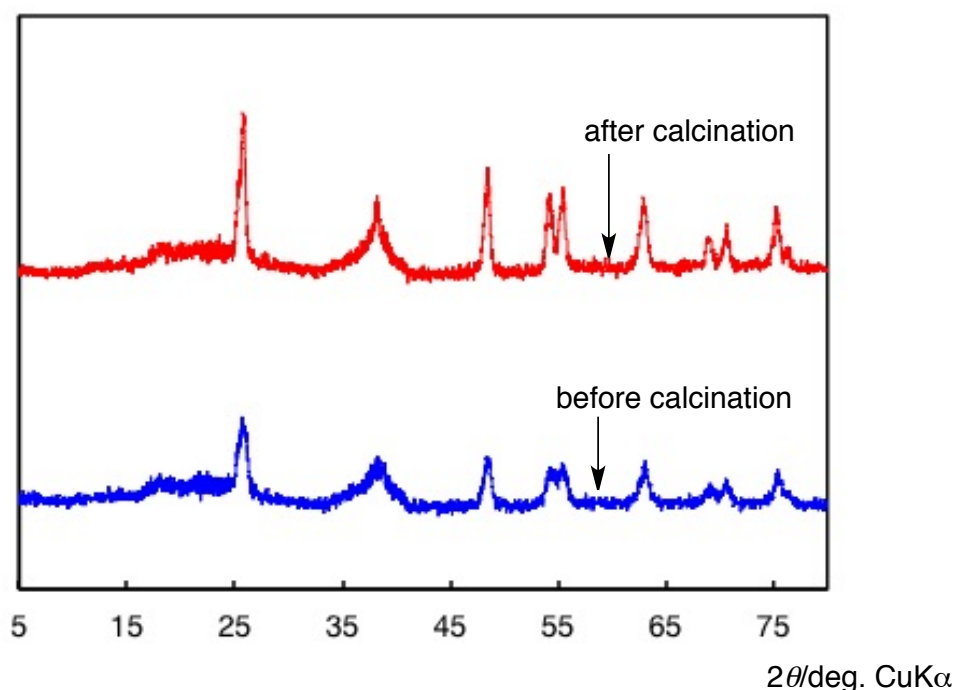


Fig. 4-17 X-ray Diffraction Patterns of **FA6**/SiO₂/*an*-TiO₂ nanocomposites - encapsulated BPA (Run 2 in Table 4-3) before and after calcination at 1000 °C.

The photocatalytic activity of **FA6/SiO₂/an-TiO₂** nanocomposites – encapsulated fullerene (Run 9 in Table 4-3) before and after calcination at 1000 °C was evaluated in terms of the decolorization of methylene blue dye (MB) under UV light irradiation (λ_{max} 365 nm) in order to clarify the presence of *an*-TiO₂ nanoparticles in the present nanocomposites even after calcination at 1000 °C. The residual amounts of MB were estimated by the decrease of the absorbance at λ_{max} : 652 nm related to MB by UV light irradiation, and the results were summarized in Fig. 4-18.

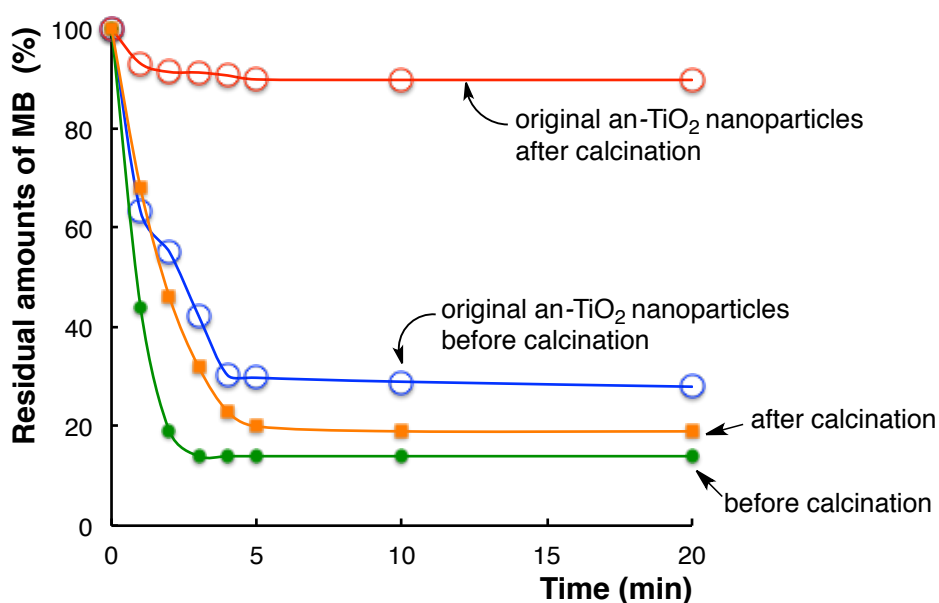


Fig. 4-18 Relationship between the residual amounts of methylene blue dye and photoirradiation (λ_{max} : 365 nm) time in the presence of **FA6/SiO₂/an-TiO₂** nanocomposites – encapsulated C₆₀: full diamonds and squares (or original *an*-TiO₂ nanoparticles: open circles) before and after calcination at 1000 °C (used sample: Run 9 in Table 4-3): Concentration of methylene blue dye: 2.5 mg/dm³; Concentration of nanocomposites (or original *an*-TiO₂ nanoparticles before and after calcination at 1000 °C): 25 mg/dm³.

Original *an*-TiO₂ nanoparticles before calcination can exhibit a good photocatalytic

activity for the decolorization of MB, although the original *an*-TiO₂ nanoparticles are unable to give any photocatalytic activity even after 20 min-photoirradiation due to the phase transformation to rutile, of whose structure affords in general no photocatalytic activity for TiO₂ nanoparticles. However, interestingly, **FA6/SiO₂/*an*-TiO₂** nanocomposites – encapsulated fullerene before calcination were found to exhibit a higher photocatalytic activity for the decolorization of MB than that of the parent *an*-TiO₂ nanoparticles before calcination under similar conditions. More interestingly, **FA6/SiO₂/*an*-TiO₂** nanocomposites – encapsulated fullerene after calcination were able to exhibit the same photocatalytic activity as that before calcination.

Fig. 4-18 shows that the photocatalytic activity of **FA6/SiO₂/*an*-TiO₂** nanocomposites – encapsulated fullerene before and after calcination for the decoloring ability of MB at the initial UV light irradiation time from 1 to 5 min can increase effectively, compared to that of the parent *an*-TiO₂ nanoparticles before calcination. Thus, the photocatalytic activity of **FA6/SiO₂/*an*-TiO₂** nanocomposites and **FA6/SiO₂/*an*-TiO₂** nanocomposites – encapsulated *Ar-H* has been studied under the initial 1 ~ 5 min-photoirradiation under similar conditions. These results are shown in Table 4-4.

Table 4-4 Relationship between the consumed amounts of MB (initial concentration: 2.5 mg/dm³) (in percentage) and UV light irradiation time (1 ~ 5 min) in the presence of **FA6**/SiO₂/*an*-TiO₂/**Ar-H** nanocomposites (25 mg/dm³).

Run*	Nanocomposites	Consumed MB (%)									
		UV light irradiation time									
		Before calcination					After calcination at 1000 °C				
		1	2	3	4	5 (min)	1	2	3	4	5 (min)
	<i>an</i> -TiO ₂ nanoparticles**	37	45	58	70	70	7	9	9	9	10
1	FA6 /SiO ₂ / <i>an</i> -TiO ₂	58	78	83	83	83	15	26	34	38	40
3	FA6 /SiO ₂ / <i>an</i> -TiO ₂ /BPA	30	56	79	86	87	24	40	51	59	64
6	FA6 /SiO ₂ / <i>an</i> -TiO ₂ /BINOL	41	65	77	82	83	24	41	53	61	66
9	FA6 /SiO ₂ / <i>an</i> -TiO ₂ /C ₆₀	56	81	86	86	86	32	54	68	77	80

* Each Run No. corresponds to that of Table 4-3

** Concentration of nanoparticles: 25mg/dm³

As shown in Table 4-4, the photocatalytic activity of these nanocomposites before and after calcination at 1000 °C at 1 ~ 5 min-photoirradiation for the decolorization of MB is higher than that of original *an*-TiO₂ nanoparticles. Interestingly, a higher photocatalytic activity for the decolorization of MB during the initial photoirradiation time: 1 ~ 5 min was observed in **FA6**/SiO₂/*an*-TiO₂ nanocomposites – encapsulated **Ar-H** (Runs 3, 6 and 9 in Table 4-4) after calcination, compared to that of **FA6**/SiO₂/*an*-TiO₂ nanocomposites (Run 1 in Table 4-4) after calcination. Such higher photocatalytic activity would be due to the effective oleophilic-oleophilic interaction between the aromatic compounds in the **FA6**/SiO₂/*an*-TiO₂ nanocomposites and MB. It was previously reported that the SiO₂ lattice in the titania–silica composites, which were prepared by the sol–gel reaction of titanium oxychloride and sodium

silicate in the presence of surfactants such as cetyltrimethylammonium bromide,^{48, 49)} can lock the Ti–O species through the formation of Ti–O–Si species to prevent the phase transformation to rutile during the calcination process. Fluorine-doped nanosized anatase TiO₂ particles can be in general prepared by using hydrofluoric acid as a source of fluorine, and these fluorine-doped TiO₂ nanoparticles can enhance the photocatalytic activity, compared to that of original one.^{50 ~ 57)} This result is due to the formation of Ti–F species on the facets, especially surface terminating Ti–F bonds in the surface Ti–O–Ti networks.^{50 ~ 57)} Hydrogen fluoride should be formed in the **R_F–OH**/SiO₂/*an*-TiO₂ nanocomposite matrices to give a nonflammable characteristic for the encapsulated low molecular weight aromatic compounds into their composite matrices. Therefore, the higher photocatalytic activity and extremely thermostable anatase titanium oxide related to the **R_F–OH**/SiO₂/*an*-TiO₂ nanocomposites even after calcination at 1000 °C would be due to the formation of Ti–F and Ti–O–Si species, respectively.

4.4. Conclusion

A variety of fluorinated aliphatic alcohols/SiO₂ nanocomposites were prepared by the sol-gel reactions of TEOS in the presence of both silica nanoparticles and the corresponding alcohols under alkaline conditions. These obtained nanocomposites can give no weight loss corresponding to the contents of the alcohols even after calcination at 800 °C. In addition, these fluorinated nanocomposites were applied to the surface modification of glass to exhibit the superoleophobic and superhydrophilic characteristics on the surface. There have been hitherto some reports on the creation of both superhydrophobic and superoleophobic (superamphiphobic) surface with fluorinated derivatives such as fluorinated monoalkyl phosphate,^{40, 41)} fluorine-end-capped polyurethane,⁵⁸⁾ and fluoroalkyl end-capped oligomer.⁵⁹⁾ In addition, much attention has been also focused on the design, fabrication, and application of bio-inspired superoleophobic and smart surfaces, including superoleophobic-superhydrophobic surfaces,⁶⁰⁾ especially underwater superoleophobic surfaces have attracted a great deal of attention owing to their important practical applications.⁶¹⁾ However, to the best of my knowledge, studies on the creation of the superoleophobic and superhydrophilic surfaces have been hitherto very limited except for the present study. Thus, the present technology for the creation of the superoleophobic and

superhydrophilic surface has high potential for the applications to a wide variety of fields.

In addition, fluorinated aliphatic alcohol/SiO₂/*an*-TiO₂ nanocomposites have been prepared under the similar sol-gel reactions. The encapsulation of low molecular weight aromatic compounds such as BPA, BINOL and fullerene was found to proceed into these fluorinated nanocomposite cores. Interestingly, these obtained fluorinated SiO₂/*an*-TiO₂ nanocomposites can keep the anatase structures even after calcination at 1000 °C, although the parent *an*-TiO₂ nanoparticles undergoes the perfect phase transformation from anatase to rutile under the similar calcination conditions. These fluorinated nanocomposites before and after calcination were found to exhibit a higher photocatalytic activity than that of the parent *an*-TiO₂ nanoparticles before calcination under the similar conditions. More interestingly, fluorinated SiO₂/*an*-TiO₂ nanocomposites – encapsulated aromatic compounds enabled their photocatalytic activity to enhance more effectively, compared to the corresponding fluorinated SiO₂/*an*-TiO₂ nanocomposites. In this way, the present fluorinated SiO₂/*an*-TiO₂ nanocomposites – encapsulated aromatic compounds have high potential for the applications to the fields such as dye sensitized solar cell due to their not only good photocatalytic activity relative to anatase titanium oxide even after calcinations appropriately at 1000 °C but also the extremely thermal stable encapsulated low molecular weight aromatic compounds.

References

- 1) W. R. Dolbier, *J. Fluorine Chem.*, **126**, 157 (2005).
- 2) B. Ameduri, *Macromolecules*, **44**, 44, 2394 (2011).
- 3) T. Imae, *Curr. Opinion Colloid Interface Sci.*, **8**, 307 (2003).
- 4) B. Ameduri, *Chem. Rev.*, **109**, 6632 (2009).
- 5) B. Ameduri and B. Boutevin, *J. Fluorine Chem.*, **104**, 53 (2000).
- 6) B. Ameduri and B. Boutevin, "Well-Architected Fluoropolymers: Synthesis, Properties and Applications", *Elsevier, Amsterdam* pp231- 348 (2004).
- 7) J. -F. Berret, D. Calvet, A. Collet, and M. Viguier, *Curr. Opinion Colloid Interface Sci.*, **8**, 296 (2003).
- 8) T. Imae, H. Tabuchi, K. Funayama, A. Sato, T. Nakamura, and N. Amaya, *Colloids Surfaces A: Physicochem. Eng. Aspects*, **167**, 73 (2000).
- 9) P. Lebreton, B. Ameduri, and B. Boutevin, *Corpart, J. M. Macromol. Chem. Phys.*, **203**, 522 (2002).
- 10) M. J. Monteiro, M. M. Adamy, B. J. Leeuwen, A. M. Van Herk, and M. Destarac, *Macromolecules*, **38**, 1538 (2005).
- 11) A. E. Feiring, E. R. Wonchoba, F. Davdson, V. Percec, and B. Barboiu, *J. Polym. Sci.*

- Part A: Polym. Chem.*, **38**, 3313 (2000).
- 12) M. Destarac, K. Matyjaszewski, E. Silverman, B. Ameduri, and B. Boutevin, *Macromolecules*, **33**, 4613 (2000).
- 13) Z. Shi and S. Holdcroft, *Macromolecules*, **38**, 4193 (2005).
- 14) Y. Patil and B. Ameduri, *Polym. Chem.*, **4**, 2783 (2013).
- 15) F. Boschet, G. Kostov, B. Ameduri, A. Jackson, and B. Boutevin, *Polym. Chem.*, **3**, 217 (2012).
- 16) H. Sawada, *Chem. Rev.*, **96**, 1779 (1996).
- 17) H. Sawada and T. Kawase, *Kobunshi Ronbunshu*, **58**, 147 (2001).
- 18) H. Sawada and T. Kawase, *Kobunshi Ronbunshu*, **58**, 255 (2001).
- 19) H. Sawada, *J. Fluorine Chem.*, **105**, 219 (2000).
- 20) H. Sawada, *J. Fluorine Chem.*, **121**, 111 (2003).
- 21) H. Sawada, *Prog. Polym. Sci.*, **32**, 509 (2007).
- 22) H. Sawada, *Polym. Chem.*, **3**, 46 (2012).
- 23) P. Gomez-Romero and C. Sanchez, *Functional Hybrid Materials*; Wiley-VCH, Weinheim, (2004).
- 24) S. Yano, N. Okubo, and K. Takahashi, *Macromol. Symp.*, **108**, 279 (1996).
- 25) P. Fabbri, M. Messori, M. Montecchi, S. Nannarone, L. Pasquali, F. Pilati, C. Tonelli,

- and M. Toselli, *Polymer*, **47**, 1055 (2006).
- 26) Y. -C. Chen, C. -C Tsai, and Y. -D. Lee, *J. Polym. Sci. Part A: Polym. Chem.*, **42**, 1789 (2004).
- 27) J. -W. Cho and K. -I. Sul, *Fibers Polym.*, **2**, 135 (2001).
- 28) H. Sawada, T. Tashima, H. Kakehi, Y. Nishiyama, M. Kikuchi, M. Miura, Y. Sato, and N. Isu, *Polym. J.*, **42**, 167 (2010).
- 29) H. Sawada, X. Liu, Y. Goto, M. Kikuchi, T. Tashima, and M. Nishida, *J. Colloid and Interface Sci.*, **356**, 8 (2011).
- 30) S. Soma, Y. Mizuguchi, M. Sugiya, and H. Sawada, *J. Polym. Sci. Part A: Polym. Chem.*, in press.
- 31) H. Sawada, T. Narumi, S. Kodama, M. Kamijo, R. Ebara, M. Sugiya, and Y. Iwasaki, *Colloid Polym. Sci.*, **285**, 977 (2007).
- 32) H. Sawada, M. Kikuchi, and M. Nishida, *J. Polym. Sci. Part A: Polym. Chem.*, **49**, 1070 (2011).
- 33) H. Sawada, T. Tashima, and S. Kodama, *Polym. Adv. Technol.*, **19**, 739 (2008).
- 34) H. Sawada, T. Narumi, S. Kodama, M. Kamijo, R. Ebara, M. Sugiya, and Y. Iwasaki, *Colloid Polym. Sci.*, **285**, 977 (2007).
- 35) H. Sawada, H. Kakehi, T. Tashima, Y. Nishiyama, M. Miura, and N. Isu, *J. Appl. Polym.*

- Sci.*, **112**, 3482 (2009).
- 36) H. Sawada, T. Tashima, Y. Nishiyama, M. Kikuchi, G. Kostov, Y. Goto, and B. Ameduri, *Macromolecules*, **44**, 1114 (2011).
- 37) X. Yao, Y. Song, and L. Jiang, *Adv. Mater.*, **23**, 719 (2011).
- 38) J. Feng, B. Huang, and M. Zhong, *J. Colloid Interface Sci.*, **336**, 268 (2009).
- 39) R. Taurino, E. Fabbri, M. Messori, F. Pilati, D. Pospiech, and A. Synytska, *J. Colloid Interface Sci.*, **325**, 149 (2008).
- 40) K. Tsujii, T. Yamamoto, T. Onda, and S. Shibuichi, *Angew. Chem. Int. Ed. Eng.*, **36**, 1011 (1997).
- 41) S. Shibuichi, T. Yamamoto, T. Onda, and K. Tsujii, *J. Colloid Interface Sci.*, **208**, 287 (1998).
- 42) S. Srinivasan, S. Chhatre, M. J. Mabry, E. R. Cohen, and H. G. McKinley, *Polymer*, **52**, 3209 (2011).
- 43) S. Guo, H. Yoshioka, H. Kakehi, Y. Kato, M. Miura, N. Isu, B. Ameduri, and H. Sawada, *J. Colloid Interface Sci.*, **387**, 141 (2012).
- 44) D. A. H. Hanaor and C. C. Sorrell, *J. Mater. Sci.*, **46**, 855 (2011).
- 45) X. Peng and A. Chen, *Adv. Funct. Mater.*, **16**, 1355 (2006).
- 46) G. Madras, B. J. McCoy, and A. Navrotsky, *J. Am. Ceram. Soc.*, **90**, 250 (2007).

- 47) G. Wu, J. Wang, D. F. Thoma, and A. Chen, *Langmuir*, **24**, 3503 (2008).
- 48) A. Hilonga, J.-K. Kim, P. B. Sarawade, and H. T. Kim, *J. Mater. Sci.*, **45**, 1255 (2010).
- 49) A. Hilonga, J.-K. Kim, P. B. Sarawade, and H. T. Kim, *J. Mater. Sci.*, **45**, 1264 (2010).
- 50) S. Liu, J. Yu, B. Cheng, and M. Jaroniec, *Adv. Colloid Interface Sci.*, **173**, 35 (2012).
- 51) G. Liu, C. Sun, H. G. Yang, S. C. Smith, L. Wang, G. O. Lu, and H.-M. Cheng, *Chem. Commun.*, **46**, 755 (2010).
- 52) W. Ho, J. C. Yu, and S. Lee, *Chem. Commun.*, 1115 (2006).
- 53) D. Zhang, G. Li, X. Yang, and J. C. Yu, *Chem. Commun.*, 4381 (2009).
- 54) G. Wu, J. Wang, D. F. Thomas, and A. Chen, *Langmuir*, **24**, 3503 (2008).
- 55) M. Liu, L. Zhao, S. Ju, Z. Yan, T. He, C. Zhou, and W. Wang, *Chem. Commun.*, **46**, 1664 (2010).
- 56) X. Han, Q. Kuang, M. Jin, Z. Xie, and L. Zheng, *J. Am. Chem. Soc.*, **131**, 3152 (2009).
- 57) G. H. Yang, G. Liu, S. Z. Qiao, C. H. Sun, Y. G. Jin, S. C. Smith, J. Zou, H. M. Cheng, and G. Q. Lu, *J. Am. Chem. Soc.*, **131**, 4078 (2009).
- 58) Q. Xie, J. Xu, L. Feng, W. Tang, X. Luo, and C. C. Han, *Adv. Mater.*, **16**, 302 (2004).
- 59) Y. Goto, H. Takashima, K. Takishita, and H. Sawada, *J. Colloid Interface Sci.*, **362**, 375 (2011).
- 60) K. Liu, Y. Tian, and L. Jiang, *Prog. Mater. Sci.*, **58**, 503 (2013).

- 61) M. J. Liu, S. T. Wang, Z. X. Wei, Y. L. Song, and L. Jiang, *Adv. Mater.*, **21**, 665 (2009).
- 62) N. Isu, *J. Soc. Cosmet. Chem. Jpn.*, **40**, 187 (2006).
- 63) S. Nishimoto, Y. Sawai, Y. Kameshima, and M. Miyake, *J. Jpn. Soc. Colour Mater.*, **87**, 50 (2014).

Conclusions

The results obtained from this study are summarized as follows:

1. Fluoroalkyl end-capped vinyltrimethoxysilane oligomer/anatase titanium oxide $[R_F-(VM-SiO_2)_n-R_F/an-TiO_2]$ nanocomposites were prepared by the sol-gel reaction of the corresponding oligomer with anatase titanium oxide nanoparticles under alkaline conditions. Interestingly, anatase titanium oxide in the obtained fluorinated oligomeric anatase titanium oxide nanocomposites can preserve completely its structure without any phase transformation from anatase to rutile even after calcination at 1000 °C, although the parent anatase titanium oxide nanoparticles completely change into rutile type under similar conditions. More interestingly, this fluorinated oligomeric anatase titanium oxide nanocomposite even after calcination at 1000 °C was able to exhibit the same photocatalytic activity as that before calcination. This is the first example of such extremely thermally stable characteristic and higher photocatalytic activity of anatase titanium oxide in the composites after calcination at 1000 °C. Especially, the thermally stable $R_F-(VM-SiO_2)_n-R_F/an-TiO_2$ nanocomposites will have high potential for the applications to a variety of fields such as dye sensitized solar cell,

because these nanocomposites can exhibit good photocatalytic activity relative to anatase titanium oxide even after calcination at 1000 °C.

2. Fluoroalkyl end-capped vinyltrimethoxysilane oligomer/anatase titanium oxide nanocomposite-encapsulated low molecular weight aromatic compounds [Ar-H] such as bisphenol A [BPA], 1,1'-bi(2-naphthol) [BINOL], and fullerene (C₆₀), named as [R_F-(VM-SiO₂)_n-R_F/*an*-TiO₂/Ar-H] were prepared by the sol-gel reactions of the corresponding oligomer in the presence of *an*-TiO₂ nanoparticles and Ar-H under alkaline conditions. Thermogravimetric analyses measurements show that R_F-(VM-SiO₂)_n-R_F/*an*-TiO₂ nanocomposite-encapsulated BPA and BINOL, were found to give no weight loss corresponding to the contents of these aromatic compounds even after calcination at 800 °C. Anatase TiO₂ in these fluorinated nanocomposites can keep its crystalline structure without phase transformation into rutile even after calcination at 1,000 °C, although the original anatase TiO₂ nanoparticles underwent a complete phase transformation into rutile under similar conditions. Notably, R_F-(VM-SiO₂)_n-R_F/*an*-TiO₂/Ar-H nanocomposites can give a good photocatalytic activity even after calcination at 1000 °C for the decolorization of methylene blue under UV light irradiation. More interestingly, these fluorinated nanocomposites before and after calcination were found to exhibit a higher photocatalytic

activity than that of the corresponding $R_F-(VM-SiO_2)_n-R_F/an-TiO_2$ nanocomposites under similar conditions.

3. Vinylidene fluoride (VDF) and functional comonomers such as $CF_2=CFCO_2Me$, $CFH=CFCO_2H$, and $CF_2=CFC_3H_6OCOMe$ copolymers [poly(VDF-co-M)] were applied to the preparation of the corresponding fluorinated copolymers/anatase titanium oxide, and /silica/anatase titanium oxide nanocomposites, respectively. These nanocomposites possess high thermal stabilities. For example, poly(VDF-co- CF_2CFCO_2Me)/silica/anatase titanium nanocomposites only give 2% weight loss even after calcination at 800 °C. Anatase titanium oxide in the fluorinated copolymers/anatase titanium oxide nanocomposites underwent an effective transformation into rutile after calcination at 1000 °C. However, fluorinated copolymers/silica/anatase titanium oxide nanocomposites preserved completely its anatase structure without any phase transformation into rutile. Interestingly, these fluorinated nanocomposites exhibit a higher photocatalytical activity for the discoloration of methylene blue compared with original anatase titanium oxide nanoparticles. Especially, poly(VDF-co- CF_2CFCO_2Me)/silica/anatase titanium nanocomposites before and after calcination displayed a higher photocatalytic activity than the other VDF copolymers nanocomposites.

4. Four kinds of fluorinated aliphatic alcohols/SiO₂ nanocomposites were prepared by the sol-gel reactions of TEOS in the presence of both silica nanoparticles and the corresponding alcohols under alkaline conditions. Fluorinated alcohols in these obtained nanocomposites can give no weight loss even after calcination at 800 °C. The modified glass surfaces treated with these fluorinated silica nanocomposites were found to exhibit the superoleophobic and superhydrophilic characteristics. Similarly, fluorinated aliphatic alcohol/silica/anatase titanium oxide nanocomposites and these nanocomposites encapsulated low molecular weight aromatic compounds such as bisphenol A, 1,1'-bi(2-naphthol) and fullerene, were also prepared by the similar sol-gel reactions. TGA results showed that the encapsulated bisphenol A and 1,1'-bi(2-naphthol) exhibit nonflammable characteristic even at 800 °C. Anatase structure in these fluorinated silica/anatase titanium oxide nanocomposites can keep without any transformation into rutile even after calcination at 1000 °C. Interestingly, these fluorinated nanocomposites before and after calcination were found to exhibit a higher photocatalytic activity than that of the original anatase titanium oxide nanoparticles before calcination under the similar conditions. More interestingly, fluorinated silica/anatase titanium oxide nanocomposites-encapsulated aromatic compounds possess superior photocatalytical ability, compared to the corresponding fluorinated silica/anatase titanium oxide nanocomposites.

Publications

- 1) S. Guo, H. Yoshioka, H. Kakehi, Y. Kato, M. Miura, N. Isu, B. Ameduri, and H. Sawada, “Fluoroalkyl end-capped vinyltrimethoxysilane oligomer/anatase titanium oxide nanocomposites possessing photocatalytic activity even after calcination at 1000 °C”, *J. Colloid Interface Sci.*, **387**, 141 ~ 145 (2012).
- 2) S. Guo, T. Ogasawara, T. Saito, H. Kakehi, Y. Kato, M. Miura, N. Isu, and H. Sawada, “Preparation and photocatalytic activity of fluoroalkyl end-capped vinyltrimethoxysilane oligomer/anatase titanium oxide nanocomposites - encapsulated low molecular weight aromatic compounds”, *Colloid Polym. Sci.*, **291**, 2947 ~ 2957 (2013).
- 3) S. Guo, H. Yoshioka, Y. Kato, H. Kakehi, M. Miura, N. Isu, A. Manseri, H. Sawada, and B. Ameduri, “Photocatalytic activity of vinylidene fluoride - containing copolymers/anatase titanium oxide/silica nanocomposites”, *Eur. Polym. J.*, **58**, 79 ~ 89 (2014).
- 4) S. Guo, S. Soma, K. Okuno, T. Saito, T. Nakagawa, K. Sato, and H. Sawada, “Preparation and properties of fluorinated aliphatic alcohol/silica nanocomposites - Application to the encapsulation of anatase titanium oxide nanoparticles into these composite cores”, *Composites: Part B*, DOI:10.1016/j.compositesb.2014.09.020

(not described in this thesis)

- 5) S. Guo, X. Wu, J. Zhou, J. Wang, B. Yang, and B. Ye, “MWNT/Nafion composite modified glassy carbon electrode as the voltammetric sensor for sensitive determination of 8-hydroxyquinoline in cosmetic”, *J. Electroanal. Chem.*, **655**, 45 ~ 49 (2011).
- 6) S. Guo, Q. Zhu, B. Yang, J. Wang, and B. Ye, “Determination of caffeine content in tea based on poly(safranin T) electroactive film modified electrode”, *Food Chem.*, **129**, 1311 ~ 1314 (2011).
- 7) B. Yang, F. Wang, S. Guo, and B. Ye, “Electrochemical behavior and voltammetric determination of 2,4,6-Triaminopyrimidine at glassy carbon electrode modified with multi-walled carbon nanotubes/Nafion”, *Anal. Sci.*, **26**, 1071 ~ 1075 (2010).

Acknowledgements

The author would like to express her deepest gratitude to her supervisor, Prof. Sawada, who has offered her the valuable guidance during her academic studies. Without his patient instruction and expert suggestions, the completion of this thesis would not have been possible.

Secondly, she deeply thanks to Prof. Isoshi Nukatsuka, Prof. Masaaki Okazaki, Prof. Toshiyuki Abe and Associate Prof. Masanobu Sagisaka for their kind advice. She would also like to thank all the students in Sawada Laboratory, especially Dr. Hiroaki Yoshioka, Dr. Tetsushi Kijima, Mr. Taiki Tsuzuki-ishi and Mr. Tomoya Saito. They have provided her great help during the three years.

Thanks for the financial support from China Scholarship Council and Hirosaki University.

Finally, her thanks would also go to her beloved families for their boundless love and whole-hearted support over all these past years.